NON-ORTHOGONAL MULTIPLE ACCESS: A COMPREHENSIVE ANALYTICAL STUDY AND OPTIMISATION IN FADING CHANNELS

A thesis submitted to the University of Manchester for the degree of
Doctor of Philosophy
in the Faculty of Science and Engineering

2022

By
Adel Saleh S. Alqahtani

Department of Electrical and Electronic Engineering

TABLE OF CONTENTS

Word count: 32979

LIST OF TABLES

LIST OF FIGURES

List of Acronyms

5G	fifth generation
AF	amplify-and-forward
A-UP	adaptive user pairing algorithm
AWGN	additive white Gaussian noise
BER	bit error rate
BS	base station
CDF	cumulative distribution function
C-NOMA	cooperative non-orthogonal multiple accesses
CR-NOMA	cognitive radio NOMA
CSI	channel state information
DF	decode-and-forward
DKL	conditions and the Dinkelbach
EC	ergodic capacity
EE	energy efficiency
EH	energy harvesting
F-NOMA	fixed NOMA
FPA	fixed power allocation
FR	fixed relaying
FS	web page size
FSPA	full search power allocation
FTPA	fractional transmit power allocation
HD	half-duplex
HNG	Hungarian algorithm

HTTP	Hypertext Transfer Protocol
IBFS	initial basic feasible solution
IP	information process
IPM	interior point method
IRS	intelligent reflecting surfaces
ISDF	incremental-selective DF
KKT	Karush-Kuhn-Tucker
LCM	Least Cost Method
LMCM	least and most cost method
LOS	line of sight
MIMO	multiple-input-multiple-output
MISO	multiple input single output
ML	maximum likelihood
MMS	maximum segment size
MODI	modified distribution method
MQAM	M-ary quadrature amplitude modulation
MSO	mean score opinion
NLOS	non-line of sight
NNFF	nearest near user and farthest far user
NNNF	nearest near user and nearest far user
NOMA	non-orthogonal multiple accesses
NWCM	North-West Corner Method
OFDM	orthogonal frequency division multiple accesses
OMA	orthogonal multiple access
OP	outage probability
PDF	probability density function
QoE	quality of experience
QoS	quality of service
RNRF	random near user and random far user
RTT	round trip time
RVs	random variables
SC	superposition coding

SF-CDRT	selective DF with coordinated direct and relay transmission
SIC	successive interference cancellation
SINR	Signal to Interference and Noise Ratio
SISO	single input single output
SNR	signal-to-noise ratio
SSM	streamlined simplex method
SSTM	Stepping Stone Method
SUAAs	sub-carrier user assignment algorithms
SWIPT	simultaneous wireless information and power transfer
TCP	Transmission Control Protocol
TSR	time switching-based relaying
UAV	unmanned aerial vehicle
VAM	Vogel's Approximation Method
VLC	visible light communication

List of Symbols

$\mathcal{I}$	Indoor user
$\mathcal{P}_{\mathrm{s}}$	Total transmitted power at BS
$\mathcal{O}$	Outdoor user
η	SIC Imperfect factor
κ	Channel fading parameter
μ	Channel fading parameter
α	Channel fading parameter
β	Power allocation factor
r	UAV-relay
g_i	Small scale fading
PL	Path loss
f	Carrier frequency
L_{fs}	Free space path loss
L_t	Transition propagation path loss
L_{in}	Indoor propagation path loss
L_{pc}	Perpendicular path loss
L_{pt}	Parallel penetration loss
L_i	Internal wall lose
n	Number of internal walls
χ	Indoor path loss parameter
ρ	Signal to noise ratio
γ	Instantaneous SNR
$\tilde{\gamma}$	Average SNR

σ	Noise power
$\mathrm{I}_v(.)$	Modified Bassel function
$\mathcal{Q}_{(.)}$	Generalized Marcum-Q function
α_1	Power allocation factor of $\mathcal{I}$
α_2	Power allocation factor of $\mathcal{O}$
x_{sc}	Superimposed NOMA signal
τ	Time splitting factor
h	Channel frequency response
B	System bandwidth
$\mathcal{P}$	Signal power
$\mathcal{P}_{\mathrm{r}}$	Transmitted power at UAV-relay
R	Data target rate
$R_{\mathcal{I}}$	Indoor target data rate
$R_{\mathcal{O}}$	Outdoor target data rate
$\mathcal{P}_{\mathrm{c}}$	Circuit power
E_{total}	Total harvested power
δ	Energy amplifier efficiency
$d_{r\mathcal{O}}$	Distance between UAV-relay and outdoor user
$d_{r\mathcal{I}}$	Distance between UAV-relay and indoor user
$d_{r\mathcal{I}}$	Distance between UAV-relay and external wall
d_{in}	Distance between interior wall and indoor user
d_{sr}	Distance between BS and UAV-relay
θ	Grazing angle between UAV-relay and exterior wall
d_{out}	Distance between UAV-relay and exterior wall
$f_{\gamma(\gamma)}$	Probability density function
$F_{\gamma(\gamma)}$	Cumulative density function
$\mathbb{S}$	Set of all possible constellation points
$\hat{x}$	Estimated symbol
$\tilde{C}_{\mathcal{I}}$	Ergodic capacity of indoor user
$\tilde{C}_{\mathcal{O}}$	Ergodic capacity of outdoor user
$\tilde{\gamma}_{1,1}$	Average power link between BS and UAV-relay
$\tilde{\gamma}_{1,2}$	Average power link between UAV-relay and $\mathcal{I}$

$\tilde{\gamma}_{2,3}$	Average power link between UAV-relay and $\mathcal{O}$
$\mathrm{P}^{\mathcal{O}}$	Outage Propability of $\mathcal{O}$
T	Total time interval of the frame
x_1	Symbol of $\mathcal{I}$
x_2	Symbol of $\mathcal{O}$
$\hat{x}_1$	Estimated symbol of $\mathcal{I}$
$\hat{x}_2$	Estimated symbol of $\mathcal{O}$
Ω	The mean power of h
$\mathbb{E}[.]$	The expectation operator
B_{sc}	subcarrier bandwidth
λ	Lagrange multiplier
$\mathcal{L}_1$	amount of congestion window cycles
$\mathcal{L}_2$	amount of slow begin cycles

Abstract

Accommodating the rapid growth of data-intensive wireless applications requires highly innovative mechanisms to enable efficient use of the available radio spectrum while satisfying various metrics of quality of service (QoS) and quality of experience (QoE). To this end, non-orthogonal multiple access (NOMA) technique has emerged as a potential multi-access technology that can meet future wireless demands. In this thesis, various analytical works are performed to evaluate non-orthogonal multiple access (NOMA), particularly in advanced fading channels, where different wireless communication scenarios are investigated. For example, the conventional NOMA method for a limited multiple number of users is analysed by deriving closed-form expressions of outage probability (OP), bit error rate (BER) and ergodic capacity (EC). Furthermore, a cooperative NOMA scheme supported by UAV-relay is being investigated, where assigned nodes are served in different environments, that is, indoor and outdoor channel deployments. Therefore, comprehensive and analytical studies are provided to evaluate the ability of NOMA to pair indoor and outdoor users. Furthermore, the sum data rate for the previous case of user pairing is also being optimised by proposing a couple of algorithms such as the streamlined simplex method (SSM) and the least- and most-cost method (LMCM). On the other hand, the fairness rate of the indoor user is optimised by applying the Max-Min optimisation technique, since it has been considered to have the lowest channel gain due to challenges posed by its environment. In addition, different performance metrics, such as the achievable data rate and the fairness index, are analysed to evaluate the efficiency of the proposed algorithms. Ultimately, intelligent reflecting surface (IRS) technology is combined with NOMA to improve system performance, where the QoS and QoE of indoor users are being evaluated. The results achieved show the potential significance of applying NOMA in terms of system and link-level efficiency. They also broaden our understanding of the impact of channel fading, resource allocation, target data rates, path-loss models, distance, number of IRS reflectors, and others on the system performance.

Declaration

I here by declare that the thesis entitled “Non-Orthogonal Multiple Access: A Comprehensive Analytical Study and Optimization in Fading Channels” submitted by me, for the award of the degree of *Doctor of Philosophy* to University of Manchester is a record of bonafide work carried out by me under the supervision of Dr. Emad Alsusa, School of Electrical and Electronic Engineering University of Manchester, UK.

I further declare that the work reported in this thesis has not been submitted and will not be submitted, either in part or in full, for the award of any other degree or diploma in this university or any other university.

Copyright

Acknowledgements

Praise be to Allah, who has rewarded me with perseverance, patience, and health to complete my thesis. With enormous pleasure and a profound feeling of appreciation, I would like to express my sincere gratitude to my supervisor, **Dr. Emad Alsusa**; Without his encouragement and continued support, this project would not have been completed successfully. I am also gratitude to **Dr. Arafat Al-dawick** for his assistance, and his exceptional technical skills in his respective domains and consistent constructive criticism on my research. Furthermore, I would like to thank the **Saudi Arabia Cultural Bureau (SACB)** in London and **King Khalid University (KKU)** for their kind sponsorship, which enabled me to finish my Ph.D. study. I also would like to express my deepest appreciation to my mother, **Mrs. Fatimah Al-Nasir**, for all the sacrifices she made during my studies and for always being there for spiritual support and encouragement when I mostly need it. In fact, I would not have accomplished anything in my life if it were not for her unwavering love and prayer. In addition, a special heartfelt gratitude goes to my sweetheart **Mrs. Norah Alqahtani**. Words cannot express how grateful I am to you for accompanying me on this journey and for your ongoing support. My love for my two beautiful young children, **Basell** and **Shahad**, is overwhelming, and you have inspired me to thrive in my studies. Last but not least, I would like to thank my Ph.D. colleagues, **Abdulakarim Al hanif, Turki Alharbi, Mohammad Alawad, Mohammed Aljarrah, Abdulmajeed M. Alenezi, and Salah Almaghthawi**, for their encouragements and unlimited support throughout my research.

List of Publications

- **Journal Papers**

  1. A. Alqahtani, E. Alsusa, A. Al-Dweik and M. Al-Jarrah, ”Performance Analysis for Downlink NOMA Over α-μ Generalized Fading Channels,” in IEEE Transactions on Vehicular Technology, vol. 70, no. 7, pp. 6814-6825, July 2021, op0l;[
  2. A. Alqahtani, E. Alsusa, and A. Al-Dweik, ”UAV-Enabled Cooperative NOMA with Indoor- Outdoor User-Paring in κ-μ Channels,” (Submitted to IEEE IoT).
  3. A. Alqahtani, and E. Alsusa, ”Low-Complexity Indoor-Outdoor User Pairing and Resource Optimization in DL-NOMA system,” (Under process to be submitted to IEEE Access).
  4. A. Alqahtani, and E. Alsusa, ”QoS and QoE in IRS-assisted Indoor NOMA System over $\kappa - \mu$ Fading Channels,” (Under process to be submitted to IEEE Transactions on Communications).

- **Conference Papers**

  1. A. Alqahtani and E. Alsusa, ”Performance Analysis of Downlink NOMA System over α-η-μ Generalized Fading Channel,” in IEEE VTC2020-Spring conference, pp. 1-5, May 2020,
  2. A. Alqahtani, E. Alsusa, and A. Al-Dweik, ”Outage Probability of Indoor-outdoor C-NOMA Enabled UAV-Relay Over κ-μ Fading,” in IEEE VTC2022-Spring conference, Jun. 2022.
  3. A. Alqahtani, and E. Alsusa, ”Optimization Technique of Indoor-Outdoor User Pairing in DL-NOMA System,” in ICUFN, July 2022.

CHAPTER 1

Introduction

1.1 Trends in Mobile Networks

Wireless communications play an important role in the lives of most people nowadays. Recently, unprecedented demands for developing advanced mobile devices have increased, as most entertainment, online services, and others are being offered to the end user with a substantial amount of data and high download and upload speeds. At the end of the 19th century, Macroni and Maxwell demonstrated the possibility of wireless communication. The standardisation of this technology has been developed since 1957, established with the Swedish Mobile Telephone System, which at the time offered communication for 125 users. In 1980, the second generation (2G) of wireless communications was developed by a new standardisation called the Global System of Mobile (GSM). It was the first digital system that was widely used at the time. After that, multiple standers have been launched, such as direct-sequence code division multiple access (DS-CDMA) and Pan-American Digital advanced mobile phone system (D-AMPS). Shortly afterwards, the user's demand for high data rates became crucial; therefore, the third generation (3G) was developed based on code-division multiple access (CDMA) technology. However, the user's thirst for higher amounts of data rate continued to increase, and the demand for new technologies to fulfil these requirements is ongoing. Therefore, efficient modulation techniques such as orthogonal frequency division technique (OFDM) became a well-developed solution since it provides more flexibility when bringing different parameters that can be configured and controlled despite the effect of propagation conditions [1].

To this end, most of the current research is approaching a new era of promising technologies that could emerge under 5G and beyond. After decades of developing different wireless communication techniques, a potential technique called non-orthogonal modulation access technique (NOMA) has overcome most known orthogonal technologies such as TDMA, FDMA, CDMA and OFDMA in terms of different system require-

ments [2]. After the commercial deployment of fourth generation (4G), most academic researchers have shifted their focus to investigating 5G cellular networks. The rapid revolution in wireless communication technology is a promising sign for modifying many methods of communications such as in 3G and 4G to become more advanced by adequately treating a considerable amount of data in a short period of time, which could be less than one millisecond latency. These tremendous improvements are capable of beneficially contributing to the new era of 5G system. Recently, 5G has been considered the most recent development in wireless communication, where many researchers have theoretically demonstrated its ability to provide a significant decrease in latency, as well as a larger data rate capacity to serve multiple users, [2]. Therefore, the potential expectations that 5G can offer are represented by a high amount of data rate between 10-20 Gbps, which is more than the current amount provided by Long-Term Evolution (LTE), and the latency is roughly considered as short as 1 ms. In addition to this remarkable growth in 5G, concerns about meeting these expectations are still under massive investigation in academia and industry. Furthermore, extensive research has been carried out on different aspects of 5G. To illustrate, a new radio access technology has to be designed to handle this superior communication. As a consequence, the non-orthogonal multiple access (NOMA) technique is being strongly recognised as the main candidate for beyond 5G, as it outperforms current orthogonal multiple access techniques in different terms of measurements, such as high performance and spectral efficiency [1–5].

1.2 Motivation for the Thesis

The requirement for high capacity and data speed in mobile networks is increasing enormously with the growth of traffic. NOMA is one of the most promising radio access technologies that offers improved spectral efficiency, high transmission speed, and low transmission latency [4, 5]. Furthermore, NOMA impressively exceeds the current orthogonal multi-access system (OMA) in terms of high throughput performance by implementing an advanced energy allocation scheme. Therefore, analysing the performance of NOMA is essential, precisely when it emerges in different channel fading distributions, different transmission environments, and new compatible wireless technologies. Despite the importance of the existing literature on NOMA, there is little work to explore different NOMA performance metrics on composite fading channels, such as $\alpha - \mu$ and $\kappa - \mu$ fading channels. Therefore, this thesis is crucial because it provides a holistic analysis and in-depth insights on the significant impacts of the aforementioned channel variations on NOMA. Furthermore, in most current studies, NOMA signals are aimed to be propagated through outdoor-to-outdoor or indoor-to-indoor channels, while users can often be indoor while served by an outdoor base station (BS). As such,

outdoor-to-indoor channels, or vice versa, are an important consideration that requires further investigation by the research community. Moreover, NOMA shows high potential improvements in terms of system performance when it joins other recent wireless communication technologies, such as intelligent reflecting surface (IRS). Thus, it is worth investigating these particular combinations of IRS, and NOMA.

1.3 Aims and Objectives

The main objective of this research is to investigate and analyse the performance of the NOMA system on different generalised fading channels, in which a conventional non-cooperative NOMA scheme, a cooperative UAV-assisted relay NOMA scheme, and user pairing optimisation are applied for the indoor-outdoor NOMA system. The specific objectives of the research are described as follows:

- Introduce a general key investigation of the NOMA system by deep exploration of the current literature to understand fundamental concepts, recent ideas, and proposed techniques that should be applied in this research.
- Analyse a conventional NOMA system in a downlink scenario with multiple users to achieve closed-form analytical expressions of different vital performance metrics such as outage probability (OP), average bit error rate (ABER), and ergodic capacity (EC) over generalised fading channels such as models α-μ and κ-μ in different scenarios.
- Consider NOMA for indoor users, where they can be served by an outdoor base station (BS). This scenario introduces some challenges in characterising wireless channels, particularly when a UAV is applied. Therefore, our objective is to address these limitations to accurately analyse and optimise the system performance of indoor-outdoor NOMA.
- Provide an extensive analytical evaluation of the cooperative performance of NOMA for indoor-outdoor NOMA users considering other advanced technologies such as UAV-relay and practical successive interference cancellation (SIC). Different performance matrices, such as outage probability (OP), ergodic capacity (EC), throughput, and energy efficiency (EE), must be evaluated for such a system model.
- Propose new user pairing algorithms for indoor-outdoor NOMA that participate in maximising the sum data rate. These algorithms are known as the streamlined simplex method (SSM) and the least and most cost method (LMCM). To measure

the potential efficiency of the proposed algorithm, our aim is to apply a random user pairing method as a benchmark.

- Maximise the fairness rate of indoor NOMA users, as they exhibit a low data rate due to their extreme attenuation factors. Therefore, the Max-Min optimisation method is proposed to improve the individual data rate of the indoor NOMA user.

- Evaluate the performance of IRS-assisted NOMA for multiple indoor users in $\kappa - \mu$ fading channels by evaluating quality of service (QoS), defined in the form of outage probability (OP), bit error rate (BER), ergodic capacity (EC), and throughput and QoE, given in the mean score opinion (MOS).

1.4 Key Contributions

- The main contributions of Chapter 4 can be summarised as follows:
  - Derive exact OP expressions for NOMA with two and three-user NOMA over $\alpha - \mu$ channels under different constraints. The OP is testified when the users' demand of data rates is below certain QoS requirements. Moreover, the case when the NOMA users' rate is less than the OMA users is considered.
  - Investigate the link performance and provides exact closed-form BER expressions using M-QAM modulation technique.
  - Derive closed-form expressions for the ergodic capacity.
  - All provided closed-form expressions in this research are formulated with the aid of advanced mathematical functions such as the Meijer G-function and Fox H-function, which leads to more tractable analysis. In addition, the order statistics is also employed to provide more general results. The obtained mathematical expressions of all the aforementioned performance metrics are validated using extensive Monte Carlo simulation results.

- The main contributions of Chapter 5 can be summarised as follows:
  - Derive the SINR of indoor and outdoor NOMA users to find exact OP expressions over a generalised $\kappa - \mu$ fading channel when the user's demand for data rates is dropped below certain QoS requirements.
  - With the aid of the Meijer G and Fox H functions, derive an exact analytical expression for EC. In addition, closed-form expressions are obtained for the throughput and EE of a two-user NOMA system under ideal and practical assumptions.

  - Evaluate the performance of downlink NOMA signals propagating through outdoor-to-indoor and outdoor-to-outdoor channels, where both channels are ranked according to their instantaneous fading coefficients.
  - Discuss the path-loss characteristics of the indoor and outdoor users, since NOMA users are classified according to the product of their distance-dependent path loss and channel fading gains.
  - Extend the system model to include the DF UAV-relay with HD mode and consider practical issues such as imperfect SIC (η) in all the derivations.
  - Validate the precision of the derived expressions using Monte Carlo simulations.

- The main contributions of Chapter 6 can be summarised as follows:
  - Study a NOMA Downlink system model with multiple users operating simultaneously in indoor and outdoor environments
  - Propose an effective algorithm that uses the streamlined simplex method (SSM) to improve the performance of the sum data rate performance for indoor-outdoor user pairing.
  - Propose a low complexity user pairing algorithm, named the least and most cost method (LMCM) and demonstrate its effectiveness for indoor-outdoor user pairing.
  - Apply the Max-Min optimisation method to obtain optimal power allocation that can maximise individual data and fairness rates of the indoor user.
  - Validated the performance of the proposed algorithms using extensive simulations.

- The main contributions of Chapter 7 can be summarised as follows:
  - Derive the SINR of multiple indoor users to find exact and asymptotic OP expressions over a generalised κ-μ fading channel when the user's data rate demand falls below certain QoS requirements.
  - Derive exact and asymptotic analytical expressions for the EC with the aid of the Fox H function and the Meijer G function. In addition, closed-form expressions are obtained for the throughput of a three-internal-user NOMA system under ideal assumptions.
  - Evaluate link performance and provide exact and asymptotic closed-form BER expressions using the M-QAM modulation technique.

- Discuss the quality of experience (QoE) of indoor NOMA users supported by an IRS.
- Evaluate the performance of NOMA downlink signals propagating through outdoor-to-indoor channels, where they are ranked based on their instantaneous fading coefficients, and discuss the path loss characteristics of indoor and outdoor users.
- Validate the accuracy of the derived expressions using Monte Carlo simulations.

1.5 Thesis Structure

The rest of this thesis is organised as follows.

- **Chapter** (2) provides theoretical background and overview of different areas covered in this thesis. It includes some of the fundamental knowledge of wireless channel models. This chapter also presents different types of cooperative wireless communication and explains the significant differences among them. In addition, a brief overview of different multiple access techniques applied through different generations of mobile communication is illustrated.
- **Chapter** (3) presents the literature review of NOMA and explains its fundamental concept including the multiplexing signals and successive interference cancellation (SIC) technique, particularly, for downlink communication networks. This chapter also presents the key differences between OMA and NOMA system.
- **Chapter** (4) focuses on analysing the system performance of DL-NOMA for the conventional scenarios. The closed-form expressions of outage probability (OP), ergodic capacity (EC), and bit error rate (BER) of the DL-NOMA system are obtained in different scenarios.
- **Chapter** (5) discusses an important scenario of propagating NOMA signals known as outdoor-to-indoor channels, where the attenuation factors are different from the known case of outdoor NOMA. In this chapter, an analytical framework is carried out for cooperative communication, which is done by a UAV-relay assisted with NOMA to enhance the system coverage. In particular, different closed expressions of system performance are attained with the aid of some generalised hypergeometric functions such as the Fox H function and Meijer G function.
- **Chapter** (6) examines different proposed algorithms for the user pairing issue of indoor-outdoor NOMA. It describes these algorithms in detail along with the

conventional user-pair method as a benchmark. It also presents the maximisation technique applied to indoor users to improve their fairness rates.

- **Chapter** (7) represents a study of IRS-based NOMA system, where the quality of service (QoS) and quality of experience (QoE) are investigated. Furthermore, different exact and asymptotic closed-form expressions for different performance metrics such as OP, BER, and EC have been provided. In addition, the mean score opinion (MSO) has been applied in this chapter to measure the QoE, where the web page size is considered as a performance metric.

- **Chapter** (8) provides the conclusion of this thesis and outlines the future extension works. This chapter is followed by a list of the main bibliography.

CHAPTER 2

Theoretical Backgrounds

2.1 Chapter Introduction

Wireless networks are being considered as one of the most significant and developed segment in the communication system over the past few decades. It grants a reliable, secure, and high-speed connectivity between two or more users through invisible links. In comparisons with the wired networks, the wireless communication is a preferable selection due to many reasons such as the effective reducing cost of the infrastructures. Early wireless communication networks applied the line of site (LOS) techniques to transmit the desired message by fundamentally using flash mirrors, smoke signals, and others. These classic patterns of transmitting data have been developed and transformed by telegraph networks and after that by telephone. In 1895, Macroni invented the first radio transmission on a distance of fewer than 18 miles, which declares the birth of the most powerful technology by that time, namely Radio communication. Recently, a large area was being covered with enhanced signal quality, less power consumption and small handsets design. However, the initial phase of wireless networks came with inadequate performance coupled with different challenges in security and cost issues. By contrast, the current generations of wireless communication have overcome most of these restrictions and provided numerous advanced solutions. It can be noticed that the most efficient segment of wireless communication is represented in the cellular networks, which bravely applies the concept of reducing transmitted signal power over the distance. Thus, it allows multi subscribers to reuse the same frequency over different locations in a suitable manner in order to reduce the interference among them while raising their amounts [1, 3].

On the other hand, due to the limited conditions of the radio wave environment, in which the connection between BS and users will be established, the obstacles in performing a noiseless channel with no interference becomes the core concern in the cellular systems. As a consequence, extensive research works have been carried out

to address these challenges and endured whenever the requirements get more complex. Moreover, by considering the prime sector in the cellular system, represented in the wireless channels among different nodes, attention should be paid to the channel impairments caused by noise, interference, fading, and others since they play a major role in designing a wireless communication system. Hence, the characteristics of the channel are randomly fluctuated due to the mobility of users. In addition to that, in the absence of any obstacles between the users, the channel can be characterized as a line of site (LOS) channel while in the presence of any obstacles, the channel can be known as a non-line of sight (NLOS). Therefore, the transmitted signals are manipulated by the effect of several factors such as path loss and shadowing. The path loss is caused by different reasons such as the dissipation of radiated power and the effect of the propagation channel. It is chiefly used to model the loss of transmitted signal between the transmitter and the receiver over a large distance. However, shadowing occurs when the transmitted signals are attenuated by any obstacle that can absorb, reflect, scatter, or even diffract them. The main difference between the path loss and the shadowing effect is mainly based on the distance. To illustrate, the Path loss is caused by a variation in the received signal over a long distance (100-1000)m while the shadowing occurs over a short distance (10-100)m. The variation in the received signals that occurred by path loss and shadowing effect are known as large scale propagation effects because it happens over large distances. However, the variations that formed over very short distances due to multipath fading is commonly referred to the small scale propagation effects. Figure 2.1 illustrates the impact of large and small scale propagation effects [1, 3].

2.2 Fading in Wireless Channels

Electromagnetic waves are radiated through different environments, where three fundamental phenomena can occur. Some of these main effects are known as reflection, diffraction and scattering, and they mostly appear in urban areas where there is an NLOS path. Since the radiated waves travel through different paths, the interactions between them exhibit multipath fading and reduce the strength of these signals due to the distance increments between the transmitter and the receiver. Reflection occurs when the transmitted signal hits buildings, solid surfaces, water or walls. Part of that signal could be absorbed and the other could be reflected based on the material's property of that reflector. Diffraction generally occurs when the transmitted signals are obstructed by the edges of a solid surface. The extra waves produced by the effect of these mechanisms are banded around the object or presence in space. Scattering exists when the travelled signals are propagated through a medium that has smaller dimensional objects such as street signs and lamp posts, etc.

The propagated signal travelled through different paths to the receiver undergoes

different impacts of changes known as fading. This transmitted signal might be reflected, diffracted, or scattered by different types of obstacles while travelling to the receiver side. Each path is considered to have different types of fading, attenuation, and delay. The combination of these paths is commonly known as multipath propagation. However, the received signals from different paths can be constructively or destructively added, which eventually causes rapid and random fluctuation in the amplitude of the received signal. Therefore, the fading can be identified by two major groups known as large scale fading and small scale fading. The large-scale propagation model has slow variations in the envelope of the signal, and it is used to predict the transmission coverage region, as well as to estimate the mean of the received signal over a large distance, (multi hundreds or thousands of meters), between the transmitter and receiver. However, the small-scale propagation model experiences significant fluctuations over the received signal due to multipath fading and occurs over very short distance and periods of time (in seconds). It is usually represented by statistical means and known as multipath channel effects, [1]. Hence, fig.2.1 briefly shows the types of fading phenomena.

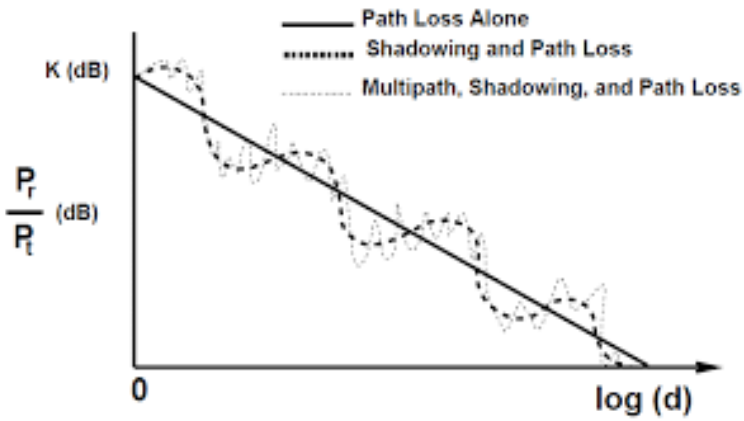

Fig. 2.1 large-scale (distance-dependent path loss and shadowing) and small-scale (fading) propagation effects, [1].

2.2.1 Large Scale Propagation Model

This phenomenon occurs when the transmitted signal is attenuated through a propagated path over a large distance, between the transmitter and the receiver, and shadowed by large objects such as buildings, mountains, trees, etc. The significant impact of large-scale fading on the received signal power can be evaluated by utilizing one of the following two models.

2.2.1.1 Log-Distance Path loss

In the presence of an unobstructed LOS channel, the common propagation model used to predict the received signal strength in such an environment is called the Free-space propagation model [1]. Because of the complex environmental conditions of the mobile radio system, the free space model is not accurate enough. Therefore, different path loss models are being developed to more accurate prediction in urban, rural, and indoor environments. These models are mainly based on analytical and empirical measurements. The average path loss of these models is defined as a function of distance by considering the path loss exponent (n). Thus, the distance dependent path loss model over significant distance can be given as follow [1].

$$PL_{(dB)}(d) = PL(d_0) + 10(n)\log\left(\frac{d}{d_0}\right) \tag{2.1}$$

or

$$PL_{(dB)}(d) \propto \left(\frac{d}{d_0}\right)^n \tag{2.2}$$

where n refers to the path loss exponent that indicates the increment rate between path loss and distance. d_0 is the close-in reference distance, and d is the transmitter-receiver separation distance. As a matter of fact, the value of the path loss exponent relies on the specification types of the propagation environments. To illustrate, when the path loss exponent is $(n = 2)$, the path of the transmitted signal is considered free of obstructions, which refers to a Free space environment. As long as the path loss exponent value is carefully selected based on the environment type, the path loss would be accurately estimated. However, it is very common that in the large coverage area, the reference distance d_0 is about (1 km) wheres in the small coverage area is less than (100 m), [3]. Thus, the path loss can be calculated through the Free space path loss model shown in equation (2.1) or by field measurements, where the reference distance is considered. Table 2.1 shows various values of path loss exponent obtained in different mobile radio environments. Path loss can be usually expressed in terms of a direct loss in dB. Therefore, the calculation of elements including the expected signal becomes straightforward. The equation below represents the path loss for a free space propagation model, where the propagation is done through air-to-air (A2A) channels.

$$PL_{(dB)}(d) = 20\log_{10}(d) + 20\log_{10}(f) + 32.45 \tag{2.3}$$

where d is the distance between the transmitter and the receiver, and f indicates the frequency.

Environment	Path loss exponent (n)
Free space	2
Urban area	2.7-3.5
shadowed urban area	3-5
indoor (LOS)	1.6-1.8
Obstructed in buildings	4-6
Obstructed in factories	2-3

Table 2.1 path loss exponent value in different propagation environments[1]

2.2.1.2 Log-Normal Shadowing

The log-normal shadowing occurs when the propagated signal is blocked in its path by large obstacles such as mountains, hills, or infrastructures. The most known model to address the shadowing fading is known as log-normal shadowing, which is empirically performed to describe the fluctuation in the received power in both outdoor and indoor scenarios. The log-normal distribution can be given as [6].

$$p(\psi) = \frac{\delta}{\sqrt{2\pi}\sigma_{\psi dB}\psi}\exp\left(-\frac{(10\log_{10}\psi - \mu_{\psi dB})^2}{2\sigma^2_{\psi dB}}\right), \tag{2.4}$$

where $\psi = \frac{P_t}{P_r}$ is the ratio of transmit-to-receive power. $\mu_{\psi dB}$ is the mean of $\psi(dB) = 10\log_{10}\psi$, and $\delta = \frac{10}{\ln 10}$.

2.2.2 Small-Scale Propagation Model

For small-scale fading, the received signal's strength fluctuates rapidly over very short distance and in a short period of time. There are two main categories of small fading based on the spread of multipath delay known as Flat fading and frequency selective fading. These multipath fading types depend on the propagation environment. Fig.2.2, briefly, explains these categories of small scale fading.

- **Flat Fading:** The received signal experiences flat fading when the coherence bandwidth of the mobile channel (Bc), which has a static gain and linear phase response, is much greater than the bandwidth of the transmitted signal (Bs) i.e., $Bc >> Bs$. The coherence bandwidth of the channel (Bc) indicates the time dispersion of the channel as

$$B_c \propto \frac{1}{\sigma_\tau}. \tag{2.5}$$

  where the root-mean-square (RMS) delay spread is defined as σ_τ. However, if the symbol period (Ts) is much larger than RMS delay spread σ_τ, i.e., $T_s >> \sigma_\tau$,

then the transmitted signal undergoes flat fading.

- **Frequency Selective Fading:** It is known as time dispersion fading since the bandwidth of the mobile channel (B_C) is smaller than the bandwidth of the transmitted signal (B_S), i.e., ($Bc << Bs$) or if the symbol period (T_S) is less than the delay spread σ_τ, i.e., $T_s << \sigma_\tau$,. In this case, the received signal undergoes the frequency selective fading due to symbol time dispersion that leads to Inter Symbol Interference (ISI) impact. It should be noted that frequency selective fading is much more difficult to be modulated than flat fading [3].

On the other hand, there are two different categories of fading based on doppler scattering: High-speed fading and slow fading. These doppler diffusion fading types depend on the speed of the receiver relative to the transmitter. These types of doppler scattering based fading are given as follows.

- **Fast Fading:** It occurs when the symbol period (T_S) is larger than the coherence time of the channel (T_C) , which is the time period when the channel impulse is constant, i.e., ($T_S >> T_C$). The frequency dispersion in fast fading can be described as
$$T_C \propto \frac{1}{B_D}. \tag{2.6}$$
However, when the doppler spread (B_D) is larger than the signal bandwidth (B_S), then the fast-fading occurs, where the signal becomes distorted.

- **Slow Fading:** In contrast with fast fading, the slow fading is formed when the doppler spread (B_D) is smaller than the signal bandwidth (B_S), i.e., ($B_D << B_S$) and the symbol period (T_S) is less than the coherence time of the channel (T_C) , i.e., ($T_S << T_C$).

2.3 Composite Channel Fading Models

The most significant common models that has been used to characterize the received envelope of the flat fading signal are known as simple models, such as Rayleigh and Rician model, and complex generalized models such as Nakagami-m , Weibull, $\alpha - \mu$, $\kappa - \mu$ fading models, etc.

2.3.1 The α-μ fading model

The α-μ distribution is a small scale fading model that mainly characterizes the impact of two vital parameters known as the non-linearity α, and the number of multipath

clusters μ. The model uses μ to describe the number of clusters where each of which consists of a number of multipath signal components propagate in a non-homogeneous environment. Each cluster has different scattered waves with random phases, but similar time delay. These clusters are expected to exhibit identical powers of the scattered waves. As a result, the envelope is produced by a nonlinear function of the modulus of the sum of the multipath components. Generally speaking, increasing the value of μ for a fixed α implies that the fading becomes less severe and the channel envelope tends to be centered around 1. On the contrary, reducing μ leads to severe fading as the channel envelope will be condensed near the 0 region. Fixing μ and changing α results generally in the same behavior [7].

By changing μ and α, a wide range of fading characteristics can be obtained. For example, the Weibull distribution can be attained by setting $\mu = 1$, and $\alpha/2$ becomes the fading parameter. Rayleigh fading can be obtained by setting $\{\alpha = 2, \mu = 1\}$. The negative exponential distributions can be obtained using $\{\alpha = 1, \mu = 1\}$. Nakagami-m is obtained by setting $\alpha = 2$, and μ becomes the fading parameter. The one-sided Gaussian distributions can be obtained by setting $\{\alpha = 2, \mu = 1/2\}$, [7].

Moreover, the probability density function (PDF) of the instantaneous SNR, γ, is given as [8],

$$f_\gamma(\gamma) = \frac{\alpha\mu^\mu\gamma^{\alpha\mu/2-1}}{2\Gamma(\mu)\tilde{\gamma}^{\alpha\mu/2}} \exp\left(-\mu\left(\frac{\gamma}{\tilde{\gamma}}\right)^{\alpha/2}\right) \tag{2.7}$$

where $\tilde{\gamma}$ is the average power, which is given in Table I, as [8]. However, the cumulative distribution function (CDF) of the instantaneous SNR is obtained by integrating the PDF in (2.7) and using property in [9, p. 3.381.8] to solve the integration. Therefore, the CDF can be written as

$$F_\gamma(\gamma) = \int_0^\gamma f_\gamma(g)dg = \frac{\mathbb{G}(\gamma)}{\Gamma(\mu)} \tag{2.8}$$

where $\mathbb{G}(\gamma) \triangleq \gamma_{inc}\left(\mu, \mu\left(\frac{\gamma}{\tilde{\gamma}}\right)^{\frac{\alpha}{2}}\right)$, $\Gamma(.)$ and γ_{inc} indicate the gamma function and the incomplete gamma function which are also defined in [9].

2.3.2 The κ-μ fading model

The κ-μ distribution represents the small-scale variations of the fading signals in a LOS environment. The signal of κ-μ fading constitutes different clusters ($\mu > 0$), of multipath and scattered waves of identical power, as well as a dominant arbitrary power component constructed inside each cluster. Moreover, the rate between these total power components is indicated as $(\kappa > 0)$. The generalised κ-μ fading model constitutes other well-known vital distributions as special cases, such as the One-Sided Gaussian ($\kappa \to 0$, $\mu = 0.5$), the Rayleigh ($\kappa \to 0$, $\mu = 1$), the Rice (Nakagami-n)

($\kappa = K$, $\mu = 1$), and the Nakagami-m ($\kappa \to 0$, $\mu = m$). Furthermore, the PDF of the instantaneous SNR of the κ-μ fading channel is given by [10],

$$f_\gamma(\gamma) = \frac{\mu(1+\kappa)^{\left(\frac{\mu+1}{2}\right)}\gamma^{\left(\frac{\mu-1}{2}\right)}}{\kappa^{\left(\frac{\mu-1}{2}\right)}\mathrm{e}^{(\mu\kappa)}\bar{\gamma}^{\left(\frac{\mu+1}{2}\right)}}\exp\left(\frac{-\mu(1+\kappa)\gamma}{\bar{\gamma}}\right) \times \mathrm{I}_{\mu-1}\left(2\mu\sqrt{\frac{\kappa(1+\kappa)\gamma}{\bar{\gamma}}}\right) \quad (2.9)$$

where the instantaneous SNR is given as $\gamma \triangleq \rho|h|^2 = \frac{\mathcal{P}}{\sigma^2}|h|^2$, and ρ represents the transmitted SNR, h indicates the channel frequency response, $\mathcal{P}$ is the transmit power. In addition, the average SNR can be demonstrated as $\bar{\gamma} \triangleq \mathbb{E}[\gamma] = \Omega\frac{\mathcal{P}}{\sigma^2}$ with $\mathbb{E}[.]$ denoting expectation and Ω defines the mean power of h, i.e, $\mathbb{E}|\Omega| = [|h|^2]$. $\mathrm{I}_v(.)$ is the modified Bessel function of the first kind. To produce a more tractable analysis, (2.9) is simplified to a further equivalent representation, precisely for $\mathrm{I}_v(.)$, by employing the series representation of $\mathrm{I}_v(.)$ given in [9, p. 8.445]. Therefore, (2.9) is rewritten as

$$f_\gamma(\gamma) = \frac{1}{\mathrm{e}^{(\mu\kappa)}}\sum_{n=0}^{\infty}\frac{\mu^{2n+\mu}\,\kappa^n\,(1+\kappa)^{n+\mu}}{n!\,\Gamma(n+\mu)\,\bar{\gamma}^{(n+\mu)}} \times \gamma^{(n+\mu-1)}\,\exp\left(-\frac{\gamma\mu(1+\kappa)}{\bar{\gamma}}\right). \quad (2.10)$$

The corresponding cumulative distribution function (CDF) of the κ-μ fading channel is given as [10],

$$F_\gamma(\gamma) = 1 - \mathcal{Q}_\mu\left[\sqrt{2\kappa\mu}\,,\ \sqrt{2\left((1+\kappa)\,\mu\gamma/\bar{\gamma}\right.}\right] \quad (2.11)$$

where $\mathcal{Q}_{(.)}$ is the generalised Marcum-Q function. Therefore, an alternative representation of (2.11) is obtained by integrating (2.10) and recalling the identity of [9, p. 3.381.3]. Therefore, the corresponding CDF is given as

$$F_\gamma(\gamma) = \frac{1}{\mathrm{e}^{(\mu\kappa)}}\sum_{n=0}^{\infty}\frac{(\kappa\mu)^n}{n!\,\Gamma(n+\mu)}\gamma_{inc}\left(n+\mu\,,\ \frac{\mu(1+\kappa)\gamma}{\bar{\gamma}}\right). \quad (2.12)$$

Furthermore, the PDF of a sum of N independent and identically distributed (i.i.d.) $\kappa - \mu$ random variables (RV) is given as in [11].

$$f_\gamma(\gamma) = \frac{1}{\mathrm{e}^{(N\mu\kappa)}}\sum_{c=0}^{\infty}\frac{(N\mu)^{2c+N\mu}\,\kappa^c\,(1+\kappa)^{c+N\mu}}{c!\,\Gamma(c+N\mu)\,\bar{\gamma}^{(c+N\mu)}} \times \gamma^{(c+N\mu-1)}\,\exp\left(-\frac{\mathrm{N}\mu(1+\kappa)\gamma}{\bar{\gamma}}\right). \quad (2.13)$$

However, the related cumulative density function (CDF) of the sum of the fading channels N of $\kappa - \mu$ is achieved by integrating the above PDF and is given in the form of the Fox H function with the aid of [12, pp. 8.4.3.1, 8.4.6.5] and [13, p. 6.2.8]. Thus,

$$F_\gamma(\gamma) = \frac{1}{\mathrm{e}^{(N\mu\kappa)}} \sum_{c=0}^{\infty} \frac{(N\kappa\mu)^c}{c!\,\Gamma(c+N\mu)} \times \mathrm{H}_{1,2}^{1,1}\left[\frac{N\mu(1+\kappa)\gamma}{\bar{\gamma}}\middle| \begin{matrix}(1,1)\\(c+N\mu,1),(0,1)\end{matrix}\right]. \tag{2.14}$$

2.4 Multiple Access Techniques

In the scenario of multi-users, the radio spectrum resources are allocated in an orthogonal or non-orthogonal manner among several users. Multiple access is a technology that allows multiple mobile users to share the spectrum assigned more effectively. It is applied in different multi-user channel schemes: Downlink channel, which is called the broadcast channel, and uplink channel, which is also known as the multiple access channel. The key major factor of both schemes is mainly related to efficient signaling allocation in dedicated channels that ensure no interruption in data transmission. This way can be achieved from the signal space domain of the system, such as time division, frequency division, code division, or any combination of them. In general, multiple-access techniques split the entire space domain into channels and then allow different users to allocate them. The most common multiple access techniques are Time Division Multiple Access (TDMA), Frequency Division Multiple Access (FDMA), and Code Division Multiple Access (CDMA).

In the early stage of mobile communication deployment, the FDMA technique, where transmission is continuous over time, was used in a way that multiple users are assigned with different frequency channels. The channel in FDMA has guard bands to mitigate interference and Doppler effects. Moreover, the channel may not undergo frequency-selective fading if the channel is sufficiently narrow band. However, when the system dimensions are divided into non-overlapping channels and each user is assigned to a specific time slot, then TDMA is performed. By doing so, the inter-symbol interference (ISI) is presented in TDMA due to the use of a wide-band system. Therefore, a digital transmission scheme is required because continuous transmission is no longer available, reducing overhead functions such as channel estimation. The main advantage of TDMA is simply assigning a single user to different channels with multiple time slots. However, the drawbacks of TDMA are synchronisations among two users in the uplink channel and the channel characteristics changing over different cycles of time slots.

On the other hand, CDMA emerges with a different technique, where each user is assigned a different unique spreading code and allowed to share the same resource (i.e., time or frequency) simultaneously. On the receiver side, the spread codes are used

to separate multiple users. In the downlink, orthogonal spreading codes are utilised, such as Walsh-Hadamard codes, while in the uplink non-orthogonal spreading codes are applied. The major advantage of non-orthogonal CDMA is represented in unlimited available channels that can be obtained by different users but with the expense of mutual interference between users. Alternatively, OFDMA can be attained by grouping the direct sequence spread spectrum with FDMA to divide the bandwidth into sub-bands to improve the frequency diversity. Thus, different users are assigned to different sub-bands, including their signal spread, so the interference is reduced. However, to expose the limitations of user's number and channel access, another powerful technique that can sufficiently contribute to enhancing the system's performance is essentially needed. Recently, NOMA has become the most powerful multiple access technique that can support the next generation. Table 2.2 shows a brief summery of some advantages and disadvantages among them.

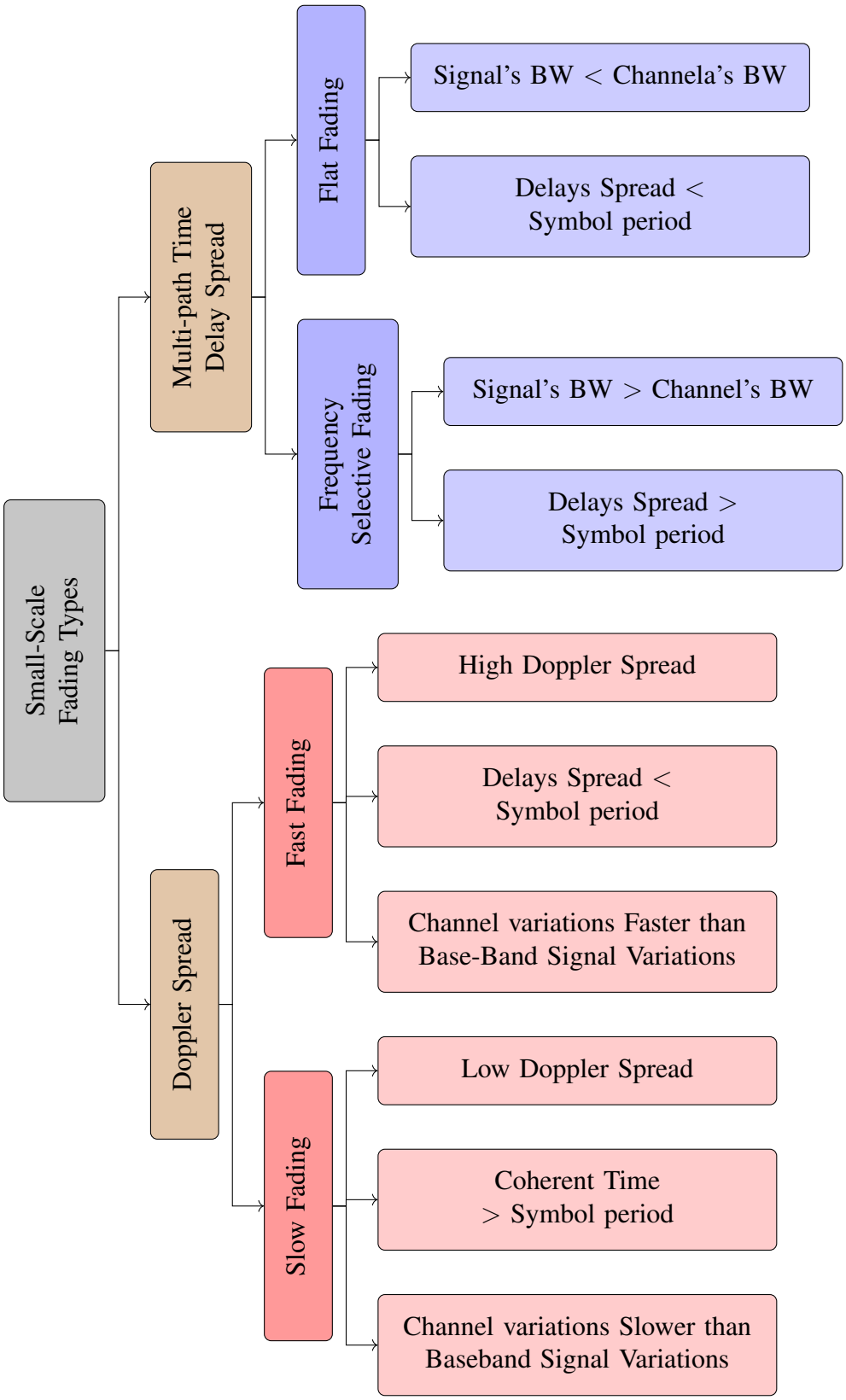

Fig. 2.2 Cooperative Relaying Techniques

Scheme		Pros	Cons
OMA	FDMA	- No limitations on base-band or modulation. - Less interference due to guard band - No need for time networking	- Cross-talk issue. -Insufficient use of bandwidth -Complexity of band pass filters.
	TDMA	- No interference when transmission is simultaneous - Cost-effective technology - No frequency guard needed	- Hand off complexity - Less number of users - Insufficient use of bandwidth
	CDMA	- Capacity and security improvements - Higher number of shared users than FDMA/TDMA. - More reliability	- System complexity - Necessity of guard band and time. - QoS decreases by the increase of users.
	OFDMA	- Less inter-symbol interference (ISI) - Robust and reliable - Frequency diversity	- Insufficient use of spectrum. - High sensitivity to noise phase - Co-channel interference complexity
NOMA	P-NOMA	- Sufficient utilisation of spectrum - Serving multiple users simultaneously - No frequency time guards	- High interference - Receiver complexity - Energy consumption
	C-NOMA	- Lower symbol interference than CDMA - Adequate receiver complexity	- Higher ISI compared with OFDMA

Table 2.2 Summery of the main multiple access technologies

2.5 Cooperative Wireless Communication

Cooperative Wireless communication is applied according to the aim of improving the diversity between a source and a destination. It conveys the information effectively between two different nodes in order to improve the achievable data rate with less energy consumption. The simplest form of cooperative wireless communication requires three different nodes known as source, relay, and destination along with wireless channels. The information can be transferred among these nodes by at least two different and independent relay channels in a cooperative paradigm. The signals passed through the relay node is processed by different cooperative communication protocols. The main classes of these protocols involve fixed and adaptive relaying techniques as shown in fig. 2.3.

2.5.1 Relaying Protocols

There are two main fundamental classes of cooperative relaying protocols known as fixed relaying and adaptive relaying. In the case of fixed relaying, channel resources between the source and destination are allocated deterministically. In addition, the fixed relay strategy has four different protocols known as amplify-and-forward (AF), decode-and-forward (DF), compress-and-forward (CF) and coded cooperation (CC) techniques. These fixed protocols mentioned above can work in a fixed manner. However, the adaptive relaying technique, which involves selective and incremental relaying protocols, has built-in adaptability to set handoff by itself, as in low SNR or severe channel fading. Therefore, fixed and adaptive relaying techniques can be described, respectively, as follows.

- **The Fixed Relaying Protocols**

  1. **The Amplify-and-Forward (AF) Relay:**

     It is considered a transparent transmission mechanism since it amplifies the received signal and forwards it to the destination without a decoding process, which tends to work as the traditional repeater [14]. In the case of a fixed amplify-and-forward (AF) relay, the source communicates with the destination in two different time slots through different independent cooperative channels. First, the relay receives the transmitted signal from the source and multiplies it by amplifying the gain. Afterwards, it resends the amplified signal to the destination in the second time slot. In case the destination observes two independent received signals, i.e. through cooperative

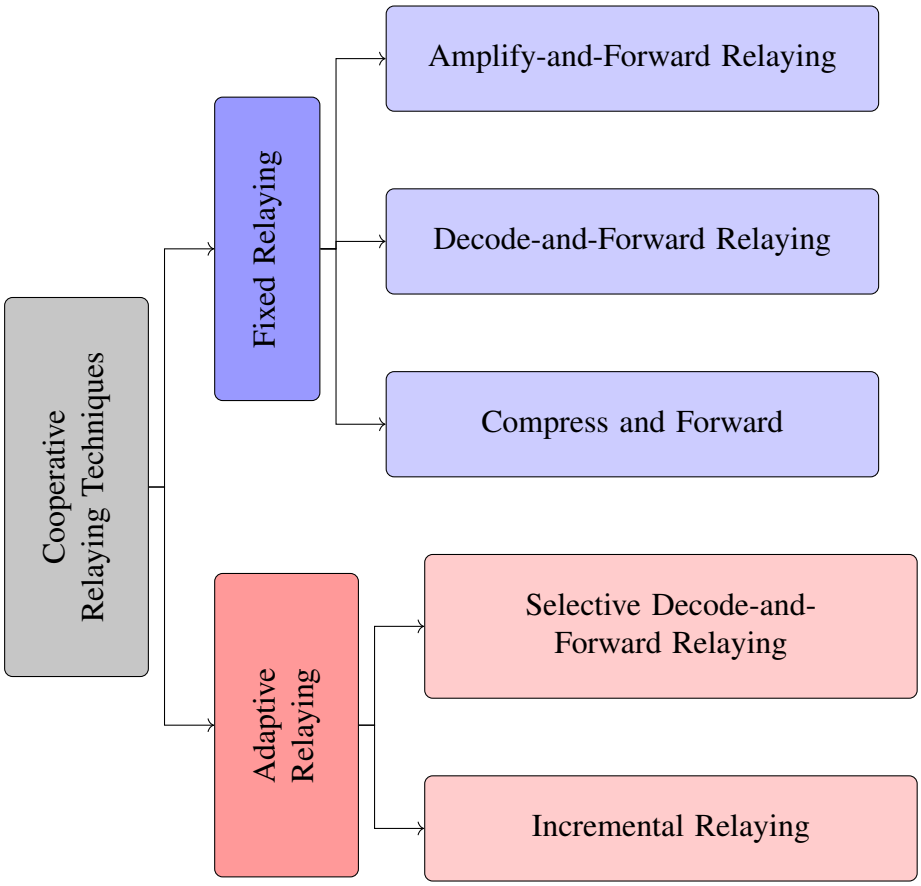

Fig. 2.3 Cooperative Relaying Techniques

and direct channels, then it can combine them to attain a maximum diversity order. Moreover, the main advantage of AF is that it simplifies hardware complexity since no decoding process is required. However, the main disadvantage of AF is that it amplifies residual noise, which degrades the performance of the system.

2. **The Decode-and-Forward (DF) Relay:**

   It is described as a regenerative transmission protocol since it works in a fixed manner of relaying. In contrast to AF, it rationally decodes the received signal transmitted by the source in the first time slot, and then re-encodes and forwards it to the destination in the second time slot. Finally, the destination can combine the received signals transmitted through direct and cooperative links using one of the diversity combining techniques. Furthermore, the DF relay has the ability to eliminate the residual noise in the second time slot when the decoding process is applied. However, it has a high computational delay and complex hardware, as well as it may introduce a propagation error. This error of unsuccessful decoding of the received signal occurs when the channel conditions between the source and the relay are very poor.

3. **The Compress-and-Forward (CF) Relay:**

   It is also considered a regenerative transmission protocol. The main concept of CF is that it only compresses the received signal using a Wyner-Ziv code and forwards it to the destination without any decoding process. The destination receives two different signals, one directly from the source, and the other is the compressed signal sent by the relay. Then, it correlates these received signals and decodes the originally transmitted signal. As a consequence, CF introduces a significant improvement of system performance and outperforms other techniques such as AF and DF, precisely when the distance between the relay and the destination is low.

2.5.2 Half and Full Duplex Modes

The way that cooperative communication is done through a relay can be described either by half-duplex (HD) communication or full-duplex (FD) communication. In HD mode, communication is done in a fixed manner, so the relay has no ability to connect to the other nodes in a simultaneous approach. Furthermore, the source-relay channel and the relay-destination channel are considered orthogonal in the time domain or in the frequency domain. This provides more reliability but with less efficient use of bandwidth as more time slots are introduced. Unlike HD mode, FD mode can send and receive information simultaneously, which mainly improves the spectral efficiency

of the system by reducing the consumption of time slots. This approach can improve the reliability and spectral efficiency of the system, but with high self-interference and implementation complexity. This high level of self-interference is caused by the simultaneous transmission and reception of the signals at the relay. Therefore, the demand for self-interference cancellation in the FD mode is highly needed [14].

2.6 Chapter Summary

This chapter provides the relevant background theory needed for this thesis. a brief history of wireless networks and its revolution in recent decades are introduced. After that, some challenges that restrict the benefits of wireless communication since the medium of connection is no longer presented through wire links is also discussed. Nevertheless, in wireless communication, radio waves have become the main carrier of multiple signals. Therefore, a radio channel model that considers both large- and small-scale propagation effects is investigated. Therefore, some of these models apply throughout the simulation work in this thesis. In addition, this chapter also presents different types of cooperative wireless communication and explains the significant differences among them. Finally, an overview of different multiple access techniques applied through the different generations of mobile communication is illustrated.

CHAPTER 3

Literature Review and Fundamentals of NOMA

3.1 Chapter Introduction

Over the past few decades, the revolution of wireless communication has developed rapidly from generation to generation in different terms of channel access technology. To illustrate, the predominant techniques that have been introduced in the first generation (1G) of mobile communication until the current fourth generation (4G) are known as FDMA, TDMA, CDMA, and OFDMA, respectively. Each technique has gained some features that can outperform others, which are mainly represented in system capacity, data rate, power consumption, etc. These technologies are characterised into three different domains: time, frequency, and code. The access method to the channel among different users can be well organised in orthogonal scheme by either assigning a user with a time slot such as TDMA or with a particular frequency such as FDMA or with a code according to CDMA or a combination of using all previous resources such as OFDMA. The advanced requirements of previous generations have been met by OFDMA, where resource blocks are divided into orthogonal variant sub-channels to increase the number of assigned users,[3] However, in the next generation of mobile communication, termed 5G and beyond and beyond, the roof of potential requirements is dramatically increased to massive expectations that lead to demands to improve spectral efficiency, reduce latency, increase data rate, increase connectivity, and improve energy efficiency.

Recently, a large number of researchers have been investigating a new radio access technology to overcome the aforementioned obstacles and fulfil the promising requirements of 5G and beyond. Therefore, non-orthogonal The multiple access technique has been proposed to be a multiple access candidate for 5G and beyond and beyond since it copes with such requirements. Yet, channel multiple access technologies can be divided

into two main categories: orthogonal multiple access (OMA), such as OFDMA, or non-orthogonal multiple access, such as NOMA. In OMA, an individual user can access the channel using orthogonal resources in the frequency, time, or code domain. This kind of scheme advocates reducing the interference among users but with a limited number of supported users. In contrast, in the NOMA scheme, different users can share the same resources simultaneously, but they are variants in new domains called the power domain or code domain NOMA. The potential sequence of this scheme represents in the user suffering from a substantial amount of interference, so the interference management should be carefully considered in the new radio access technology. Generally, NOMA is represented in two different domains, in the power and code domains. In power domain NOMA, the superposition coding is performed fully on the transmitter side, while successive interference cancellation (SIC) is applied on the receiver side. In the NOMA code domain, users are assigned different codes instead of power and multiplexed over the same resources with high complexity. However, the power domain is much less complex than the code domain because it does not require additional bandwidth as the code domain. Subsequently, It is intended to concentrate heavily on the power domain of NOMA in this thesis [15].

3.2 Literature Review

Sophisticated multiple access techniques have been recognised as one of the most developed aspects over successive generations in wireless communication, [16]. Historical improvements in wireless communication, in particular, in terms of multiple access (MA), have emerged over the past few decades. For example, in the first generation of mobile communication (1G), digital control signaling was used along with FDMA, which was imposed on analogue frequency modulation. In the second generation (2G), TDMA was introduced and used [17]. In the third generation (3G), CDMA, which was proposed by Qualcomm, has become the dominant multiple access technique at that time [18]. To overcome the limitations of the aforementioned techniques, OFDM has been adopted for the fourth generation (4G), [17]. In general, a single user is allowed to be supported by the same frequency and time resource block (RB) in FDMA, TDMA, and OFDMA. Unlike orthogonal multiple access techniques, CDMA with the aid of multiple unique codes, different users can be served within the same resource block (RB). On the other hand, several investigations have been conducted towards the application of NOMA in long-term evolution LTE, 5G and beyond and 6G and beyond networks. The authors in [19], aim to determine appropriate techniques to mitigate the interference caused by multicast NOMA by deep exploring the opportunities and challenges of NOMA in multicast networks. Another investigation of NOMA has occurred in a multi-cell downlink phase by adapting a Coordinated Multipoint (CoMP) transmis-

sion pattern that considered a distributed power allocation scheme in each cell [20]. As a further advance, a substantial number of surveys have been published on the contributions and recent studies of NOMA on different issues such as NOMA in the power domain, the performance of NOMA and OMA, uplink and downlink NOMA in single cell cellular systems, and other issues [21, 22].

NOMA is categorised into two main types known as the NOMA power domain and the NOMA code domain. In [23, 24], the authors explained in detail the fundamental concepts of NOMA Power Domain NOMA. In contrast to the current access domain, as in OMA, a new domain has emerged known as the power domain, which is considered a baseline for NOMA. In this particular domain, multiple users can be allowed to share the same resources, but with a different amount of power. Performing superposition coding (SC) on the transmitter side and successive interference cancellation (SIC) on the receiver side are the main fundamental concepts that are applied in the NOMA power domain NOMA. According to information theory, NOMA optimally achieves the capacity region of the downlink broadcast channel in contrast to OMA, [25]. Different aspects of important issues in the NOMA power domain, such as signalling overhead, multiuser power allocation, error propagation in SIC and user mobility, were studied [24]. NOMA is also being investigated in the MIMO system to obtain an additional enhancement of spectral efficiency by comparing the output performance between MIMO-NOMA and MIMO-OMA in [26–30]. Furthermore, the system-level performance of NOMA was analysed at the power domain, and the simulation shows the result of the data rate for both the edge cell user and the centre cell user, as well as the fairness for both in [4, 31–33].

On the other hand, NOMA for the code domain performs the multiplexing approach in the code domain. Code domain NOMA has some similarities to CDMA in certain points. CDMA allows multiple users to share the same available resource block (frequency/time) but with different unique spreading codes. By contrast, the major difference between both techniques is that code domain NOMA applies a user-specific spreading sequence that is limited to either a non-orthogonal cross-correlation sequence or spare sequence. This scheme can be divided into three main classes known as low density spread CDMA (LDS-CDMA) [34], spare code multiple access (SCMA) [35], and OFDM based on low density spread (LDS-OFDM) [36]. Furthermore, a large volume of research studied the potential solutions of NOMA in different terms of performance challenges. For example, in [37], the path loss performance of NOMA is being evaluated in two different cases. Firstly, when each user has allocated a specifically targeted data rate, then the quality of service (QoS) of each user can be measured by calculating the outage probability. In addition, when the user rate is totally based on the channel quality, the ergodic sum rate can estimate the NOMA performance.

Other research studies have been carried out on the cooperative NOMA in order

to enhance the efficiency of the system in terms of capacity and reliability. [38] discusses the fundamental concept of the cooperative NOMA scheme, which assists users with poor channel quality by forcing users with good channel quality to act as relays to decode the signals for them. In cooperative NOMA, the available information in NOMA network is completely attained. The authors in [39] discovered that cooperative NOMA scheme performs better than non-cooperative scheme under slow fading link. Furthermore, another cooperative scheme between different BS's within different cells has been investigated by the authors in [40]. In general, NOMA cooperative system can operate in two different modes called NOMA relay channels and the NOMA multiple-relay channels. Several research studies have shown the significant of applying relay in a wireless network to reduce the effects of fading and shadowing on the transmitted signals. In [38] Ding *et al.* proposed a cooperative NOMA scheme where the users with best channel gains work as relays. This leads to the reinforcement of transmission efficiency with the users with less channel gains. The results indicate that users with the channel privileges have the ability to decode other users signals by applying the successive detection technique. On the other hand, NOMA with multiple-relay channel has been well investigated in the literature. In [41], Mohamad *et al.* proposed a multi-nodes that include multiple users that aimed to contact with other nodes via multiple relays. They analysed the outage achievable rate for multiple relay channels.

It has been shown that NOMA is compatible with other different advanced technologies that can fulfill the requirements of 5G, 6G and beyond such as machine-to-machine (M2M), intelligent reflecting surface (IRS), internet of things (IoT), and other recent technologies. For instance, NOMA transmission system can be applied with machine-to-machine (M2M) communication. In [42], Zhang *et al.* proposed a cooperative NOMA network with full-duplex (FD) communication mode, where the BS performs NOMA to serve multiple users. The authors proposed to apply FD mode to improve the outage performance of the less channel gain users. On the other hand, NOMA has been applied for massive connectivity of Narrow-Band-IoT to support machine-to-machine (M2M) networks. In [43], the authors proposed NOMA scheme with user clustering for an NB-IoT system, where M2M devices are allocated to different orders within NOMA clusters to allow transmission over the same frequency resource.

3.3 Comparison between OMA and NOMA system

NOMA is a strong candidate for 5G and beyond, as it provides a significant set of features over OMA and meets the 5G and beyond requirements. To distinguish NOMA from conventional OMA scheme, several features and drawbacks of both schemes are listed here.

- **Throughput and spectral efficiency:**
  In the NOMA system, a similar frequency resource is allocated to different users with different channel conditions. It significantly improves the spectral efficiency even though the interference is quite large, but it can be resolved by the SIC technique. However, in OMA, a selected frequency/time resource is allocated to each user in orthogonal base. Thus, the spectral efficiency and throughput are clearly degraded [15].

- **Massive Connectivity:**
  one of the remarkable features of NOMA has the ability to advocate a massive number of user or device connections simultaneously due to the non-orthogonal property which the classical scheme of OMA does not have [44].

- **User Fairness and Low Latency:**

  In the traditional OMA scheme, signaling overhead and transmission latency are recognised as higher than NOMA as they are mainly based on access grant requests that take approximately 15.5 ms before data transmission, [45]. However, in Uplink NOMA, there is access to grant free transmission which helps in decreasing the amount of latency and signalling overhead. For example, in Uplink SCMA, predefined resources, such as codebooks or pilots, can significantly provide grant-free multiple access. It should be noted that the SIC process may experience an additional delay that restricts the decoding speed [45]. On the other hand, the scheduling of users in OMA is mainly related to channel conditions, so users with good channel conditions have the initial priority over those who have bad channel conditions. This approach cannot exist in 5G and beyond where massive connections are highly needed. Therefore, NOMA overcomes OMA by serving multiple users with different scenarios of channel conditions at the same time [44].

- **Compatibility, complexity, and signal processing:**

  From a theoretical point of view, NOMA has the ability to exist together with current OMA techniques in harmony due to its new domain features. On the other hand, NOMA appears to have a less complex design than other techniques such as PDMA, SDMA, MUSA, [44]. Ultimately, the inability and limited performance of OMA encourage many researchers to discover NOMA to meet the promising requirements of 5G and beyond. However, as NOMA becomes a potential grant solution for the next generation, it also has different drawbacks that could limit its overall performance. To further elaborate, the receiver complexity in the NOMA scheme is a sensitive issue that must be considered in future research. Performing SIC over a large number of users on the receiver side may produce extra latency

and complexity in decoding users' signals. The probability of gaining errors in successive decoding may be potentially increased by errors produced during the uncorrected decoding process. The other limitation of NOMA is represented in channel feedback overhead Channel State Information (CSI).

- **Energy Efficiency (EE):** The potential expectations of 5G and beyond networks include 10 times higher energy efficiency than 4G networks. Energy efficiency is defined as the sum data rate over the total consumed power of the circuit. Therefore, NOMA can offer higher energy efficiency than OMA since it provides high data rate. In addition, NOMA system effectively utilises the available resource allocation by allocating different users with different amount of power based on their channel conditions. This leads to highly effective energy consumption. However, in OMA, there is some wasting energy due to the incompetent utilisation of the available resource allocation among users.

Table (3.1) represents some of the key differences between OMA and NOMA system.

Scheme	OMA	NOMA
Pros	low inter-cell Interference	Sufficient use of Spectrum
	Low Receiver complexity	Low Latency
	Less Energy Consumption	Unlimited served user
Cons	Insufficient use of Spectrum	High inter-cell Interference
	High Latency	High Receiver complexity
	Limited served users	High Energy Consumption

Table 3.1 Comparison Between OMA and NOMA.

Figs. 3.1 and 3.2 show the comparison between NOMA and OMA in terms of the upper bound capacity regions of the downlink scenario. For analysis purposes, the channel is considered asymmetric to show the difference in received SNR for both users, and it is assumed that the channel gain of the cell edge user (U_1) is less than the channel gain of the cell centre user (U_2). In both figures, it can be noticed that the capacity of the upper bound of NOMA is outside the region of OMA, which means that the NOMA scheme can obtain a better performance gain than OMA. Fig. 3.1 shows the feasible rate regions $R1$ and $R2$ for NOMA and OFDMA, respectively. As demonstrated in fig. 3.1, NOMA produces greater rate pairings than OFDMA, where the rates are equal to the single user capacities, disregarding the corners. Therefore, when fairness is set to high, both users exhibit 1.6 bps/Hz throughput with both multiple-access techniques. However, when fairness is less, both total capacity and individual throughput increase with

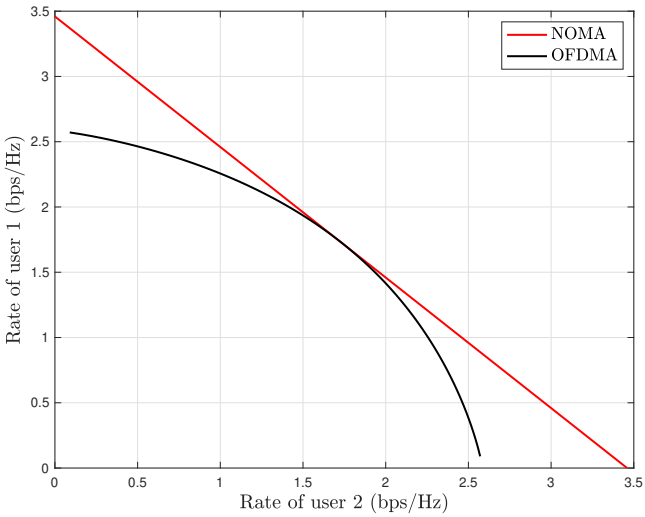

Fig. 3.1 Rate of two users with NOMA and OFDMA, SNR of ($U_1 = 10$ dB and $U_2 = 10$ dB).

NOMA. On the other hand, fig. 3.2 plots rate pairings, where the channel is asymmetric, i.e. ($U_1 = 20$ dB, $U_2 = 0$ dB). NOMA delivers substantially higher rate pairings than OFDMA, especially for the distant user, U_1. As a consequence, NOMA is considered the most powerful candidate for the next generation, since it obtains a higher spectral efficiency [21, 46].

3.4 Basic Concept of NOMA

3.4.1 Code Domain NOMA

Code domain NOMA is motivated by uplink CDMA and can be divided into different techniques. For instance, low-density spreading CDMA (LDS-CDMA), which is used to mitigate the impact of interference in a basic CDMA. In addition, another class of C-NOMA is called low-density spreading-based OFDM (LDS- OFDM), where the transmitted message is spread and transmitted on a particular set of subcarriers, then an algorithm called Message-Passing Algorithm (MPA) is performed at the receiver to decode multi-user signals. It is also a combined technique of SCMA and LDS-CDMA.Finally, another technique called Sparse Code Multiple Access (SCMA) is considered a new domain of C-NOMA since it improves the system with low complexity.[34]

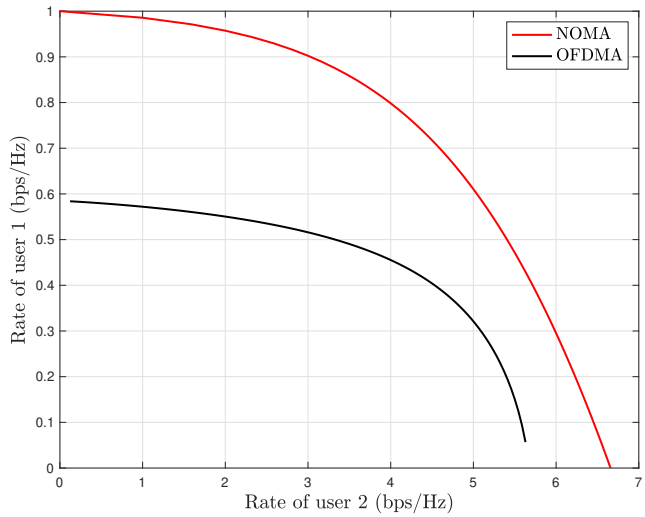

Fig. 3.2 Rate of two users with NOMA and OFDMA, SNR of ($U_1 = 20$ dB and $U_2 = 0$ dB).

3.4.2 Power Domain NOMA

The fundamental concept of NOMA in the power domain (PD-NOMA) is defined, as different users will be assigned different amounts of power depending on their channel conditions. Moreover, a significant portion of power will be given to the far user who has a poor channel condition, while the near user who has the best channel condition will be assigned with a smaller amount of power. It is mainly designed as the transmitter side performs SC, where the receiver side implements SIC. In the case of two users with different channel conditions, the near user treats the far user's signal as interference, so it first operates the SIC to cancel the interference and then decodes its signal. However, the far user treats the near-user's signal as noise and then decodes its signal without performing SIC.

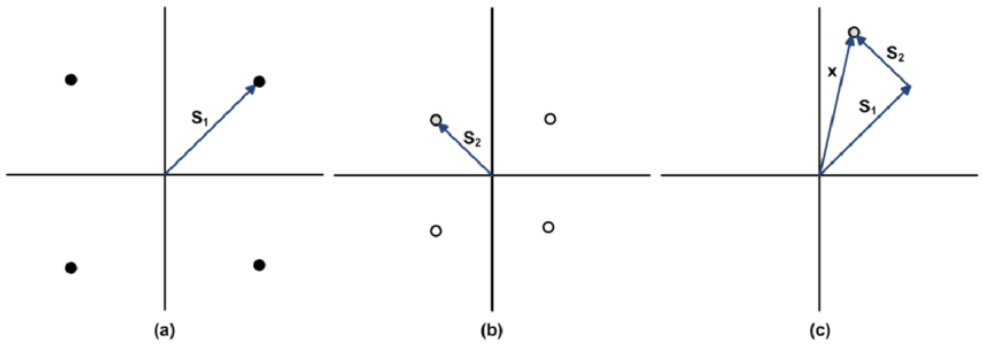

Fig. 3.3 SC encoding : (a) first user's signal constellation (s_1) (b) second user's signal constellation (s_2) (c) superimposed signal constellation, [21].

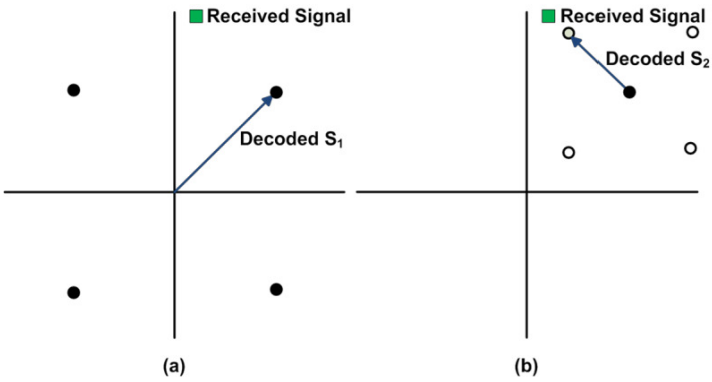

Fig. 3.4 SC decoding: (a) decoding the second user's signal (b) decoding the first user's signal, [21].

3.4.2.1 Superposition Coding (SC)

The key element that allows simultaneous communication between a single source and multiple receivers is known as superposition coding (SC). Significantly, it improves the spectral efficiency by multiplexing all transmitted and modulated signals from different users in the power domain. Fig. 3.3 illustrates the practical SC method, where the strong user signal is superposed with the weak user signal, [21]. Vanken in [47], investigated a new approach of SC using standard single-user coding and decoding blocks. In the Quadrature Phase Shift Keying (QPSK) case, SC consists of two point-to-point encoders, which can be expressed as : $f_1\{0,1\}^{\lfloor 2TR_1 \rfloor}$ C^T and $f_2\{0,1\}^{\lfloor 2TR_2 \rfloor}$ C^T. The input bits will be assigned to two output bits $s_1(n)$ and $s_2(n)$, and T denotes the length of the block. $R1$ and $R2$ indicate the rate of data transmission for the first user and the second user, respectively. $\lfloor . \rfloor$ means the floor operator and C indicates the code library. Consequently, the SC output sequence of two users is as follows.

$$X(n) = \sqrt{P\beta_1}s_1(n) + \sqrt{P\beta_2}s_2(n) \tag{3.1}$$

where P is the total transmission power assigned to both users, and β indicates the fraction of P which is subject to the following restriction: $\beta_1 + \beta_2 = 1$, [21].

3.4.2.2 Successive Interference Cancellation (SIC)

Initially, SIC was initially proposed by Cover [5] in order to decode the superposed signal. The main idea of SIC is to successfully decode signals from different users. Once the first user's signal is decoded, it will be subtracted from the original received signal before the second user's signal gets decoded. It is highly important that users are ordered according to their channel conditions or signal strengths to perform SIC in a sufficient manner. Fig. 3.4 illustrates the SIC process of the SC signal. The following steps show the SIC processes for the case of two users that implemented the QPSK mod-

ulation technique as shown in fig. 3.4. The far user, with weak signal, performs the decoder $g_1\{0,1\}^{|2TR_1|}$ on y_1 where it is equal to $y_1(n) = \sqrt{P\beta_1}h_1s_1(n) + \sqrt{P\beta_2}h_1s_2(n)$ to decode its message $s_1(n)$ directly considering $s_2(n)$ as noise. Thus, no need to employ SIC at this stage. However, the near-user, with strong signal, implements the SIC as follows: Firstly, it uses the decoder $g_2\{0,1\}^{|2TR_2|}$ to decode the far user's signal. Second, it subtracts that decoded signal $(\sqrt{P\beta_1}h_2s_1(n))$,where h_2 indicates the gain in channel of the near user, from the received signal superposed, which is $y_2(n) = y_2(n) - \sqrt{P\beta_2}h_2s_1(n)$ [21]. .

3.4.3 Transmit Power Allocation Techniques

In NOMA, power allocation becomes the fundamental core issue since it significantly contributes to the applicability of NOMA. Obtaining the optimal data rate for NOMA users is mainly affected by the power allocated to each user because it is operating in the power domain. Each of the current power allocation schemes intends to compensate sufficiently in increasing the achievable data rate. Here, it is intended to discuss two different techniques of power allocation as follows:

- **Fixed Power Allocation (FPA)**:

  The most common power allocation technique is called fixed power allocation (FPA), where knowledge of channel state information (CSI) and complex derivation are not required. Hence, the previous method is not the optimal way to allocate the transmitting power among users, but it is the simplest scenario. For instance, in the case of two users, if the total power is assumed to be normalised to the unit, then each user will be assigned to a fixed portion of the total transmitting power. Thus, the cell edge user $(U1)$ with poor channel condition gets more power than the cell centre user $(U2)$, that is, $\beta_1 > \beta_2$. This basic technique has a low performance compared to the other power allocation techniques, since it does not efficiently change power according to other parameter changes such as channel gain.

- **Fractional Transmit Power Allocation (FTPA)**:

  This scheme comes up with a less complex operation and better performance than FPA, but it is still considered a fundamental technique. It is implemented as a power control in the LTE uplink scenario. In this method, the power control is equivalent to a particular variation of channel quality among users. Therefore, the transmitted power of the user k can be shown as:

$$p(k) = \frac{P_t}{\sum_{j\in K} h_j / (B * N_0)} \left(\frac{|h_k|^2}{BN_0}\right)^{-\alpha_{FTPA}} . \tag{3.2}$$

The decay factor varies according to ($0 \leq \alpha_{FTPA} \leq 1$). Nevertheless, if the factor gets zero value, then all users will have the same power, but when it is increased, then the far user gets a high power allocation factor. [48].

- **Equal resource block power allocation (ERPA)**:

  A low complexity sub-optimal approach that assigns the power equally among all the resource blocks can be found as in [49]. Therefore, the total transmission power in each RB (P_{RB}) is given as follow.

$$P_{RB} = P_s^F + P_s^N = \frac{P_t}{S_{RB}} \tag{3.3}$$

  where P_s^F and P_s^N are the allocated power for the far and near users, respectively. P_t is the total transmit power, and S_{RB} is the total number of resource block. According to [49], the optimized sub-optimal power allocation for the near and far users are given respectively as follows.

$$P_s^N = -\frac{(|h_N|^2 + |h_F|^2)B_s N_0}{2|h_N|^2|h_F|^2} + \frac{\mathcal{F}\sqrt{B_s N_0}}{2|h_N|^2|h_F|^2\sqrt{\Gamma_1}} \tag{3.4}$$

$$P_s^F = \frac{2|h_N|^2|h_F|^2 P_{RB} + (|h_N|^2 + |h_F|^2)B_s N_0}{2|h_N|^2|h_F|^2} - \frac{\mathcal{F}\sqrt{B_s N_0}}{2|h_N|^2|h_F|^2)\sqrt{\Gamma_2}} \tag{3.5}$$

  where $\Gamma_1 = 2^{\frac{1}{R_N}}$ and $\Gamma_2 = 2^{\frac{1}{R_F}}$. $\mathcal{F}$ is also given in Appendix A in [49].

3.5 Chapter Summary

Over the past few decades, different multiple access techniques have contributed significantly to enhancing the performance of cellular communication. However, NOMA has emerged as a potential solution to meet the requirements of the next 5G and beyond and beyond of mobile communication, as it impressively improves spectral efficiency, provides low latency, increases transmission throughput at the cell edge user, and offers massive connectivity. In addition to NOMA, there are several multiple access techniques that have also shown some potential developments by different research studies for the next generation of mobile communication, such as SCMA, MUSA, PDMA, and RSMA. In this chapter, the main concepts of NOMA, such as superposition coding (SC), successive interference cancellation (SIC), and power allocation techniques, particularly for the downlink scenario have been investigated and highlighted its literature review in different aspects of research concerns. The main differences between the conventional multiple access method, known as OMA, and NOMA are presented in this chapter. In the next chapter, an analytical work on the performance of the DL-NOMA system on fundamental channel models is provided.

CHAPTER 4

Performance Analysis for Downlink NOMA over α-μ Generalized Fading Channels

A. Alqahtani, E. Alsusa, A. Al-Dweik, and M. Al-Jarrah
Published in: IEEE Transactions on Vehicular Technology in 2020.

Abstract

This work presents a performance analysis for downlink non-orthogonal multiple accesses (DL-NOMA) systems where the channel gains follow the α-μ fading distribution. Specifically, closed-form expressions are derived for DL-NOMA in terms of the outage probability (OP), bit error rate (BER), and ergodic capacity (EC). The OP analysis considers two main scenarios, the first is when the individual user's rate is required to satisfy a certain quality of service (QoS), while the second is when the individual user's NOMA rate is less than that of the conventional orthogonal multiple access (OMA) rate. Moreover, the derived BER performance is generalized for the case of M-ary quadrature amplitude modulation (MQAM). The results demonstrate the interplay between the system performance, the power allocation coefficients, target data rates, and the channel fading parameters. Moreover, the OP results reveal that NOMA users with OMA data rate experience higher outage compared to NOMA with fixed target data rate. The accuracy of the derived expressions is validated using extensive Monte Carlo simulation.

Keywords— Non-orthogonal multiple access (NOMA), outage probability (OP), ergodic capacity (EC), α-μ fading

4.1 Chapter Introduction

Non-orthogonal multiple access (NOMA) has been recognized as a promising technology for future wireless communications as it allows multiple users to simultaneously share the same transmission resources to improve the spectral efficiency. In power domain NOMA, the base-station (BS) broadcasts the superimposed signal to all users in the same time slot and frequency band, but with different power values. Typically, users with poor channel conditions are allocated more power than users with good channel conditions. As such, users with high power can detect their signals by treating low-power signals as additive noise. Low-power users, i.e., users with good channel conditions, can detect their signals using successive interference cancellation (SIC) [5].

4.2 Related Work

Due to its desirable features, NOMA has been considered extensively in the literature. For example, Baidas *et al.* [50] attempted to analyze downlink NOMA (DL-NOMA) in terms of signal-to-noise ratio (SNR), achievable bit rate, and outage probability (OP) over independent not identically distributed (i.n.i.d) Rayleigh fading channels. In [51], the OP performance of DL-NOMA and orthogonal multiple access (OMA) systems is analyzed over η-μ and κ-μ fading channels with predefined target data rates. The presented results show that NOMA OP is less than OMA for a given target data rate. A study of OP for NOMA over Nakagami-m fading channels is presented in [52], where exact closed-form expressions for the individual users and overall system are obtained for a wide range of diversity orders. Agarwal *et al.* [53] investigated the OP of multiple NOMA users in downlink and uplink scenarios over sum of Gamma distributions, where closed-form OP expressions are obtained. The study considers the statistical channel state information (CSI) and the instantaneous CSI-based ordering schemes. It also provides some analytical expressions of the diversity order and outage floor for downlink and uplink scenarios, respectively. Moreover, OP and ergodic capacity (EC) performance metrics have been also investigated for cooperative NOMA system. In [54], the authors presented the analysis of OP and EC for uplink NOMA based cooperative scheme. They provided exact analytical expressions of OP and EC over Rayleigh fading channels. NOMA is also investigated in [55] for the κ-μ shadowed fading channel, where the EC is evaluated. The presented results indicate that increasing the number of multi-path clusters has a significant impact on the NOMA gain and users' performance. Moreover, the effective capacity under quality of service (QoS) requirements for multiple NOMA users is studied in [56], where the results show that NOMA outperforms OMA.

The bit error rate (BER) performance of NOMA has also been considered in the

literature. For example, Kara and Kaya [57] examined the BER of downlink and uplink NOMA, where phase shift keying (PSK) modulation is used and exact closed-form BER expressions over Rayleigh fading channels are derived for the scenario of imperfect SIC. The results demonstrate the impact of imperfect SIC for different cases of power assignments and channel quality in downlink and uplink scenarios. In addition, the BER is investigated in [58] for a NOMA system using binary phase shift keying (BPSK), where closed-form BER expressions are attained. The study composes the ideal and practical scenarios of the SIC process, and the results show that diversity and array gains can be achieved at high SNR when considering perfect SIC. However, in the case of imperfect SIC, the system performance exhibits error-floor at high SNRs. The work in [59] investigates the BER performance of uplink NOMA, where the boundary values of a two-user NOMA over asymmetric channels are disclosed and derived. Moreover, the authors of the same study derived closed-form of BER expressions on both sides of the boundary value for uplink NOMA users. Unlike the previous studies, the authors of [60] attempted to investigate the BER performance of an uplink NOMA scheme while employing a joint maximum-likelihood detector (ML) instead of SIC at the base station with multiple antennas. In addition, the derived closed-form BER expressions are attained by considering quadrature phase shift keying (QPSK) modulation, and the results reveal that the ML detector significantly outperforms the SIC. Lee and Kin [61] considered the symbol error rate (SER) of NOMA under imperfect SIC using quadrature amplitude modulation (QAM), where exact closed-form expressions are presented for individual DL-NOMA users under Rayleigh fading channels. The authors of [62] and [63] have addressed the BER performance for various NOMA communication systems and modulation schemes. More specifically, Assasf *et al.* [62] derived the exact BER expressions with imperfect SIC under Nakagami-m fading channels for two and three users' scenarios, while [63] derives an upper bound on the BER. In addition, both works consider the optimal power allocation that minimizes the average BER and achieve fairness among different users. Furthermore, our recent work in [64] investigates the performance of NOMA under the α-η-μ generalized fading channel. However, the work considers only the BER performance and it is limited to the two-user scenario.

The α-μ fading model is considered for cooperative detect and forward (DF) DL-NOMA in [65], where the OP and average channel capacity are analyzed. The authors considered a system with one user whose data is being transferred to the destination via a relay. It was shown that the system efficiency is increased because two data symbols are transmitted during the two time slots, rather than one symbol as in the case of conventional relaying systems. Although the work considers the α-μ fading channel model, the presented analysis is not directly applicable to non-cooperative NOMA where each data symbol belongs to a different user, and transmitter/receiver has to support more than two multiplexed signals when the number of users is more than two. Moreover,

the work did not provide BER analysis.

4.3 System Model

Consider a DL-NOMA system in a single cell equipped with a BS which broadcasts a superimposed single stream towards L users. Without loss of generality, the channels' coefficients between the L users and BS are assumed to be in ascending order, i.e., $|h_1|^2 \leq |h_l|^2 \leq \cdots \leq |h_L|^2$. Using the NOMA principle, the BS superimposes the L users' information symbols after assigning each user a particular power level. Therefore, the transmitted NOMA signal is given by

$$x_{sc} = \sum_{l=1}^{L} \sqrt{\beta_l P_t} s_l, \tag{4.1}$$

where the total transmit power P_t is normalized to unity, β_l is the power allocation coefficient, and s_l is the transmitted symbol of the lth user. The power coefficients are typically assigned such that $\beta_1 > \beta_2 > \cdots > \beta_L$. More details about the power allocation can be found in [66].

The received signal in flat fading channels after phase compensation at the lth user can be written as [67],

$$y_l = |h_l| x_{sc} + n_l, \;\; l \in \{1, 2, \ldots, L\}, \tag{4.2}$$

where the channel envelope $|h|$ follows the α-μ distribution and $n_l \sim \mathcal{CN}(0, \sigma^2)$ is an additive white Gaussian noise (AWGN). The received signal at the lth user is detected using the SIC detector where symbols $s_1, s_2, \ldots, s_{l-1}$ are detected and subtracted from y_l, and then s_l is detected. Generally speaking, the SIC process can fail, and hence, the interference will not be cancelled. However, in certain scenarios the SIC process can be assumed to be perfect, i.e., each SIC-user can successfully eliminate the interfering signals of the first $l-1$ users. This assumption is typically adopted to make the analysis more tractable without sacrificing much information, particularly at high signal-to-noise ratios (SNRs). For the case of $i > l$, the lth user treats the ith user's signal as noise, and thus, it is independent of the SIC process. For the perfect SIC case, the achievable data rate of the lth user, $1 \leq l \leq (L-1)$, is mathematically given as [68],

$$R_l = \log_2 \left(1 + \frac{\gamma_l \beta_l}{\gamma_l \sum_{i=l+1}^{L} \beta_i + 1} \right), \tag{4.3}$$

where $\rho = P_t/\sigma^2$ is the transmitted signal power to noise ratio (SNR), and $\gamma_l = \frac{\eta_l}{\beta_l} \triangleq \rho |h_l|^2$, where η_l is the instantaneous SNR. It is worth noting that R_l is subject to $R_{j \to l} \geq \tilde{R}_j$,

where $\tilde{R}_j$ denotes the target data rate of jth user which signifies the QoS requirement, and $R_{j\to l}$ is the data rate of the lth user to decode the jth user's signal, $j \leq l$, given as

$$R_{j\to l} = \log_2\left(1 + \frac{\gamma_l \beta_j}{\gamma_l \sum_{i=j+1}^{L} \beta_i + 1}\right). \tag{4.4}$$

It can be noticed that the achievable data rate of the Lth user is

$$R_L = \log_2\left(1 + \eta_L\right) \tag{4.5}$$

where $\eta_L \triangleq \gamma_L \beta_L$. Ultimately, it is intended to apply the order statistics approach to model the differences in the users-to-BS distances. As a result, the PDF and the CDF of the random variable of lth ordered user's γ_l can be respectively represented as [69],

$$f_{\gamma_l}(\gamma) = \Xi f_\gamma(\gamma) \times \left[F_\gamma(\gamma)\right]^{l-1}\left[1 - F_\gamma(\gamma)\right]^{L-l}, \tag{4.6}$$

$$F_{\gamma_l}(\gamma) = \Xi \sum_{n=0}^{L-l} \binom{L-l}{n} \frac{(-1)^n}{l+n}\left[F_\gamma(\gamma)\right]^{l+n}, \tag{4.7}$$

where Ξ is given in Table 4.1. by submitting (2.7) into (4.13), the final formula for the OP of the lth user for a given target data rate can be obtained as in (4.8).

4.4 Performance Analysis over α-μ Channels

4.4.1 Outage Probability (OP)

This section investigates the outage probability of a three-user, $L = 3$, NOMA system. OP is evaluated for two different scenarios as discussed in the following subsections.

4.4.1.1 Outage probability with a predefined target rate

Proposition 1. The outage probability of the lth user with a fixed data rate over α-μ fading is given by,

$$P_l^{out} = \Xi \sum_{n=0}^{L-l} \binom{L-l}{n} \frac{(-1)^n}{l+n} \times \left[\frac{\gamma_{inc}\left(\mu, \mu\left(\frac{\tau_l^*}{\tilde{\gamma}_l}\right)^{\alpha/2}\right)}{\Gamma(\mu)}\right]^{l+n}, \tag{4.8}$$

where $\tau_l^* = \max\{\tau_1, \cdots, \tau_l\}$, and τ_l is defined in (4.10).

Proof. According to [68], each user is supposed to have a predefined data rate known as $\tilde{R}_l$, therefore, two main probabilities are supposed to be considered. First, when a user can eliminate other user's signal i.e., $E_{l,j} = (R_{j\to l} \geq \tilde{R}_j)$, where $1 \leq j \leq l$, and when NOMA satisfies the user's QoS requirement, i.e., $(R_l \geq \tilde{R}_l)$. Thus, the OP of the lth user is observed as follows,

$$P_l^{out} = 1 - P\left(E_{l,1}^c \bigcap \cdots \bigcap E_{l,l}^c\right), \tag{4.9}$$

where $E_{l,j}^c$ is the complementary set of $E_{l,j}$ which is defined as follows

$$\begin{aligned} E_{l,j}^c &= (SINR_{j\to l} > \varepsilon_j) \\ &= \left(\frac{\gamma_l \beta_j}{\gamma_l \sum_{i=j+1}^{L} \beta_i + 1} > \varepsilon_j\right) \\ &= \left(\gamma_l > \frac{\varepsilon_j}{\beta_j - \varepsilon_j \sum_{i=j+1}^{L} \beta_i} \triangleq \tau_j\right), \end{aligned} \tag{4.10}$$

where $\varepsilon_j = 2^{\tilde{R}_j} - 1$ for $1 \leq j \leq l$. The probability event in (4.10) is constrained by $(\beta_j > \varepsilon_j \sum_{i=j+1}^{L} \beta_i)$. Therefore, (4.9) is rewritten as

$$P_l^{out} = 1 - P\left(\gamma_l > \tau_l^*\right) = \int_0^{\tau_l^*} f_{\gamma_l}(\gamma) d\gamma \tag{4.11}$$

where $\tau_l^* = \max\{\tau_1, \cdots, \tau_l\}$. Consequently, (4.6) is plugged into (4.11), and manipulated by using the binomial expansion defined in [9]. Thus, (4.11) is rewritten as

$$P_l^{out} = \Xi \int_0^{\tau_l^*} \sum_{n=0}^{L-l} \binom{L-1}{n} \times (-1)^n \left[F_\gamma(\gamma)\right]^{l+n-1} f_\gamma(\gamma) d\gamma \tag{4.12}$$

which after further manipulations becomes

$$P_l^{out} = \Xi \sum_{n=0}^{L-l} \binom{L-l}{n} \frac{(-1)^n}{l+n} \left[\int_0^{\tau_l^*} f_\gamma(\gamma) d\gamma\right]^{l+n}. \tag{4.13}$$

However, the complementary outage event of user L is obtained as $E_L^c = 1 - P(\gamma_l \beta_L > \varepsilon_L)$, where $\varepsilon_L = 2^{\tilde{R}_L} - 1$, and $\tilde{R}_L$ indicates the target data rate of user L. Thus, the outage probability of user L can be calculated as follows

$$P_L^{out} = 1 - P\left(\gamma_l > \frac{\varepsilon_L}{\beta_L} \triangleq \tau_L\right) = \int_0^{\tau_L} f_{\gamma_L}(\gamma) d\gamma. \tag{4.14}$$

Similarly, the previous steps from (4.11)-(4.13) is followed to find the final outage

probability of user L . Hence, the proof is complete. □

4.4.1.2 Outage probability of NOMA individual rate less than OMA individual rate

In Sec. 4.4.1.1 above, the OP was considered with a given fixed rate. However, to get more insights, another scenario is considered where the user's rate in NOMA is less than OMA. As a consequence, the above probability event of the lth user with $l < L$ can be evaluated with the help of (4.3)-(4.5) as

$$\begin{aligned} P(R_l^N < R_l^O) &= P\left[\left(1+\frac{\gamma_l\beta_l}{\gamma_l\sum_{i=j+1}^{L}\beta_i+1}\right)^L < \Theta\right] \\ &= P\left[\left(1+\gamma_l^2\left(\sum_{i=l}^{L}\beta_i\right)\right)^L - (1+\gamma_l)\left(1+\gamma_l\sum_{i=l+1}^{L}\beta_i\right)^L < 0\right] \\ &= \int_{\Omega_l} f_{\gamma_l}(\gamma)d\gamma_l \end{aligned} \tag{4.15}$$

where Ω_l is a set of intervals in which the function in the left hand-side of the inequality is negative, R_l^N indicates the NOMA data rate defined in (4.3), R_l^O is the OMA data rate which is also defined as $R_l^O = \frac{1}{L}\log_2\left(1+\rho\left|h_l\right|^2\right)$, and $\Theta \triangleq 2^{LR_l^O} = 1+\rho\left|h_l\right|^2$. To find the SNR threshold which determines the outage in the previous equation, the inequality should be solved by finding the roots of the resulting polynomial and then finding the intervals in which the polynomial is negative.

However, for the Lth, the event that its achievable rate with the NOMA transmission is less than OMA transmission, i.e., $P(R_L^N > R_L^O)$, can be mathematically derived in a similar fashion but with the aid of (4.5) and the binomial expansion theorem. Thus, after some manipulations, the OP of user L can be found as

$$\begin{aligned} P_L^{out} &= P\left(R_L^N < R_L^O\right) \\ &= P\left(-\gamma_L + \sum_{k=1}^{L}\binom{L}{k}\left(\gamma_L\beta_L\right)^k < 0\right) \\ &= \int_{\Omega_L} f_{\gamma_l}(\gamma)d\gamma_l. \end{aligned} \tag{4.16}$$

Similar to the previous case, $l < L$, the roots of the polynomial are evaluated and then the intervals in which the function is negative are considered.

For the first user of a two-user NOMA system, an inequality with quadratic equation

with a single real positive root is obtained, and thus the OP can be found as

$$P(R^N_{1|L=2} < R^O_{1|L=2}) = P\left(\gamma_{1|L=2} < \frac{1-2\beta_2}{\beta_2^2}\right)$$
$$= F_{\gamma_{1|L=2}}(\phi_{1|L=2}) \tag{4.17}$$

where $\phi_{1|L=2} = \frac{1-2\beta_2}{\beta_2^2}$. Thus, the OP of the lth user can be expressed as

$$P^{out}_{1|L=2} = \Xi \sum_{n=0}^{1} \binom{L-1}{n} \times \frac{(-1)^n}{l+n} \left[F_{\gamma_l}(\phi_{1|L=2})\right]^{l+n}. \tag{4.18}$$

where $F_{\gamma_l}(\gamma)$ is given in (2.8).

For the second user, P^{out}_L can be obtained as

$$P^{out}_{L|L=2} = P\left(\gamma_L < \frac{1-2\beta_L}{\beta_L^2}\right) = F_{\gamma_l}(\phi_{L|L=2}) \tag{4.19}$$

where $\phi_{L|L=2} = \frac{1-2\beta_L}{\beta_L^2}$.

By following similar procedure for $L = 3$ scenario, the OP for the first user can be found as

$$P(R^N_1 < R^O_1) = 1 - F_{\gamma_{1|L=3}}(\phi_{1|L=3}) \tag{4.20}$$

where $\phi_{1|L=3}$ with $a = -(1-\beta_1)^3$, $b = 1 - 3(1-\beta_1)^2$ and $c = 2 - 3(1-\beta_1)$.

For the second user, a polynomial with a degree of 3 is obtained, and thus the polynomial could have up to 3 real positive roots depending on the values β_1, β_2 and β_3. Therefore, the OP for each set of β's should be evaluated separately. For example when $\{\beta_1, \beta_2, \beta_3\} = \{0.75, 0.2, 0.05\}$, two real positive roots are obtained $\Phi_{2|L=3} = \{5.628, 66.873\}$, and the OP can be given as

$$P^{out}_{2|L=3} = F_{\gamma_2}(\gamma_2 = 5.628) + 1 - F_{\gamma_2}(\gamma_2 = 66.873), \tag{4.21}$$

whereas when $\{\beta_1, \beta_2, \beta_3\} = \{0.8, 0.15, 0.05\}$, the polynomial does not have real positive roots, and it is positive for the whole range of γ_2. Consequently, the OP in this case is $P^{out}_{2|L=3} = 1$.

For the third user, the obtained polynomial has a single root and P^{out}_L can be given as

$$P^{out}_{L|L=3} = F_{\gamma_l}(\phi_{L|L=3}) \tag{4.22}$$

and where $\phi_{L|L=3} = \frac{-3+\sqrt{\frac{4}{\beta_L}-3}}{2\beta_L}$ with $\beta_L < 1/3$ where this condition is certainly satisfied given that $\beta_1 > \beta_2 > \beta_3$ and $\beta_1 + \beta_2 + \beta_3 = 1$.

The same procedure can be followed to obtain P^{out}_L for the scenarios in which $L \geq 4$, however, the solution of high degree polynomials is not generally traceable and thus

numerical or graphical methods could be applied in such cases.

4.4.2 Average Bit Error Rate (BER)

The average BER can be obtained by first identifying the conditional BER of each user, and then applying the averaging process defined in [6],

$$\bar{P_l^e} = \int_0^\infty P_l^e \, f_{\gamma_l}(\gamma) d\gamma, \tag{4.23}$$

where $l \in \{1, 2, 3\}$. In this subsection, two different scenarios of NOMA-user system that are modulated using QAM, where the first one includes two assigned NOMA users with different modulation orders and the second scenario considers three different users with similar modulation orders are being considered. In both cases, the average BER performance is investigated over α-μ fading model.

4.4.2.1 Case of $(L = 2)$

The signals of two NOMA users are modulated using square QAM constellation M_l, where $M_1 = M_2 = 4$ for all users. Therefore, according to [70], the conditional BER, P_i^e, of both users can be given respectively as follows,

$$P_1^{e(I)} = \frac{1}{4} \sum_{i=1}^{2} \operatorname{erfc}\left(\sqrt{\frac{\lambda_{1,i}\gamma_1}{2}}\right) \tag{4.24}$$

$$P_2^{e(I)} = \frac{1}{4} \sum_{i=1}^{5} g_i \operatorname{erfc}\left(\sqrt{\frac{\lambda_{2,i}\gamma_2}{2}}\right) \tag{4.25}$$

where $\lambda_{1,i}$, $g_i = [2, -1, 1, 1, -1]$, and $\lambda_{2,i}$ are also given in Table 4.1.

Proposition 2. The average BER of the cell edge user U_1 can be defined as

$$\bar{P_1^{e(I)}} = \frac{1}{4} \sum_{i=1}^{2} \left[\Psi_1 \mathrm{H}_{2,2}^{1,2} \left[\frac{\mu \mathcal{D}_{1,i}^{-1}}{(\tilde{\gamma}_1)^{\frac{\alpha}{2}}} \middle| \begin{matrix} \left(1 - \frac{\alpha\mu}{2}, \frac{\alpha}{2}\right), \left(\frac{1}{2} - \frac{\alpha\mu}{2}, \frac{\alpha}{2}\right) \\ (0,1), \left(-\frac{\alpha\mu}{2}, \frac{\alpha}{2}\right) \end{matrix} \right] \right.$$
$$\left. - \Psi_2 \mathrm{H} \left[\begin{matrix} \binom{0,2}{2,1} \\ \binom{1,0}{0,1} \\ \binom{1,1}{1,2} \end{matrix} \middle| \begin{matrix} (1 - \frac{\alpha\mu}{2}; \frac{\alpha}{2}, \frac{\alpha}{2})(-\frac{\alpha\mu}{2}; \frac{\alpha}{2}, \frac{\alpha}{2}) \\ (-\frac{\alpha\mu}{2}; \frac{\alpha}{2}, \frac{\alpha}{2}) \\ - \\ (0,1) \\ (1,1) \\ (\mu,1), (0,1) \end{matrix} \middle| \xi_1, \xi_2 \right] \right] \tag{4.26}$$

where Ψ_1, Ψ_2, ξ_1, ξ_2, and $\mathcal{D}_{1,i}$ are defined in Table 4.1 .

Proof. Submitting (4.6) into (4.23) give,

$$\bar{P}_l^{e(I)} = \Xi \int_0^\infty P_l^e . f_\gamma(\gamma) \times [F_\gamma(\gamma)]^{l-1} \times [1 - F_\gamma(\gamma)]^{L-l} \, d\gamma. \tag{4.27}$$

By substituting (2.7) and (2.8) in (4.27), and applying the binomial theorem with some algebraic manipulations, (4.27) becomes

$$\bar{P}_l^{e(I)} = \sum_{n=0}^{L-l} \binom{L-1}{n} \frac{(-1)^n}{(\Gamma(\mu))^{l-1+n}} \Xi \times \mathcal{B}_l \int_0^\infty P_l^e \gamma_l^{\frac{\alpha\mu}{2}-1} \mathrm{e}^{-\mu\left(\frac{\gamma_l}{\tilde{\gamma}_l}\right)^{\frac{\alpha}{2}}} \left[\mathbb{G}(\gamma_l)\right]^{l-1+n} d\gamma_l, \tag{4.28}$$

where Ξ and $\mathcal{B}_l$ are shown in Table 4.1. Now, if $L = 2$, then average BER of U_1 and U_2 can be given respectively as

$$\bar{P}_1^{e(I)} = \sum_{n=0}^{1} \begin{pmatrix} 1 \\ n \end{pmatrix} \frac{(-1)^n \, \alpha\mu^\mu}{(\Gamma(\mu))^{n+1} \; \tilde{\gamma}_1^{\alpha\mu/2}} \int_0^\infty P_1^e \times \gamma_1^{\alpha\mu/2-1} e^{-\mu\left(\frac{\gamma_1}{\tilde{\gamma}_1}\right)^{\alpha/2}} \mathbb{G}(\gamma_1)^n d\gamma_1. \tag{4.29}$$

$$\bar{P}_2^{e(I)} = \frac{\alpha\mu^\mu}{\Gamma^2(\mu)\tilde{\gamma}_2^{\frac{\alpha\mu}{2}}} \int_0^\infty P_2^e \gamma_2^{\frac{\alpha\mu-2}{2}} e^{-\mu\left(\frac{\gamma_2}{\tilde{\gamma}_2}\right)^{\frac{\alpha}{2}}} \mathbb{G}(\gamma_2) d\gamma_2. \tag{4.30}$$

With further simplifications of (4.29) it can be written as,

$$\bar{P}_1^{e(I)} = \omega_1 \int_0^\infty P_1^e \gamma_1^{\frac{\alpha\mu-2}{2}} \mathrm{e}^{-\mu\left(\frac{\gamma_1}{\tilde{\gamma}_1}\right)^{\frac{\alpha}{2}}} \left[1 - \frac{\mathbb{G}(\gamma_1)}{\Gamma(\mu)}\right] d\gamma_1, \tag{4.31}$$

where ω_1 and ω_2 are defined in Table 4.1. By substituting (4.24) in (4.31), which gives

$$\bar{P}_1^{e(I)} = \frac{\omega_1}{2} \sum_{i=1}^{2} \int_0^\infty \left[1 - \frac{\mathbb{G}(\gamma_1}{\Gamma(\mu)})\right] \gamma_1^{\frac{\alpha\mu-2}{2}} \mathrm{e}^{-\left(\frac{\gamma_1}{\tilde{\gamma}_1}\right)^{\frac{\alpha}{2}}} \times Q\left(\sqrt{\lambda_{1,i}\gamma_1}\right) d\gamma_1. \tag{4.32}$$

The integral in (4.32) is composed of two integrals that can be obtained using the distributive law of multiplication over the variables in the squared brackets. The integrals can be solved using identities [9, pp. 8.4.3.1, 8.4.14.2, 8.4.16.1], and replacing the Meijer G-function's format to the H-function's format using identity [13, p. 6.2.8]. As a

result, the first integral of (4.32) becomes

$$I_1 = \frac{1}{\sqrt{\pi}} \int_0^\infty \gamma_1^{\alpha\mu/2-1} \mathrm{H}_{0,1}^{1,0} \left[\mu \left(\frac{\gamma_1}{\tilde{\gamma}_1} \right)^{\alpha/2} \middle| \begin{matrix} - \\ (0,1) \end{matrix} \right] \times \mathrm{H}_{1,2}^{2,0} \left[\frac{\lambda_{1,i}\gamma_1}{2} \middle| \begin{matrix} (1,1) \\ (0,1), (\frac{1}{2},1) \end{matrix} \right] d\gamma_1. \tag{4.33}$$

The mathematical expression in (4.33) can be evaluated by using the Mellin transform of the two H-fox functions, given in [71], as

$$I_1 = \mathrm{H}_{2,2}^{1,2} \left[\frac{\mu \left(\tilde{\gamma}_1\right)^{\alpha/2}}{\mathcal{D}_{1,i}} \middle| \begin{matrix} \left(1 - \frac{\alpha\mu}{2}, \frac{\alpha}{2}\right) & \left(\frac{1}{2} - \frac{\alpha\mu}{2}, \frac{\alpha}{2}\right) \\ (0,1) & \left(-\frac{\alpha\mu}{2}, \frac{\alpha}{2}\right) \end{matrix} \right] \times \frac{\left(\mathcal{D}_{1,i}\right)^{-\mu}}{\sqrt{\pi}}. \tag{4.34}$$

However, to solve the second integral in (4.32), the identities applied for (4.32) are reused along with the identity [66, p. 8.4.14.2]. Thus, the following expression is obtained,

$$I_2 = \frac{1}{\sqrt{\pi}} \int_0^\infty \gamma_1^{\alpha\mu/2-1} \mathrm{H}_{1,2}^{2,0} \left[\frac{\lambda_{1,i}\gamma_1}{2} \middle| \begin{matrix} (1,1) \\ (0,1), (\frac{1}{2},1) \end{matrix} \right] \times \mathrm{H}_{0,1}^{1,0} \left[\mu \left(\frac{\gamma_1}{\tilde{\gamma}_1} \right)^{\frac{\alpha}{2}} \middle| \begin{matrix} - \\ (0,1) \end{matrix} \right] \times \mathrm{H}_{1,2}^{1,1} \left[\mu \left(\frac{\gamma_1}{\tilde{\gamma}_1} \right)^{\frac{\alpha}{2}} \middle| \begin{matrix} (1,1) \\ (\mu,1), (0,1) \end{matrix} \right] d\gamma_1. \tag{4.35}$$

The above equation can be evaluated using [72, Eq. 2.3]. Therefore, (4.35) is further simplified to

$$I_2 = \mathrm{H} \left[\begin{matrix} \\ \binom{0,2}{2,1} \\ \binom{1,0}{0,1} \\ \binom{1,1}{1,2} \\ \\ \end{matrix} \middle| \begin{matrix} \left(1 - \frac{\alpha\mu}{2}; \frac{\alpha}{2}, \frac{\alpha}{2}\right), \left(\frac{1}{2} - \frac{\alpha\mu}{2}; \frac{\alpha}{2}, \frac{\alpha}{2}\right) \\ \left(-\frac{\alpha\mu}{2}; \frac{\alpha}{2}, \frac{\alpha}{2}\right) \\ - \\ (0,1) \\ (1,1) \\ (\mu,1), (0,1) \end{matrix} \middle| \xi_1, \xi_2 \right] \times \frac{\left(\mathcal{D}_{1,i}\right)^{-\mu}}{\sqrt{\pi}} \tag{4.36}$$

where ξ_1, ξ_2 are defined in Table 4.1. By substituting (4.34) and (4.36) in (4.32), the proposition in (4.26) is obtained. Hence, the proof is complete. □

Proposition 3. The average BER of the user in the cell

center (U_2) can be given in the following,

$$\bar{P}_2^{e(I)} = \frac{1}{4}\sum_{i=1}^{5} g_i \frac{\omega_3 \left(\mathcal{D}_{1,i}\right)^{-\mu}}{\sqrt{\pi}} \mathrm{H}\left[\begin{array}{c|c|c} & (1-\frac{\alpha\mu}{2};\frac{\alpha}{2},\frac{\alpha}{2}),(\frac{1}{2}-\frac{\alpha\mu}{2};\frac{\alpha}{2},\frac{\alpha}{2}) & \\ & (-\frac{\alpha\mu}{2};\frac{\alpha}{2},\frac{\alpha}{2}) & \\ \binom{0,2}{2,1} & - & \\ \binom{1,0}{0,1} & (0,1) & \varsigma_1,\varsigma_2 \\ \binom{1,1}{1,2} & (1,1) & \\ & (\mu,1),(0,1) & \end{array}\right], \tag{4.37}$$

where ω_3, ς_1, and ς_2 are presented in Table 4.1.

Proof. To obtain the average BER of the cell center user, i.e, U_2, (4.30) is applied and the same approach of deriving from (4.31)-(5.33) is followed. However, different conditional BER, i.e., (4.25) is substituted in (4.31) instead of (4.24). Furthermore, to avoid redundancy, the repeated steps are omitted, and hence the proof is complete. □

4.4.2.2 Case of $(L = 3)$

The transmitted signals of a three-user NOMA are modulated using QAM with same order, i.e., $M_l = 4\ \forall l$, $l \in \{1,2,3\}$. Therefore, according to [62], the conditional BER, P_i^e, of all three users can be given, respectively, in terms of $\mathrm{Q}(.)$ as follows

$$P_1^{e(II)} = \frac{1}{4}\sum_{i=1}^{4} \mathrm{Q}\left(\sqrt{\lambda_{3,i}\gamma_1}\right) \tag{4.38}$$

$$P_2^{e(II)} = \frac{1}{4}\sum_{i=5}^{14} c_i \times \mathrm{Q}\left(\sqrt{\lambda_{3,i}\gamma_1}\right) \tag{4.39}$$

$$P_3^{e(II)} = \frac{1}{4}\sum_{i=15}^{33} d_i \times \mathrm{Q}\left(\sqrt{\lambda_{3,i}\gamma_1}\right) \tag{4.40}$$

where $d_i = [4, -2, 2, 1, -1, 1, -2, 2, -2, 1, 1, -1, 1, -1, 2, -1, -1, 1, -1]$, $c_i = [1, -1, 2, 1, -1, 2, 1, -1, 1, -1]$, and $\gamma_{3,i}$ can be obtained from Table 4.1.

By considering $L = 3$ and following the previous steps from (4.27)-(4.28) as well as using (4.38)-(4.40), the average BER for all three users can be computed, respectively,

as follows,

$$\bar{P}_1^{e(II)} = \frac{1}{4}\sum_{i=1}^{4}\int_0^{\infty} \gamma_1^{\frac{\alpha\mu-2}{2}} \mathrm{e}^{-\mu\left(\frac{\gamma_1}{\bar{\gamma}_1}\right)^{\frac{\alpha}{2}}} \mathrm{Q}\left(\sqrt{\lambda_{3,i}\gamma_1}\right) \times \left[\omega_4 - \mathbb{G}(\gamma_1)\left(\omega_5 + \omega_6\mathbb{G}(\gamma_1)\right)\right] d\gamma_1 \tag{4.41}$$

$$\bar{P}_2^{e(II)} = \frac{1}{8}\sum_{i=1}^{10} c_i \left[\int_0^{\infty} \gamma_2^{\frac{\alpha\mu}{2}-1} \mathrm{e}^{-\mu\left(\frac{\gamma_2}{\bar{\gamma}_2}\right)^{\frac{\alpha}{2}}} \mathrm{Q}\left(\sqrt{\lambda_{3,i}\gamma_2}\right)\left(\omega_7 - \omega_8\left[\mathbb{G}(\gamma_2)\right]^2\right)\right] d\gamma_2 \tag{4.42}$$

where $\omega_4, \ldots \omega_8$ are given in Table 4.1, and

$$\bar{P}_3^{e(II)} = \frac{1}{4}\sum_{i=15}^{33} d_i \left[\omega_9 \int_0^{\infty} \gamma_3^{\frac{\alpha\mu}{2}-1} \mathrm{e}^{-\mu\left(\frac{\gamma_3}{\bar{\gamma}_3}\right)^{\alpha/2}} \mathrm{Q}\left(\sqrt{\lambda_{3,i}\gamma_3}\right)\left[\mathbb{G}(\gamma_3)\right]^2 d\gamma_3\right]. \tag{4.43}$$

where ω_9 is given in Table 4.1, and d_i is considered as in (4.40). It is wort noting that some integrals in (4.41)-(4.43) are analytically intractable. Therefore, to the best of the authors' knowledge, there is no closed-expressions for the above equations, and thus, such integrals will be evaluated numerically.

4.4.3 Ergodic Capacity (EC)

It is assumed that the channel state information (CSI) is known for an average amount of transmit power constraint, thus the Shannon channel fading capacity which is also known as the ergodic capacity in (bits/s/Hz) is defined in [6] as

$$\bar{C}_l = B\int_0^{\infty} \log_2(1+\gamma_l\beta_l) f_{\gamma_l}(\gamma_l) d\gamma_l. \tag{4.44}$$

4.4.3.0.1 Case of (L=2)

Proposition 4. The average channel capacity of U_1 is expressed as shown in (4.45),

$$\begin{aligned}\bar{C}_1 = \frac{\omega_1}{\ln 2} \times \Bigg(& \mathrm{H}_{2,2}^{3,1}\left[\frac{\mu}{(\tilde{\gamma_1})^{\alpha/2}}\middle| \begin{matrix}\left(-\frac{\alpha\mu}{2},\frac{\alpha}{2}\right)\left(1-\frac{\alpha\mu}{2},\frac{\alpha}{2}\right)\\ (0,1)\left(-\frac{\alpha\mu}{2},\frac{\alpha}{2}\right)\left(-\frac{\alpha\mu}{2},\frac{\alpha}{2}\right)\end{matrix}\right] \\ & -\beta_2{}^{\left(\frac{-\alpha\mu}{2}\right)}\mathrm{H}_{2,2}^{3,1}\left[\frac{\mu\beta_2{}^{-\alpha/2}}{(\tilde{\gamma_1})^{\alpha/2}}\middle| \begin{matrix}\left(-\frac{\alpha\mu}{2},\frac{\alpha}{2}\right)\left(1-\frac{\alpha\mu}{2},\frac{\alpha}{2}\right)\\ (0,1)\left(-\frac{\alpha\mu}{2},\frac{\alpha}{2}\right)\left(-\frac{\alpha\mu}{2},\frac{\alpha}{2}\right)\end{matrix}\right]\Bigg) \\ & -\frac{\omega_2}{\ln 2}\left(\frac{\mu}{(\tilde{\gamma_1})^{\alpha/2}}\right)^{-\mu}\Bigg(\mathrm{H}\left[\begin{matrix}(1-\mu;\frac{2}{\alpha},1)\\ -\\ \left(\begin{smallmatrix}0,1\\1,0\end{smallmatrix}\right)\left(\begin{smallmatrix}1,2\\2,2\end{smallmatrix}\right)\left(\begin{smallmatrix}1,1\\1,2\end{smallmatrix}\right)\end{matrix}\middle| \begin{matrix}(1,1),(1,1)\\(1,1),(0,1)\\(1,1)\\(\mu,1),(0,1)\end{matrix}\middle|\varsigma_3,\varsigma_4\right] \\ & -\mathrm{H}\left[\begin{matrix}(1-\mu;\frac{2}{\alpha},1)\\ -\\ \left(\begin{smallmatrix}0,1\\1,0\end{smallmatrix}\right)\left(\begin{smallmatrix}1,2\\2,2\end{smallmatrix}\right)\left(\begin{smallmatrix}1,1\\1,2\end{smallmatrix}\right)\end{matrix}\middle| \begin{matrix}(1,1),(1,1)\\(1,1),(0,1)\\(1,1)\\(\mu,1),(0,1)\end{matrix}\middle|\varsigma_5,\varsigma_6\right]\Bigg)\end{aligned} \tag{4.45}$$

where ς_3, ς_4, ς_5, and ς_6 are defined in Table 4.1.

Proof. By noting that (4.27) is similar to (4.44) given that P_i^e is replaced by $\log_2(1+\mathcal{G}_l)$ and using the identity $\log_2(x) = \frac{\ln(x)}{\ln(2)}$, the following expression is produced,

$$\bar{C}_l = \Upsilon \int_0^\infty \ln(1+\mathcal{G}_l) f(\gamma_l)\left[F(\gamma_l)\right]^{l-1}\left[1-F(\gamma_l)\right]^{L-l} d\gamma_l, \tag{4.46}$$

where Υ and $\mathcal{G}$ are defined in Table 4.1. Now, by following the same deriving approach applied in (4.27), with respect to the logarithmic function instead of the complementary error function and considering $L = 2$, the average channel capacity for both users are given, respectively, as follows,

$$\bar{C}_1 = \frac{1}{\ln 2}\int_0^\infty \ln(1+\mathcal{G}_1)\gamma_1^{\left(\frac{\alpha\mu}{2}-1\right)}\mathrm{e}^{-\mu\left(\frac{\gamma_1}{\tilde{\gamma}_1}\right)^{\frac{\alpha}{2}}} \times \left(\omega_1\gamma - \omega_2\mathbb{G}(\gamma_1)\right) d\gamma_1 \tag{4.47}$$

$$\bar{C}_2 = \frac{\omega_2}{\ln 2}\int_0^\infty \ln(1+\mathcal{G}_2)\frac{\gamma_1^{\frac{\alpha\mu}{2}}}{\gamma_1}\mathrm{e}^{-\mu\left(\frac{\gamma_1}{\tilde{\gamma}_1}\right)^{\frac{\alpha}{2}}}\mathbb{G}(\gamma_1)d\gamma_1. \tag{4.48}$$

By noting that the integral (4.47) can be split into two integrals that can be further

extended to the following formats, respectively,

$$\mathcal{I}_1 = \int_0^\infty \ln\left(\frac{1+\gamma_1}{1+\beta_2\gamma_1}\right)\gamma_1^{\frac{\alpha\mu-2}{2}} \mathrm{e}^{-\mu\left(\frac{\gamma_1}{\tilde{\gamma}_1}\right)^{\frac{\alpha}{2}}} d\gamma_1 \tag{4.49}$$

$$\mathcal{I}_2 = \int_0^\infty \ln\left(\frac{1+\gamma_1}{1+\beta_2\gamma_1}\right)\gamma_1^{\frac{\alpha\mu-2}{2}} \mathrm{e}^{-\mu\left(\frac{\gamma_1}{\tilde{\gamma}_1}\right)^{\frac{\alpha}{2}}} \mathbb{G}(\gamma_1) d\gamma_1. \tag{4.50}$$

The steps from (4.32)-(5.33) are reused with respect to the logarithmic, which can be solved with the aid of [66, p. 8.4.16.1] as well as the other identities mentioned previously in (4.32). In addition, after applying some further algebraic manipulations, prop. 5 in (4.45) is sufficiently achieved. □

Proposition 5. The average channel capacity of U_2 is expressed as follows,

$$\bar{C}_2 = \frac{\omega_2 \mu^{-\frac{\alpha\mu}{2}}}{\ln 2\,(\tilde{\gamma}_1)^{\frac{\alpha^2\mu}{4}}} \times \mathrm{H}\left[\begin{array}{c|c|c} & (1-\mu;\frac{2}{\alpha},1) & \\ & - & \\ \binom{0,1}{1,0} & (1,1),(1,1) & \varsigma_5,\varsigma_6 \\ \binom{1,2}{2,2} & (1,1),(0,1) & \\ \binom{1,1}{1,2} & (1,1) & \\ & (\mu,1),(0,1) & \end{array}\right] \tag{4.51}$$

where ς_3, ς_4, ς_5, and ς_6 are defined in Table 4.1.

The EC of U_2 can be attained by evaluating (4.48) as such as (4.30).

4.4.3.1 Case of $(L = 3)$

By substituting $L = 3$ in (4.46), and following the same steps that were applied for (4.41)-(4.43) with respect to the logarithmic function, EC of three-user NOMA can be eventually attained. Hence, writing their expressions is omitted to avoid redundancy since the same expressions can be obtained by replacing $Q(\cdot)$ function with $\ln(1+\mathcal{G}_l)$. It can be noted that obtaining the final closed-form expressions of EC for this particular case of $L = 3$ is more challenging and intractable, therefore, numerical solutions are adopted.

4.5 Results and Discussion

In this section, DL-NOMA, with different numbers of users, is considered where the total transmit power is normalized to unity, and the fixed power allocation technique is performed. In addition, the power coefficients are distributed amongst the users according to their channel conditions basically as $(\beta_1 = 0.8, \beta_2 = 0.2)$ for two user's case, and $(\beta_1 = 0.8, \beta_2 = 0.15, \beta_3 = 0.05)$ for three user's case unless stated otherwise. It is

Table 4.1 Definitions for The Symbols Used in Formulations.

Symbol	Definition	Symbol	Definition
ω_1	$2\mathcal{B}_l$	Ψ_1	$\frac{\omega_1\left(\mathcal{D}_{1,i^*}\right)^{-\mu}}{\sqrt{\pi}}$
$\lambda_{1,1}$,$\lambda_{2,2}$	$A_1 - A_2$	ω_2,ω_3	$\frac{1}{\Gamma(\mu)}\omega_1$
Ψ_2	$\frac{\omega_2\left(\mathcal{D}_{1,j^*}\right)^{-\mu}}{\sqrt{\pi}}$	$\lambda_{1,2}$,$\lambda_{2,3}$	$A_1 + A_2$
ς_3	$\left(\mu/\left(\tilde{\gamma}_l\right)^{2/\alpha}\right)^{-2/\alpha}$	$^{\mathrm{a}}\xi_1$	$\left(\frac{\mu}{(\tilde{\gamma}_l)^{\alpha/2}}\right)/\mathcal{D}_{1,i^*}$
$\lambda_{2,1}$	A_2	ω_4	$3\mathcal{B}_l$
$^{\mathrm{b}}\varsigma_1$	$\left(\frac{\mu}{(\tilde{\gamma}_l)^{\alpha/2}}\right)/\mathcal{D}_{2,j^*}$	$\lambda_{2,4}$	$2A_1 - A_2$
ω_5,ω_7	$\frac{6}{\Gamma(\mu)}\mathcal{B}_l$	ς_5	$\beta_2\varsigma_3$
$\lambda_{2,5}$	$2A_1 + A_2$	ω_6,ω_9	$\frac{3}{\Gamma(\mu)^2}\mathcal{B}_l$
ς_2,ς_4,ς_6	1	Ψ	$\frac{1}{2\Gamma^{l-1}(\mu)}\mathcal{B}_l$
ω_8	$\frac{6}{\Gamma(\mu)^2}\mathcal{B}_l$	Ξ	$\frac{L!}{(L-l)!(l-1)!}$
L_{i^*}	$\{4\}$	Θ	$1 + \rho\left\|h_l\right\|^2$
Υ	$\frac{1}{\ln(2)}\Xi$	$\mathcal{G}_l$	$\left(\frac{\beta_l\gamma_l}{\sum_{i=j+1}^{L}\beta_i\gamma_l+1}\right)$
$\lambda_{3,1}$,$\lambda_{3,6}$,$\lambda_{3,33}$	$A_1 + A_2 + A_3$	$\lambda_{3,2}$,$\lambda_{3,11}$,$\lambda_{3,30}$	$A_1 - A_2 + A_3$
$\lambda_{3,3}$,$\lambda_{3,14}$,$\lambda_{3,24}$	$A_1 + A_2 - A_3$	$\lambda_{3,4}$,$\lambda_{3,8}$,$\lambda_{3,18}$	$A_1 - A_2 - A_3$
$\lambda_{3,5}$,$\lambda_{3,31}$	$2A_1 + A_2 + A_3$	$\lambda_{3,7}$	$A_2 + A_3$
$\lambda_{3,9}$,$\lambda_{3,20}$	$2A_1 - A_2 - A_3$	$\lambda_{3,10}$,$\lambda_{3,22}$	$A_2 - A_3$
$\lambda_{3,12}$,$\lambda_{3,28}$	$2A_1 - A_2 + A_3$	$\lambda_{3,13}$,$\lambda_{3,25}$	$2A_1 + A_2 - A_3$
$\lambda_{3,15}$	A_3	$\lambda_{3,16}$	$A_2 + A_3$
$\lambda_{3,17}$	$2A_2 + A_3$	$\lambda_{3,19}$	$2A_1 - 2A_2 - A_3$
$\lambda_{3,21}$	$2A_1 - A_3$	$\lambda_{3,23}$	$2A_2 - A_3$
$\lambda_{3,26}$	$2A_1 + 2A_2 - A_3$	$\lambda_{3,29}$	$2A_1 + A_3$
$\lambda_{3,32}$	$2A_1 + 2A_2 + A_3$	$\lambda_{3,27}$	$2A_1 - 2A_2 + A_3$
$\tilde{\gamma}_l$	$\frac{\mu^{(2/\alpha)}\Gamma(\mu)}{\Gamma(\mu+2/\alpha)}\rho$	$\mathcal{B}_l$	$\frac{\alpha\mu^{\mu}}{2\Gamma(\mu)\tilde{\gamma}_l^{\alpha\mu/2}}$
$A_1 = \sqrt{\beta_1}$, $A_2 = \sqrt{\beta_2}$, $A_3 = \sqrt{\beta_3}$, $\mathcal{D}_{1,i^*} = \left(\frac{\lambda_{1,i^*}}{2}\right)^{\alpha/2}$, $\mathcal{D}_{2,j^*} = \left(\frac{\lambda_{1,j^*}}{2}\right)^{\alpha/2}$			

$^{\mathrm{a}}\xi_1$=ξ_2,$^{\mathrm{b}}\varsigma_1$=ς_2 n^{c}=$[0,1]$, $i^* \in \{1,2\}$, $j^* \in \{1,2\ldots,5\}$

worth noting that most of the results in this section are mainly dependent on the Fox-H function, where it can be applied in Matlab as proposed in [73]. α-μ fading distribution is considered as a generalized model due to its ability to encompass other important fading models such as Rayleigh, Weibull, and Nakagami. Therefore, various selections of α and μ parameters are implemented in this section to study their significance. In addition, the BER and EC analysis for multiple-users NOMA becomes intractable when order statistics theory is applied to α-μ fading. To illustrate, the work in [67], as an example, shows the BER analysis of three-user NOMA under Rician fading channels with order statistics, which is obviously highly complex. Consequently, obtaining exact closed-form BER and EC expressions for more than two users using α-μ model with order statistics is generally intractable. To overcome this issue, a numerical tool is applied to compute the results for a three NOMA user's case.

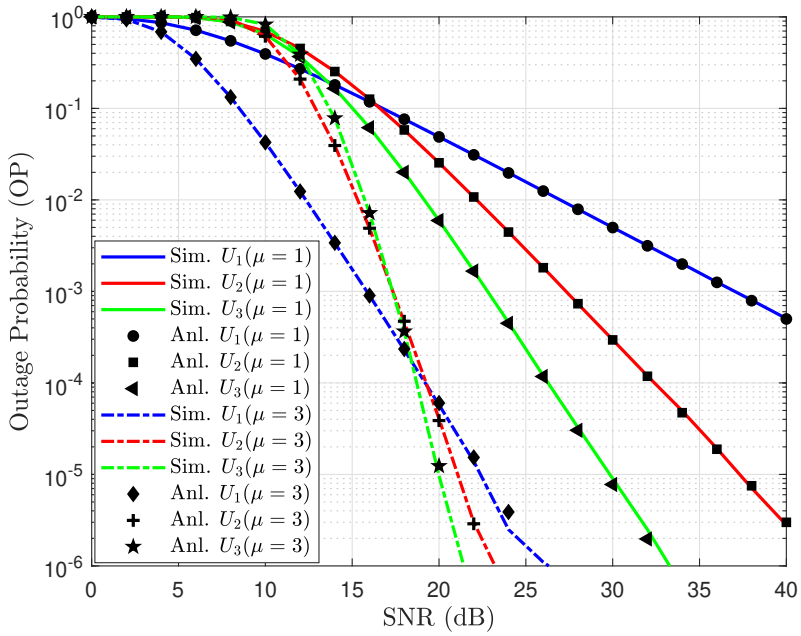

Fig. 4.1 OP of three NOMA users with fixed target data rates, $R_1 = R_2 = R_3 = 1$ bits/channel (BPCH), $\alpha = 2$.

Fig. 4.1 shows OP of all users when they fall below certain target data rates. The figure is generated for a fixed value of $\alpha = 2$, and for $\mu = [1, 3]$. It can be noted from the figure that the fading parameter μ has a direct impact on the outage performance of the users, but with different levels. For example, when μ is increased from 1 to 3, the OP of all users dramatically improves, particularly for the farthest user, U_1, where a 20 dB improvement is achieved at $OP = 10^{-3}$. The same behavior is experienced by U_2 and U_3, but the achieved improvement is less as compared with U_1. Such performance is obtained because the fading distribution for $\mu = 3$ is mostly congregated around 1, which implies mild fading. On the contrary, when $\mu = 1$, the fading envelope

becomes mostly concentrated below 1, leading to severe fading and poor performance. Therefore, power allocation and target data rates should be selected to constructively contribute to achieving reliable connections with less outage probability.

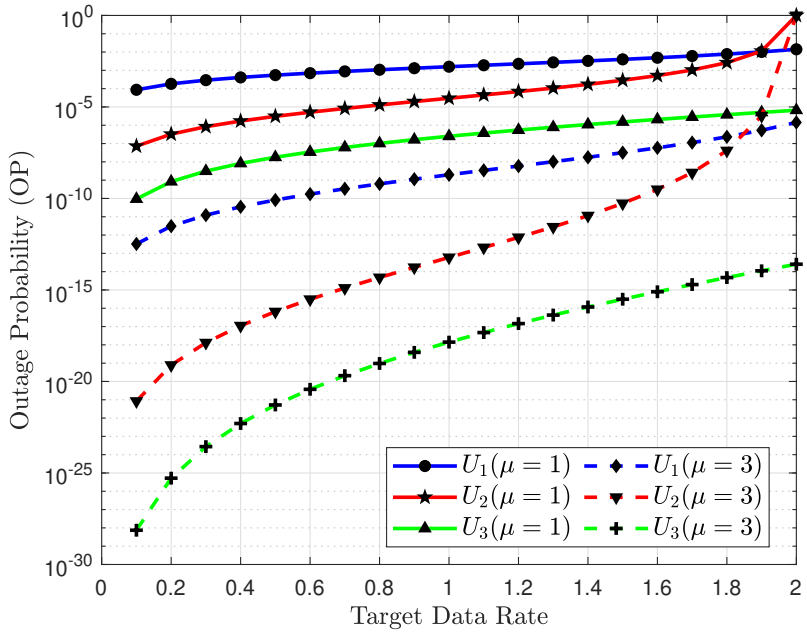

Fig. 4.2 OP versus similar target data rates for all users over fixed fading and SNR parameters i.e., $\alpha = 2$ and SNR$= 35$ dB.

Fig. 4.2 represents the case where all users exhibit identical QoS requirements defined with similar preset data rates, predefined SNR, fixed allocation power, i.e. ($\beta_1 = 0.8, \beta_2 = 0.15, \beta_3 = 0.05$), and variant fading parameters, i,e ($\alpha = 2, \mu = [1, 3]$). It can be seen from that figure that assigning a similar predefined target data rate to all users with different fading parameters has a significant impact on the system behavior. To illustrate, U_3, with the strong channel conditions, achieves the best OP performance over all values of target data rates. However, at high target data rate, U_2 suffers from high outage comparing to U_1 precisely when $\mu = 3$. The interpretation of this phenomena can be indicated as the interference amount that carried by U_2. In general, the potential impact of fading parameters can obviously contribute positively when they get increased. Moreover, undifferentiated QoS requirements for all NOMA users may lead to discriminatory outage performance, therefore, a careful selection of target data rates for all users plays a major impact on the overall system performance as explained in the next two figures.

Unlike the previous results, Fig. 4.3 shows the OP versus different combinations of target data rates and SNR values under the same assumptions used in Fig. 4.2 of power allocations and fading parameters. In this figure, each user is examined over a distinct range of target data rate with respect to others. To illustrate, it is assumed

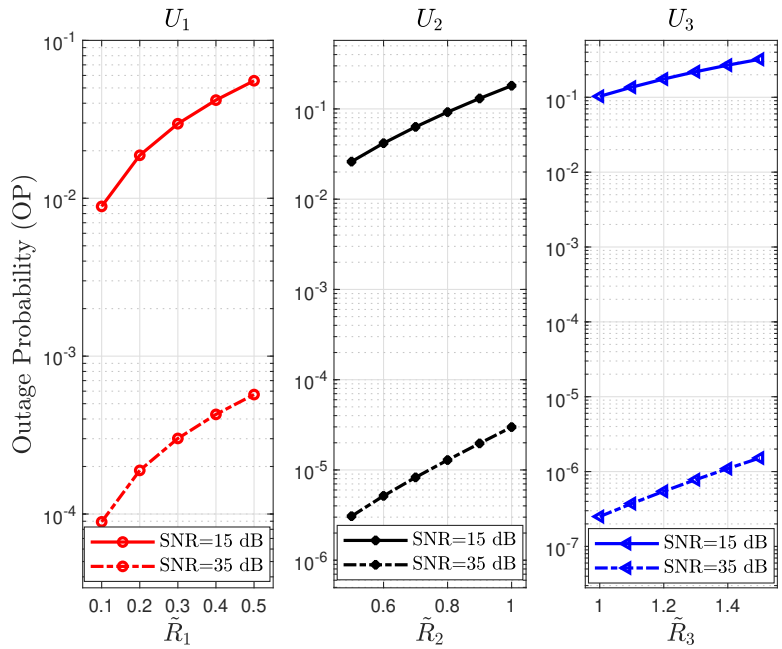

Fig. 4.3 OP versus different target data rates for all users over fixed fading and SNR parameters, i.e., $\alpha = 2$, $\mu = 1$ and SNR= $[15, 35]$ dB.

that U_1's target data rate can be fallen between any value of $(0.1 - 0.5)$. Similarly, the assigned target data rate of U_2 and U_3 can be chosen between the range of $(0.5 - 1)$ and $(1 - 1.5)$, respectively. Therefore, at high SNR, U_3 practices lower outage among other users though it is assigned with low power, but indeed with high privilege of channel conditions and QoS requirement. In contrast to Fig. 4.2, it is noticed that various combinations of predefined data rates for all users contribute to better OP performance at high SNR values, i.e., SNR= 35 dB. Generally speaking, the OP is improved when considering various combinations of QoS requirements for all users instead of being identical. As a result, Table 4.2 shows various outputs of OP for two different groups of target data rates for all users over the same selection of fading parameters as an illustration, which are categorized as: group $I = \{U_1 = 1, U_2 = 1, U_3 = 1\}$ and group $II = \{U_1 = 0.2, U_2 = 0.7, U_3 = 1\}$. These results are aggregated from Figs. 4.2 and 4.3.

Fig. 4.4 demonstrates the OP of two NOMA users with OMA rate. It shows that U_1 has an opposite behaviour with U_2. To illustrate, U_1 gains more effective OP at very low SNR comparing with U_2 which has the reveres relation. In addition, a significant impact of increasing the fading parameter μ is clearly appear on U_2 over high SNR values while less significance is granted for U_1.

Fig. 4.5 shows the second scenario of the OP performance for three user's case when the user's data rate in OMA system exceeds the similar user's data rate in NOMA system. It is expected that less outage can be attained at high SNR values, especially

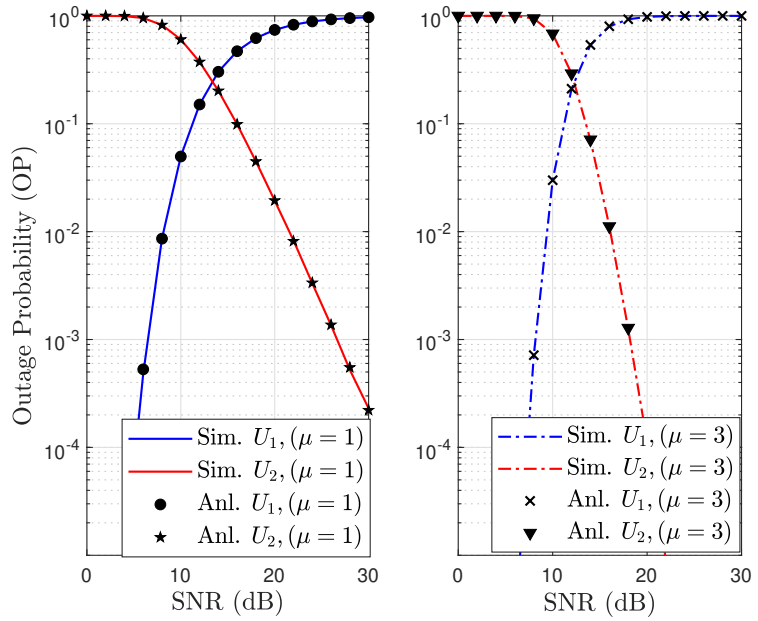

Fig. 4.4 OP of two NOMA users when their data rates are less than in OMA with different cases of fixed fading parameters as $\alpha = 2, \mu = [1, 3]$, and power allocation $(\beta_1 = 0.8, \beta_2 = 0.2)$.

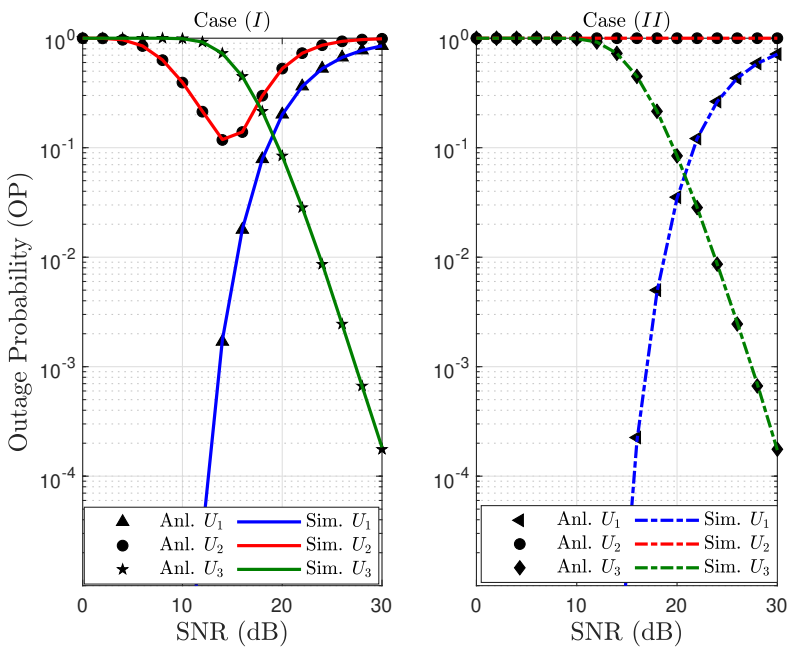

Fig. 4.5 OP of three NOMA users when their data rates are less than in OMA with different cases of power assignment and fixed fading parameters as $\alpha = 2, \mu = 1$.

for the nearest user, U_3, due to its high channel gain. However, U_1 AND U_2 have different pattern of OP than U_3. Their OP performance are mainly manipulated by the amount of assigned power allocation as it can be seen in the same figure.U_1 exhibits the similar approach in two user's case while U_2 has different outputs. In the first

scenario, where power allocation is distributed as ($\beta_1 = 0.75, \beta_2 = 0.15, \beta 3 = 0.1$), U_2 start behaving better till it reaches 10^{-1} of OP, then it practices negatively towards OP=1. On the other hand, another scenario of assigning power allocation to all users as ($\beta_1 = 0.75, \beta_2 = 0.15, \beta 3 = 0.1$) is applied, where U_2 has gained flat OP with full outage. According to the previous results and On contrast with the previous case of OP with QoS, the OP performance with OMA data rate is considered as worse than the case of OP predefined data rate. Overall, the assigned power allocation plays a major impact on the system performance.

Table 4.2 OP over different predefined target rates

Users	Outage Probability (OP)	
	Group I	Group II
	$\tilde{R}_1 = \tilde{R}_2 = \tilde{R}_3 = 1$	$\tilde{R}_1 = 0.2, \tilde{R}_2 = 0.7, \tilde{R}_3 = 1$
U_1	1.5×10^{-3}	1.8×10^{-4}
U_2	2.98×10^{-5}	8.27×10^{-6}
U_3	2.5×10^{-7}	2.5×10^{-7}

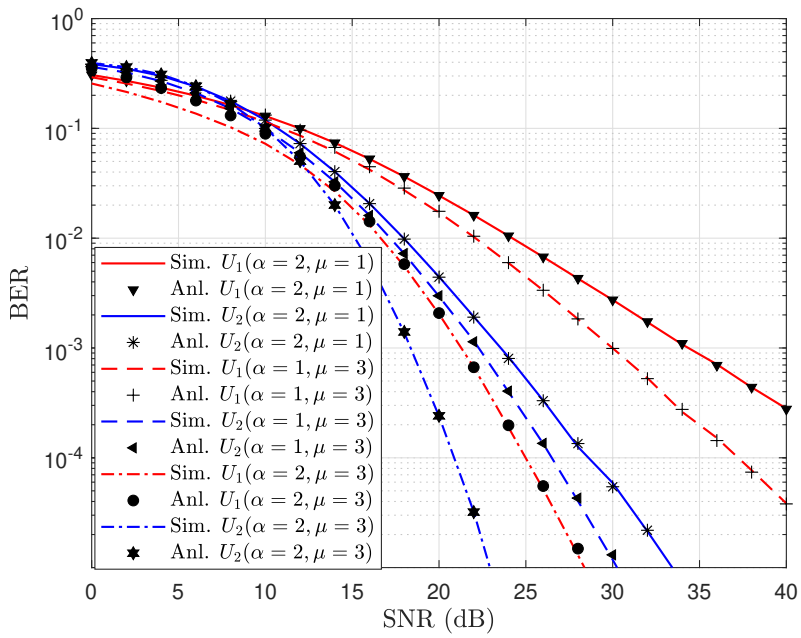

Fig. 4.6 BER versus SNR over α-μ fading channels with different values of fading parameters.

Fig. 4.6 shows the significant effect of α and μ fading parameters on the average BER of two-user NOMA, where high modulation order, M_1 and M_2, are used equally

for both users. It is noticed that a trade-off between the assigned power and BER can be observed in 4.6. To illustrate, when the α selection is fixed to 2 and $\mu = 3$, U_1 demands about 12 dB less than the case of exhibiting $\mu = 1$ to achieve 10^{-3} BER. Similarly, for the fixed selection of μ fading parameter as ($\mu = 3$) and $\alpha = 1$, U_1 requires about 8 dB more than the case of experiencing $\alpha = 2$ to attain 10^{-3} BER. The identical approach can be applied for U_2 and low performance gap can be observed at different choices of fading parameters since it exhibits better channel gain than U_1. Therefore, increasing the fading parameters can improve the BER performance and contribute in less errors at high SNR values. This figure indicates that other different fading models such as Rayleigh, Weibull and Nakagami-m can be produced by a certain choice of of α and μ fading parameters as special cases. It provides more insightful results of the link performance under different fading scenarios. Overall, the error probabilities in both users performance become less once the α and μ parameters are significantly increased, and conversely when they are assigned to lower values.

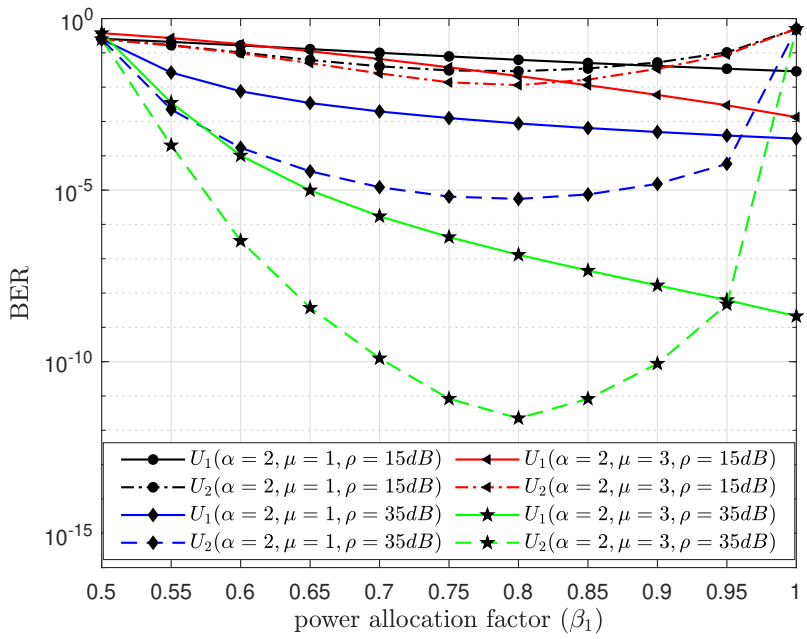

Fig. 4.7 BER versus different power allocation factors of β_1 for $L = 2$ over different fading parameters.

Fig. 4.7 shows the potential impact of the power allocation coefficient, β_n, in terms of BER. Therefore, the power allocation factor β_1 mainly improves the quality of U_1's link performance if it was much large for all cases of different fading parameters, i.e., $\alpha = 2$, and for $\mu = [1, 3]$. However, regarding U_2, the link performance provides the best outcome when the assigned power allocation is about 0.25 at high SNR values. In addition, the amount of fixed power allocation factors could corrupt the link performance when both users powers are almost assigned equally. On contrary, when both

users have a notable difference in their assigned power, then efficient BER performance is defiantly gained.

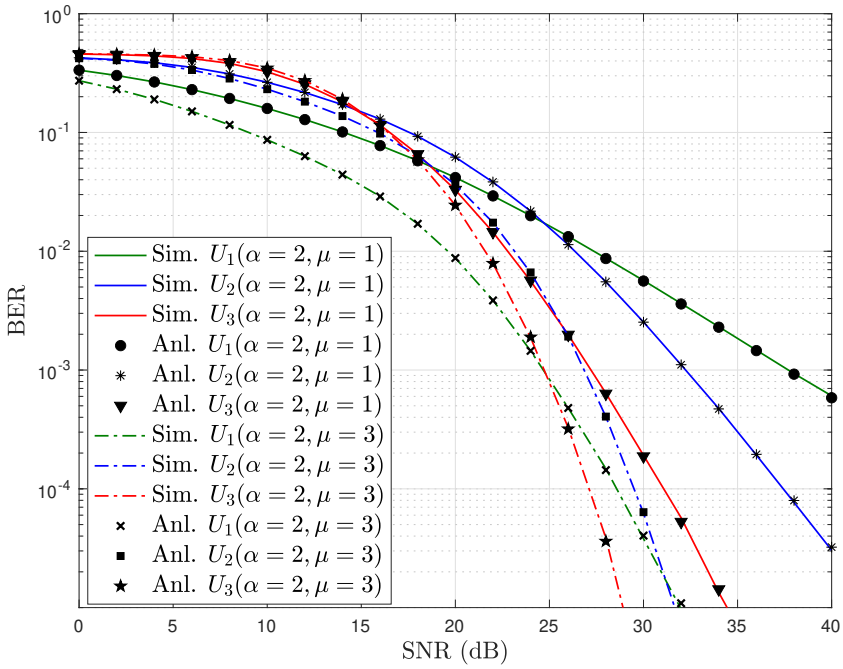

Fig. 4.8 Average BER versus SNR over α-μ fading channels with different values of μ and $\alpha = 2$ for three NOMA users that performed 4-QAM.

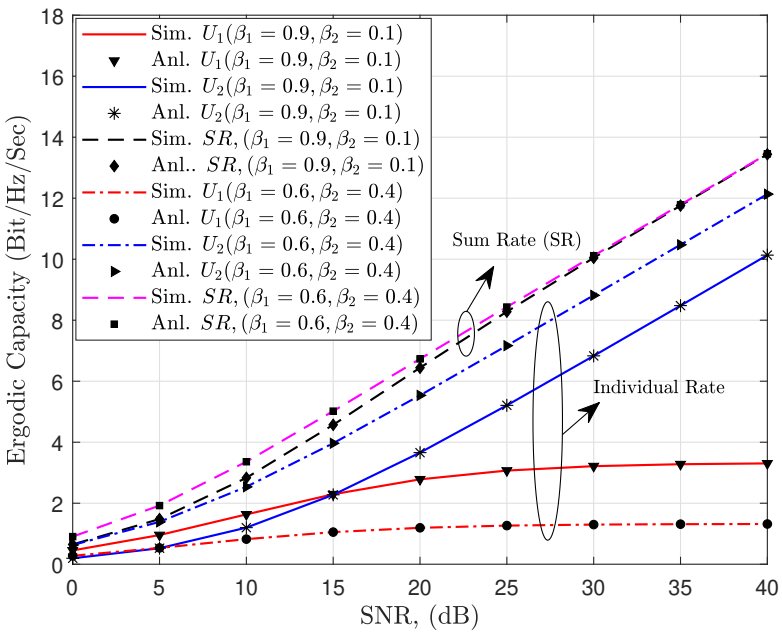

Fig. 4.9 EC versus SNR with different values of μ and $\alpha = 2$ for two NOMA users.

In Fig. 4.9, a fixed selection of fading parameter is made as $(\alpha = 2, \mu = 1)$ with various selection of power allocation factors to demonstrate the vital role of power

allocation assignment. the average channel capacity, i.e. EC, of both users is plotted along with the its simulation results including the sum and individual rates of the two NOMA users. The figure shows the impact of the power allocation parameters, where promising results for U_1 are achieved when its' allocated power is approaching to the highest values with respect to the other user. Similarly, U_2 obtains the similar output when its allocated power is increased. However, in order to have a fairness among them, a fair power allocation must be apply. Moreover, these boundaries can be disappeared in terms of sum rate at high SNR value as it is shown in the same figure.

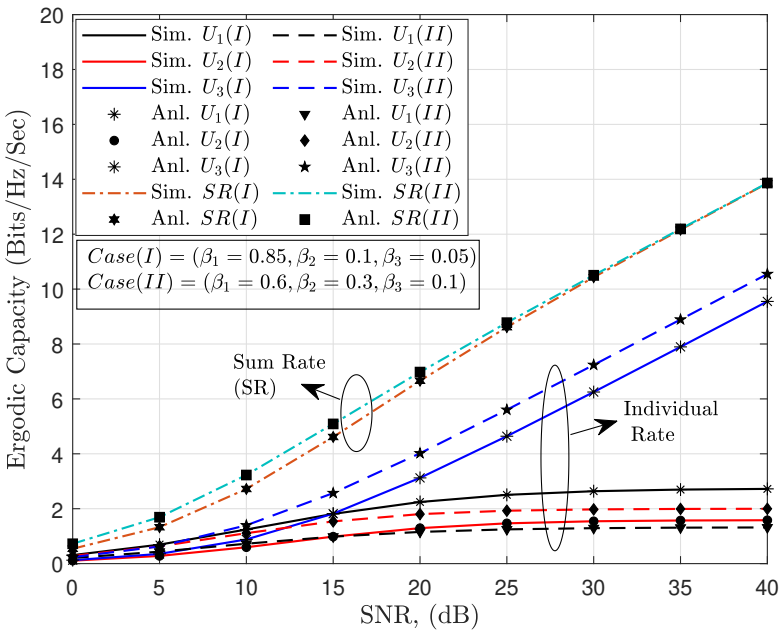

Fig. 4.10 EC versus SNR with fixed values of $\mu = 1$ and $\alpha = 2$ different power allocation β_1 and β_2 Parameters for three NOMA users.

Fig. 4.10 shows the EC performance of three NOMA users over a fixed range of α-μ fading parameters, i.e., $\alpha = 2$ and $\mu = 2$, but with different amount of power allocation. In general, U_3, with the lowest assigned power, exhibits the best capacity performance due to its privileged channel conditions while U_1 attains the lowest EC performance because of its poor channel gain, even though it occupies the large portion of allocated power. Nevertheless, the figure also indicates the EC of sum rate over different assigned channel fading parameters, where the fair performance is gained under the large combination of power allocation components. It clearly indicates to the significant role of power allocation parameters on the overall system performance.

4.6 Chapter Summary

In this chapter, exact analytical closed-forms of OP, BER, and EC for different NOMA users over α-μ fading channels are obtained with the aid of the order statistics and the advanced Fox H-function. Firstly, the OP in two different scenarios where pre-defined target data rates for all users are selected based on their QoS requirements, and when the OMA rate outperforms the NOMA rate for the same case have been evaluated. Then, the error probability for two NOMA users, applying M-QAM higher modulation, are mathematically obtained by averaging their conditional BER probability over the PDFs of their instantaneous SNRs. Then, the EC of NOMA is studied, where other special cases of similar fading models are applied to gain more insightful results. Interestingly, the results revealed that OP with OMA rate outperforms OP with fixed target data rate for all the users. Furthermore, it is noticed that the power allocation factors, fading parameters, and target rates have significant impacts on the overall performance of NOMA systems. Finally, the derived results were validated by simulations and were shown to be perfectly matching.

CHAPTER 5

UAV-Enabled Cooperative NOMA with Indoor-Outdoor users in κ-μ Channels

A. Alqahtani, E. Alsusa, and A. Al-Dweik

Under process to be submitted in: IEEE Internet of Things Journal

Abstract

This work presents performance analyses on cooperative non-orthogonal multiple accesses (C-NOMA) with a half-duplex (HD) and decode-and-forward (DF) relaying enabled by unmanned aerial vehicle (UAV). In particular, two scenarios are considered, an outdoor-indoor one, where the non-orthogonal multiple accesses (NOMA) signal propagates through an outdoor-to-indoor channel, and a conventional outdoor scenario where channel gains follow a κ-μ generalised fading model. The objectives of this work is to analyse the downlink performance of this C-NOMA system and derive closed-form expressions for the outage probability (OP), ergodic capacity (EC), throughput and energy efficiency (EE) for the users assuming imperfect successive interference cancellation (SIC). Specifically, the OP approach considers the individual users' rate where it is required to satisfy certain quality of service (QoS) requirements. The results achieved different insights into the considered performance metrics relative to key parameters such as power allocation, power splitting factor, fading parameters, and residual interference. Extensive simulation results are performed to validate the accuracy of the derived expressions.

Keywords— Non-orthogonal multiple access (NOMA), outage probability (OP), ergodic capacity (EC), κ-μ fading, UAV

5.1 Chapter Introduction

Accommodating the rapid growth of data-intensive wireless applications requires highly innovative solutions to enable efficient utilisation of available radio resources while satisfying various QoS metrics such as data rate, latency, outage, and error rate. Although fifth generation (5G) wireless networks were designed to satisfy these QoS requirements [74, 75], the constant growth of wireless applications prompts the need to find new solutions beyond 5G. To this end, NOMA has emerged as a potential multiple access technology that can fulfil future wireless demands [76]. The fundamental concept of NOMA is to multiplex the data of multiple users through superposition coding (SC) at the transmitter while taking into account the conditions of their channels. In the power domain NOMA, multiple users are assigned the same transmission resources at time and frequency, but different power levels. Therefore, users with better channel conditions may receive less transmit power, and users with poor channel conditions receive more transmit power to achieve fairness. Although weak users can decode their information directly due to the high power assigned, users with less power may use SIC to retrieve their information [77].

5.2 Related Work

There are numerous research studies on NOMA when combined with other concepts such as cooperative transmission and relays UAV. For example, the authors of [5] studied different categories of NOMA focused on key characteristics and challenges. They also provided fundamental comparisons between NOMA and orthogonal multiple access (OMA), where NOMA has been shown to outperform OMA in many popular scenarios. In addition, studies in [78] and [79] investigate the impact of ideal and practical channel state information (CSI) on NOMA systems. In [80], C-NOMA is proposed, where a dedicated relay is applied to improve the capacity and coverage of NOMA users. A C-NOMA proposed in [81] where a couple of HD users decode the received information and efficiently relay it to improve spectral efficiency. The results showed that the proposed scheme outperforms the existing HD and SR schemes in different terms of performance metrics. The authors of [82] proposed several cooperative schemes such as DF relay, known as fixed relaying (FR), selective DF with coordinated direct and relay transmission (SDF-CDRT) and incremental-selective DF (ISDF) relaying. In a study of C-NOMA given in [83], Bariah *et al.* investigated the error rate performance of relay networks based on NOMA with energy harvesting. The results indicate that the overall performance is affected by the selection of different impact factors such as the power splitting coefficient, the location of the relay, and the allocated transmit power. In [84], the authors studied the error rate of C-NOMA-based cognitive

radio networks with partial relay selection, where an exact expression of the pairwise error probability is obtained to evaluate the BER union bound. Moreover, several research studies have been conducted on systems based on the UAV relay C-NOMA. For example, the authors of [85] suggested that a UAV relay flies at a fixed altitude to assist a pair of outdoor users NOMA, and tried to maximise the sum rate of the system considered and the energy harvested at the UAV node. The work in [86] proposed an outdated relay selection algorithm for amplify-and-forward (AF) relay-assisted C-NOMA, where several UAV's are supported to assist outdoor users. The study investigates the impact of outdated coefficients, transmission signal-to-noise ratio (SNR), the number of relays, and the average channel gain components on outage performance. On the other hand, NOMA has been combined with other technologies for indoor environments. Unlike [87] and [88], where NOMA users are distributed entirely in outdoor environments, [89] shows the application of NOMA with indoor visible light communication (VLC), whereby users are distributed in an indoor environment. The study demonstrated a remarkable performance gain over OMA, where all users exhibit realistic conditions with restriction of the illumination design.

The impact of pairing of outdoor users in NOMA has been widely investigated in the literature. For example, the authors in [88] studied the impact of user pairing on two outdoor NOMA users by analysing the sum data rate of two different NOMA schemes known as the fixed NOMA (F-NOMA) and cognitive radio NOMA (CR-NOMA) systems. For F-NOMA, the authors proposed to select a pair of users whose channel conditions are distinctly different. However, for CR-NOMA, the user pairing process depends mainly on channel conditions to prioritise the primary user's QoS and/or fairness. A further study on user pairing NOMA, where the target users are randomly located in a cooperative network with simultaneous wireless information and power transfer (SWIPT), is presented in [90]. The authors proposed three different techniques for user selections based on the distance of the user from the base station. These are known as follows: random near user and random far user (RNRF) pairing, nearest near user and nearest far user (NNNF) pairing, and nearest near user and farthest far user (NNFF) pairing. The results reveal that NNFF outperforms other techniques in terms of low outage and high throughput for both near and far users. Moreover, other recent works, restricted to the deployment of outdoor-to-outdoor channels, introduced some advanced algorithms to efficiently solve the assignment problem of NOMA users. To illustrate, in [91], the authors propose two user pairing algorithms for cooperative NOMA with SWIPT applications. These algorithms are mainly established to minimise the inter-pair interference of the far user caused by zero-forcing beam-forming. In addition, a power allocation scheme is also proposed to guarantee user performance. In the case of multiple NOMA users, the study in [92] aims to improve the spectral efficiency, data rate, fairness and outage probability of multiple NOMA users by proposing two sub-carrier

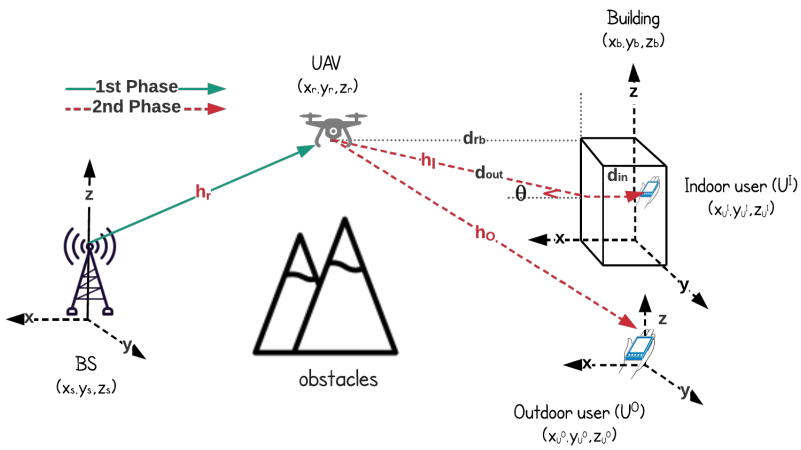

Fig. 5.1 System Model Under consideration with indoor and outdoor user positioning.

user assignment algorithms (SUAAs). The pairing procedure of both algorithms is predominantly determined by increasing the channel conditions of the designated paired users per sub-carrier to improve the data rate of each individual user. The results of that work show significant improvements over other proposed algorithms by achieving high spectral efficiency, data rate, and outage probability performance. Another study on user pairing that considered the NOMA based UAV system is presented in [93]. The authors optimised power allocation, user pairing, and UAV placement to maximise the minimum sum rate for each selected pair of users. The results illustrate the key importance of optimising the placement of UAV, where the proposed heuristic user pairing algorithm offers close performance to the optimal solution.

5.3 System Model

This work considers a communications system in which a UAV-relay is deployed to assist the communications between a terrestrial base station (BS) and two far NOMA users deployed in two environments, an indoor user ($\mathcal{I}$), and an outdoor user ($\mathcal{O}$). This system model can exist when both users are beyond the coverage of BS due to large obstacles in the path of the signal, or in an emergency case, when the ground infrastructures are hampered due to a natural event such as an earthquake. It is assumed that all terminals are equipped with a single antenna, and the entire transmission process is carried out in two different time slots, where the relay node applies the HD protocol. As depicted in Fig. 5.1, the intention is to concentrate on the downlink scenario of the C-NOMA system. It is also assumed that $\mathcal{I}$ is located inside a building that has location coordinates identified by (x_b, y_b, z_b). Similarly, each assigned user is located at different coordinates known as (x_i, y_i, z_i), where $i \in \{\mathcal{I}, \mathcal{O}\}$. Furthermore, the location coordinates for the BS and the UAV-relay are (x_s, y_s, z_s), and

(x_r, y_r, z_r), respectively. Thus, the distances between BS and UAV can be calculated as $d_{\text{sr}} = \sqrt{(x_s - x_r)^2 + (y_s - y_r)^2 + (z_s - z_r)^2}$. Similarly, the distance between UAV and the user i is given by $d_{\text{ri}} = \sqrt{(x_r - x_i)^2 + (y_r - y_i)^2 + (z_r - z_i)^2}$.

5.3.1 Channel and Path Loss Models

Without loss of generality, it is assumed that all adopted wireless channels are independent and identically distributed (i.i.d.) and follow the general κ-μ fading model [94]. It is also assumed that all CSI are available at BS. Without loss of generality, the channel coefficients between BS and all nodes are considered to be in ascending order as $|h_{\mathcal{I}}| \leq |h_{\mathcal{O}}| \leq |h_r|$, where the effects of path loss (PL) and small-scale fading (g_i) are given as $|h_i| = \frac{g_i}{\sqrt{PL_i}}$ and $i \in \{\mathcal{I}, \mathcal{O}, r\}$, [95]. In particular, g_i is modelled as κ-μ fading in this work. According to Fig. 5.1, the NOMA signal is transported over two transmission phases via a UAV relay, operated in HD mode [1], to reach both users. The first phase is established between the air-to-air channel, that is, h_r, which only has the impact of a basic loss of outdoor transmission, where the transmitted signal has a high opportunity to work in a scenario line of sight (LOS). This particular large-scale path loss is assumed to follow the free space path loss model given in [96] as

$$PL_r = 32.45 + 20\log_{10}(d_{sr}) + 20\log_{10}(f) \tag{5.1}$$

where d_{sr} is the Euclidean distance between the BS and UAV-relay nodes, and f is the frequency. On the other hand, the second phase occurs over the air-to-ground channels, i.e, $h_{\mathcal{I}}$ and $h_{\mathcal{O}}$, where $\mathcal{O}$ is assumed to have a LOS path with a UAV-relay, which causes only outdoor transmission loss. Thus, the transmission loss between the UAV and $\mathcal{O}$ is described by the free-space path-loss model as

$$PL_{\mathcal{O}} = 32.45 + 20\log_{10}(d_{r\mathcal{O}}) + 20\log_{10}(f). \tag{5.2}$$

The signal that fades from UAV to $\mathcal{I}$ shows a loss of the path from outdoor to indoor. It is assumed that the wall of the building has LOS with the transmitting antenna of UAV. An empirical propagation model of penetration loss in buildings COST 231 [96] is applied. This particular model can efficiently describe the propagation path loss for the indoor user by considering two major transmission path losses characterised by large-scale path loss and the indoor transmission path loss, which includes the building penetration loss and the indoor propagation loss. Thus, the total path loss for $\mathcal{I}$ can be calculated as

$$PL_{\mathcal{I}} = L_{fs} + L_t + L_{in} \tag{5.3}$$

[1] Half duplex (HD) mode is applied to simplify the analysis. Studying different relay protocols is out of the scope of this thesis.

where L_{fs} indicates the loss of the free space path. It can be given as in (5.1) with respect to the measured distance of $(d_{rb} + d_{in})$, where d_{in} is the distance between the wall of the building and $\mathcal{I}$, and $d_{r\mathcal{I}}$ is the distance between the wall of UAV and the external wall of the building. Furthermore, L_t is defined as the loss of path of transition propagation that includes the perpendicular loss L_{pc} and the parallel penetration loss L_{pt}. It can be presented as

$$L_t = L_{pc} + L_{pt} \times (1 - \sin(\theta))^2 \tag{5.4}$$

where θ is the grazing angle between the UAV and the exterior building wall, which can be given as $\theta = \cos^{-1}(d_{rb}/d_{out})$. In addition, the indoor propagation path-loss, L_{in}, is defined by the mean path-loss determined from the internal side of the exterior wall, which can be computed as

$$L_{in} = \max\{n\, L_i, \chi(d_{in} - 2)(1 - \sin(\theta))^2\} \tag{5.5}$$

where n is the number of internal walls, L_i defines the loss in the internal walls, and χ is the indoor path-loss parameter. Typical values for this model parameters are given in table 5.1. In this chapter, it is assumed that the link between UAV and $\mathcal{I}$ behaves more like non-line of sight (NLOS) since the signal must pass through the wall, so we believe that signal fading is more compatible with Rayleigh fading. It can be achieved as a special case of κ-μ generalised fading. We also tried to test $\mathcal{I}$ under various fading parameters of the κ-μ channel to obtain more insights.

5.4 Performance Analysis

5.4.1 Signal to Interference and Noise Ratio (SINR)

It is assumed that a fixed power allocation technique is applied in this work where α_j, $\forall j \in \{1, 2\}$, is subject to $\alpha_1 + \alpha_2 = 1$ and $\alpha_2 < \alpha_1$. In addition, α_1 and α_2 are respectively indicated for the power allocation factors of $\mathcal{I}$ and $\mathcal{O}$. In the first time interval, the observation received at UAV can be expressed as

$$y_r = h_r \times \underbrace{\left(\sqrt{\alpha_1 \mathcal{P}_{\mathrm{s}}} x_1 + \sqrt{\alpha_2 \mathcal{P}_{\mathrm{s}}} x_2\right)}_{x_{sc}} + n_r \tag{5.6}$$

where $\mathcal{P}_{\mathrm{s}}$ is the total transmitted power at BS, and x_{sc} represents the superposed signal in the first time interval where x_1 and x_2 represent the information symbols of $\mathcal{I}$ and $\mathcal{O}$, respectively, n_r indicates additive white Gaussian noise (AWGN), where $n_r \sim \mathcal{CN}(0, \sigma_r^2)$. In this work, the noise power of both users is assumed to be identi-

cal. In the first transmission phase, the UAV-relay node attempts to detect and decode the received signal for both users by performing SIC. Thereafter, it regenerates a new superimposed signal scaled with the new energy gained from UAV and forwards it to the nominated users as a second phase of communication. In order to enhance the user fairness, conventional power allocation is proposed in both time slots, i.e., $\alpha_1 > \alpha_2$, where α_1 + α_2 = 1. Since more power is assigned to the $\mathcal{I}$ symbol to ensure user fairness, the relay in the first time slot initially detects the x_1 symbol by treating the x_2 symbol as unknown additive noise. Therefore, the maximum likelihood (ML) detection of the x_1 symbol on the relay is given as

$$\hat{x}_1 = \arg\min_{x_1 \in \mathbb{S}} \left| y_r - \sqrt{\alpha_1 \mathcal{P}_{\mathrm{s}}} h_r x_1 \right|^2 \tag{5.7}$$

where the estimated symbol $\hat{x}_1$ belongs to the set $\mathbb{S}$ of all possible constellation points for $\mathcal{I}$. Therefore, Signal to Interference and Noise Ratio (SINR) at the UAV-relay to detect x_1 can be expressed as

$$\gamma_r^{x_1} = \frac{\alpha_1 \mathcal{P}_{\mathrm{s}} |h_r|^2}{\alpha_2 \mathcal{P}_{\mathrm{s}} |h_r|^2 + \sigma_r^2} = \frac{\alpha_1 \gamma_r}{\alpha_2 \gamma_r + 1} \tag{5.8}$$

where $\gamma_r \triangleq \rho_r |h_r|^2$ and $\rho_r = \frac{\mathcal{P}_{\mathrm{s}}}{\sigma_r^2}$, which is the transmitted SNR for the link between BS and UAV. On the other hand, SIC is applied to the relay to detect x_2. Therefore, ML detection of the symbol x_2 for $\mathcal{O}$ is given as

$$\hat{x}_2 = \arg\min_{x_2 \in \mathbb{S}} \left| \acute{y}_r - \sqrt{\alpha_2 \mathcal{P}_{\mathrm{s}}} h_r x_2 \right|^2 \tag{5.9}$$

where $\hat{x}_2$ is the estimated symbol of $\mathcal{O}$ and $\acute{y}_r = \left(y_r - \sqrt{\alpha_1 \mathcal{P}_{\mathrm{s}}} h_r x_1\right)$. It is readily apparent that the remaining residual signal after applying SIC is based mainly on the detection of the symbol x_1. Therefore, the SINR at the UAV-relay to detect x_2 can be given as

$$\gamma_r^{x_2} = \frac{\alpha_2 \mathcal{P}_{\mathrm{s}} |h_r|^2}{\eta \alpha_1 \mathcal{P}_{\mathrm{s}} |h_r|^2 + \sigma_r^2} = \frac{\alpha_2 \gamma_r}{\eta \alpha_1 \gamma_r + 1} \tag{5.10}$$

where the variable η indicates the effect coefficient of the incorrect SIC, where $\eta = 0$ represents the case of perfect SIC and $\eta = 1$ represents the case of completely failed SIC.

In the second time slot, the UAV-relay forwards the decoded signal to both users' destinations. Therefore, the signal received from the indoor user $\mathcal{I}$ can be expressed as

$$y^{\mathcal{I}} = h_{\mathcal{I}} \times \underbrace{\left(\sqrt{\alpha_1 \mathcal{P}_{\mathrm{r}}} x_1 + \sqrt{\alpha_2 \mathcal{P}_{\mathrm{r}}} x_2\right)}_{x_{sc}{}^{(3)}} + n_{\mathcal{I}} \tag{5.11}$$

where $\mathcal{P}_{\mathrm{r}}$ is the new total transmitted power at the UAV, and ${x_{sc}}^{(3)}$ represents the signal imposed in the second time interval, where x_1 and x_2 refer to the $\mathcal{I}$ and $\mathcal{O}$ information, respectively. $n_{\mathcal{I}}$ indicates the AWGN, where $n_{\mathcal{I}} \sim \mathcal{CN}(0, \sigma_{\mathcal{I}}^2)$. In particular, it is assumed that $\mathcal{O}$ communicates with the UAV relay in better channel conditions than the indoor user $\mathcal{I}$, so $\mathcal{O}$ is allocated less power. Consequently, $\mathcal{I}$ detects its own symbol, x_1, by considering the x_2 symbol as unknown additive noise. Therefore, the detection of ML in $\mathcal{I}$ is expressed as

$$\hat{x}_1 = \arg\min_{x_1 \in \mathbb{S}} \left| y^{\mathcal{I}} - \sqrt{\alpha_1 \mathcal{P}_{\mathrm{r}}} h_{\mathcal{I}} x_1 \right|^2. \tag{5.12}$$

Therefore, SINR of $\mathcal{I}$, in the second time slot, to detect the symbol x_1 is calculated as

$$\gamma_{\mathcal{I}}^{x_1} = \frac{\alpha_1 \mathcal{P}_{\mathrm{r}} |h_{\mathcal{I}}|^2}{\alpha_2 \mathcal{P}_{\mathrm{r}} |h_{\mathcal{I}}|^2 + \sigma_{\mathcal{I}}^2} = \frac{\alpha_1 \gamma_{\mathcal{I}}}{\alpha_2 \gamma_{\mathcal{I}} + 1} \tag{5.13}$$

where $\gamma_{\mathcal{I}} \triangleq \rho_{\mathcal{I}} |h_{\mathcal{I}}|^2$ and $\rho_{\mathcal{I}} \triangleq \mathcal{P}_{\mathrm{r}} / \sigma_{\mathcal{I}}^2$ is the SNR of the link between UAV and $\mathcal{I}$. On the other hand, the received signal at the $\mathcal{O}$ node is expressed as

$$y^{\mathcal{O}} = h_{\mathcal{O}} \times \underbrace{\left(\sqrt{\alpha_1 \mathcal{P}_{\mathrm{r}}} x_1 + \sqrt{\alpha_2 \mathcal{P}_{\mathrm{r}}} x_2 \right)}_{{x_{sc}}^{(4)}} + n_{\mathcal{O}}. \tag{5.14}$$

And the corresponding ML detection of x_1 symbol at $\mathcal{O}$ is

$$\hat{x}_1 = \arg\min_{x_1 \in \mathbb{S}} \left| y^{\mathcal{O}} - \sqrt{\alpha_1 \mathcal{P}_{\mathrm{r}}} h_{\mathcal{O}} x_1 \right|^2 \tag{5.15}$$

Thus, SINR of $\mathcal{O}$ to detect the x_1 symbol at the first level of the SIC process can be given as

$$\gamma_{\mathcal{O}}^{x_1 \to x_2} = \frac{\alpha_1 \mathcal{P}_{\mathrm{r}} |h_{\mathcal{O}}|^2}{\alpha_2 \mathcal{P}_{\mathrm{r}} |h_{\mathcal{O}}|^2 + \sigma_{\mathcal{O}}^2} = \frac{\alpha_1 \gamma_{\mathcal{O}}}{\alpha_2 \gamma_{\mathcal{O}} + 1}. \tag{5.16}$$

where $\gamma_{\mathcal{O}} \triangleq \rho_{\mathcal{O}} |h_{\mathcal{O}}|^2$ and $\rho_{\mathcal{O}} \triangleq \mathcal{P}_{\mathrm{r}} / \sigma_{\mathcal{O}}^2$ is the SNR of the link between UAV and $\mathcal{O}$. Similarly, the ML detection for the x_2 symbol at the same destination can also be written as

$$\hat{x}_2 = \arg\min_{x_2 \in \mathbb{S}} \left| \acute{y}^{\mathcal{O}} - \sqrt{\alpha_2 \mathcal{P}_{\mathrm{r}}} h_{\mathcal{O}} x_2 \right|^2 \tag{5.17}$$

where $\acute{y}^{\mathcal{O}} = \left(y^{\mathcal{O}} - \sqrt{\alpha_1 \mathcal{P}_{\mathrm{s}}} h_{\mathcal{O}} x_1 \right)$. Thus, the corresponding SINR to detect x_2 in $\mathcal{O}$ is defined as

$$\gamma_{\mathcal{O}}^{x_2} = \frac{\alpha_2 \mathcal{P}_{\mathrm{r}} |h_{\mathcal{O}}|^2}{\eta |h_{\mathcal{O}}|^2 \alpha_1 \mathcal{P}_{\mathrm{r}} + \sigma_{u_2}^2} = \frac{\alpha_2 \gamma_{\mathcal{O}}}{\eta \alpha_1 \gamma_{\mathcal{O}} + 1}. \tag{5.18}$$

5.4.2 Outage Probability (OP)

5.4.2.1 Outage Probability (OP) of The Indoor User:

The probability of outage of $\mathcal{I}$ using a UAV relay in the absence of a direct link from BS can be addressed as follows.

Proposition 6.

$$\mathrm{P}^{\mathcal{I}} = 1 - \prod_{i=1}^{2} \left(1 - \frac{1}{\mathrm{e}^{(\mu\kappa)}} \sum_{n=0}^{\infty} \frac{(\kappa\mu)^n}{n!\,\Gamma(n+\mu)} \times \mathrm{H}_{1,2}^{1,1} \left[\frac{\mu(1+\kappa)\varepsilon_{1,i}}{\bar{\gamma}_{1,i}} \middle| \begin{matrix} (1,1) \\ (n+\mu,1),(0,1) \end{matrix} \right] \right) \tag{5.19}$$

where γ_{inc} is the incomplete gamma function.

Proof. The indoor user outage events $\mathcal{I}$ occur if the following are satisfied. First, when the UAV-relay decodes the signal x_1 incorrectly in the first time interval. Second, when $\mathcal{I}$ fails to decode its own signal in the second time slot. Therefore, the probability of an outage of $\mathcal{I}$ can be expressed as

$$\mathrm{P}^{\mathcal{I}} = 1 - \mathcal{P}_{\mathrm{r}}\left(\gamma_r^{x_1} > \gamma_{th_1}, \gamma_{\mathcal{I}}^{x_1} > \gamma_{th_1}\right) = 1 - \left[(1 - \underbrace{\mathcal{P}_{\mathrm{r}}\left(\gamma_r^{x_1} < \gamma_{th_1}\right)}_{E_{11}})(1 - \underbrace{\mathcal{P}_{\mathrm{r}}\left(\gamma_{\mathcal{I}}^{x_1} < \gamma_{th_1}\right)}_{E_{12}}) \right] \tag{5.20}$$

where $\gamma_{th_1} = 2^{2R_{\mathcal{I}}} - 1$, and $R_{\mathcal{I}}$ is the target data rate of $\mathcal{I}$. Thus, substituting (5.8) into E_{11} gives the following expression.

$$E_{11} = \mathcal{P}_{\mathrm{r}}\left(\gamma_r^{x_1} < \gamma_{th_1}\right) = \mathcal{P}_{\mathrm{r}}\left(\gamma_0 < \frac{\gamma_{th_1}}{(\alpha_1 - \alpha_2\gamma_{th_1})} \triangleq \varepsilon_{1,1}\right) = F_{\gamma}\left(\varepsilon_{1,1}\right). \tag{5.21}$$

By substituting (2.12) into (5.21) to compute the first term of (5.20), we obtain the following

$$E_{11} = \frac{1}{\mathrm{e}^{(\mu\kappa)}} \sum_{n=0}^{\infty} \psi\, \gamma_{inc}\left(n+\mu\,,\ \frac{\mu(1+\kappa)\varepsilon_{1,1}}{\bar{\gamma}_{1,1}}\right) \tag{5.22}$$

where $\psi = \frac{(\kappa\mu)^n}{n!\,\Gamma(n+\mu)}$, and $\tilde{\gamma}_{1,1}$ indicates the average power link between BS and the UAV-relay. Similarly, E_{12} in (5.20) can be evaluated by recalling (5.13) and (2.12) as follows,

$$E_{12} = \mathcal{P}_{\mathrm{r}}\left(\gamma_{\mathcal{I}}^{x_1} < \gamma_{th_1}\right) = \mathcal{P}_{\mathrm{r}}\left(\gamma_1 < \frac{\gamma_{th_1}}{(\alpha_1 - \alpha_2\gamma_{th_1})} \triangleq \varepsilon_{1,2}\right) = F_{\gamma}\left(\varepsilon_{1,2}\right). \tag{5.23}$$

Therefore, (5.23) is regenerated as

$$E_{12} = \frac{1}{\mathrm{e}^{(\mu\kappa)}} \sum_{n=0}^{\infty} \psi \, \gamma_{inc} \left(n + \mu \, , \, \frac{\mu(1+\kappa)\varepsilon_{1,2}}{\bar{\gamma}_{1,2}} \right) \tag{5.24}$$

where $\tilde{\gamma}_{1,2}$ is the average power link between the UAV-relay and $\mathcal{I}$. By substituting (5.22) and (5.24) into (5.20) and applying some of the identities of the Meijer G and H functions given in [72, pp. 8.3.2.21, 8.4.16], we obtain Proposition 1. Hence, the proof is complete. □

5.4.2.2 Outage Probability (OP) of The Outdoor User

The outage probability of $\mathcal{O}$ when using UAV-relay over κ-μ fading channels can be calculated as follows.

Proposition 7.

$$\mathrm{P}^{\mathcal{O}} = 1 - \prod_{i=1}^{4} \left(1 - \frac{1}{\mathrm{e}^{(\mu\kappa)}} \sum_{n=0}^{\infty} \frac{(\kappa\mu)^n}{n! \, \Gamma(n+\mu)} \times \mathrm{H}_{1,2}^{1,1} \left[\frac{\mu(1+\kappa)\varepsilon_{2,i}}{\bar{\gamma}_{2,i}} \middle| \begin{matrix} (1,1) \\ (n+\mu,1),(0,1) \end{matrix} \right] \right) \tag{5.25}$$

where $\varepsilon_{2,1} = \varepsilon_{2,3} = \varepsilon_{1,1}$, and $\varepsilon_{2,2} = \varepsilon_{2,4} = \frac{\gamma_{th_2}}{(\alpha_2 - \eta\alpha_1\gamma_{th_1})}$. The average power link between BS and the UAV relay is $(\bar{\gamma}_{2,1} \, , \, \bar{\gamma}_{2,2})$, and between the UAV relay and $\mathcal{O}$ is $(\bar{\gamma}_{2,3} \, , \, \bar{\gamma}_{2,4})$, where $(\bar{\gamma}_{1,1} = \bar{\gamma}_{2,1} = \bar{\gamma}_{2,2})$ and $(\bar{\gamma}_{2,3} = \bar{\gamma}_{2,4})$.

Proof. Outdoor user outages, $\mathcal{O}$, occur on different occasions. First, when the UAV-relay incorrectly decodes the signal x_1 or x_2 in the first time slot. Second, when $\mathcal{O}$ cannot detect x_1 or x_2 after SIC in the second time slot. In other words, the probability of outage of $\mathcal{O}$ is based mainly on the successful decoding of the signal x_1 and x_2 over both the links from BS to UAV and from UAV to $\mathcal{O}$ after applying the SIC process, which can be expressed as

$$\mathrm{P}^{\mathcal{O}} = 1 - \underbrace{\mathcal{P}_{\mathrm{r}}\left(\gamma_r^{x_1} > \gamma_{th_1}\right)}_{E_{21}} \underbrace{\mathcal{P}_{\mathrm{r}}\left(\gamma_r^{x_2} > \gamma_{th_2}\right)}_{E_{22}} \underbrace{\mathcal{P}_{\mathrm{r}}\left(\gamma_{\mathcal{O}}^{x_1 \to x_2} > \gamma_{th_1}\right)}_{E_{23}} \underbrace{\mathcal{P}_{\mathrm{r}}\left(\gamma_{\mathcal{O}}^{x_2} > \gamma_{th_2}\right)}_{E_{24}} \tag{5.26}$$

where $\gamma_{th_2} = 2^{2R_{\mathcal{O}}} - 1$, and $R_{\mathcal{O}}$ is the target data rate of $\mathcal{O}$. Therefore, $E_{11} = E_{21}$. In order to omit the redundancy, the remaining events can be evaluated in a similar fashion to the aforementioned derivation from (5.20)-(5.24) with respect to their values SINR. Therefore, the proof is complete. □

To gain more insight into the impact of channel components on OP performance, we provide an asymptotic analysis, where OP can be determined under high SNR conditions, such as $(\bar{\gamma} \to \infty)$. We aim to apply an approximation for the modified Bessel

function of the first kind, mentioned in (2.9), as given in [97].

$$\mathrm{I}_v(u) \approx \frac{(u/2)^v}{\Gamma(v+1)} \quad 0 < |u| < \sqrt{v+1} \tag{5.27}$$

Under the high SNR scenario, that is, ($\bar{\gamma} \to \infty$) and $\left(2\mu\sqrt{\frac{\kappa(1+\kappa)\gamma}{\bar{\gamma}}} \to 0\right)$, and after considering (5.27), the modified Bessel function in (2.9) can be rewritten as follows.

$$\mathrm{I}_{\mu-1}\left(2\mu\sqrt{\frac{\kappa(1+\kappa)\gamma}{\bar{\gamma}}}\right) \approx \frac{\left(\mu\sqrt{\frac{\kappa(1+\kappa)\gamma}{\bar{\gamma}}}\right)^{(\mu-1)}}{\Gamma(\mu)} \tag{5.28}$$

Substituting (5.28) into (2.9) and following the similar approach of Sections 5.4.2.1 and 5.4.2.2 lead to the final asymptotic OP of both users.

5.4.3 Ergodic Capacity (EC)

It is known that EC can be computed by averaging the PDF of a fading channel over the AWGN capacity, given in [6] as

$$\bar{C}_i = \mathrm{B} \times \int_0^\infty \log_2(1+\gamma_i) f_{\gamma_i}(\gamma_i) d\gamma_i \tag{5.29}$$

where $i \in \{\mathcal{I}, \mathcal{O}\}$. Due to the fact that the overall capacity of a DF-relay-based system is described by the weakest link capacity, EC at $\mathcal{I}$ or $\mathcal{O}$ can be determined by the minimum capacity over the total links, i.e., the link from BS to the UAV-relay and the link between the UAV-relay to the user's destination, [98]. Therefore, we assume that the link between the UAV-relay to the user's destination is the weakest link. Therefore, we are interested in calculating EC at each user node.

Proposition 8. The average channel capacity of $\mathcal{I}$ is given as

$$\begin{aligned}\bar{C}_{\mathcal{I}} = &\frac{\mathrm{B}}{\ln(2)\, e^{(\mu\kappa)}} \sum_{n=0}^{\infty} \frac{\mu^{2n+\mu}\, \kappa^n\, (1+\kappa)^{n+\mu}}{n!\, \Gamma(n+\mu)\, \bar{\gamma}_{\mathcal{I}}^{(n+\mu)}} \\ &\times \left(\mathrm{H}_{2,3}^{3,1}\left[\frac{\mu(1+\kappa)}{\bar{\gamma}_{\mathcal{I}}} \middle| \begin{matrix} (-(n+\mu),1),(1-(n+\mu),1) \\ (0,1),(-(n+\mu),1),(-(n+\mu),1) \end{matrix}\right] \right. \\ &\left. - (\alpha_2)^{-(n+\mu)} \times \mathrm{H}_{2,3}^{3,1}\left[\frac{\mu(1+\kappa)}{\alpha_2\bar{\gamma}_{\mathcal{I}}} \middle| \begin{matrix} (-(n+\mu),1),(1-(n+\mu),1) \\ (0,1),(-(n+\mu),1),(-(n+\mu),1) \end{matrix}\right] \right)\end{aligned} \tag{5.30}$$

Proof. Substituting (5.13) into (5.29) gives

$$\bar{C}_I = \mathrm{B} \times \int_0^\infty \log_2\left(1 + \frac{\alpha_1\gamma_{\mathcal{I}}}{\alpha_2\gamma_{\mathcal{I}}+1}\right) f_{\gamma_{\mathcal{I}}}(\gamma_{\mathcal{I}}) d\gamma_{\mathcal{I}}. \tag{5.31}$$

With the help of the identity $\log_e(x) = \ln(x)/\ln(e)$ and some algebraic manipulations, (5.31) can be split into parts as

$$\bar{C}_I = \frac{\mathrm{B}}{\ln(2)} \left[\underbrace{\int_0^\infty \ln\left(1+\gamma_{\mathcal{I}}\right) f_{\gamma_{\mathcal{I}}}(\gamma_{\mathcal{I}}) d\gamma_{\mathcal{I}}}_{\mathrm{A}_1} - \underbrace{\int_0^\infty \ln\left(1+\alpha_2\gamma_{\mathcal{I}}\right) f_{\gamma_{\mathrm{I}}}(\gamma_{\mathcal{I}}) d\gamma_{\mathcal{I}}}_{\mathrm{A}_2} \right]. \quad (5.32)$$

By substituting (2.10) into the first integral of (5.32), and applying further manipulations, the following is produced:

$$\mathrm{A}_1 = \frac{1}{e^{(\mu\kappa)}} \sum_{n=0}^{\infty} \frac{\mu^{2n+\mu}\,\kappa^n\,\left(1+\kappa\right)^{n+\mu}}{n!\,\Gamma(n+\mu)\,\bar{\gamma}_{\mathcal{I}}^{(n+\mu)}} \int_0^\infty \gamma_{\mathcal{I}}^{(n+\mu-1)} \exp\left(-\frac{\gamma_{\mathcal{I}}\mu(1+\kappa)}{\bar{\gamma}_{\mathcal{I}}}\right) \ln\left(1+\gamma_{\mathcal{I}}\right) d\gamma_{\mathcal{I}}. \quad (5.33)$$

In order to solve the above integral, we need to transform exponential and logarithmic functions into their corresponding Meijer G function representations defined in [99, pp. 8.4.3.1, 8.4.6.5]. The equivalent form of the Meijer G function is applied by calling the Fox H function given in [13, p. 6.2.8]. Thus,

$$\mathrm{A}_1 = \frac{1}{e^{(\mu\kappa)}} \sum_{n=0}^{\infty} \frac{\mu^{2n+\mu}\,\kappa^n\,\left(1+\kappa\right)^{n+\mu}}{n!\,\Gamma(n+\mu)\,\bar{\gamma}_{I}^{(n+\mu)}} \times \int_0^\infty \gamma_{\mathcal{I}}^{(n+\mu-1)}\ \mathrm{H}_{0,1}^{1,0}\left[\frac{\gamma_{\mathcal{I}}\mu(1+\kappa)}{\bar{\gamma}_{\mathcal{I}}}\middle| \begin{matrix} - \\ (0,1) \end{matrix}\right]$$
$$\times\, \mathrm{H}_{2,2}^{1,2}\left[\gamma_{\mathcal{I}}\middle| \begin{matrix} (1,1),(1,1) \\ (1,1),(0,1) \end{matrix}\right] d\gamma_{\mathcal{I}}. \quad (5.34)$$

Applying the identity in [6] gives the following.

$$\mathrm{A}_1 = \frac{1}{e^{(\mu\kappa)}} \sum_{n=0}^{\infty} \frac{\mu^{2n+\mu}\,\kappa^n\,\left(1+\kappa\right)^{n+\mu}}{n!\,\Gamma(n+\mu)\,\bar{\gamma}_{\mathcal{I}}^{(n+\mu)}}$$
$$\times\, \mathrm{H}_{2,3}^{3,1}\left[\frac{\mu(1+\kappa)}{\bar{\gamma}_{\mathcal{I}}}\middle| \begin{matrix} (-(n+\mu),1),(1-(n+\mu),1) \\ (0,1),(-(n+\mu),1),(-(n+\mu),1) \end{matrix}\right]. \quad (5.35)$$

Similarly, the second integral of (5.32) is evaluated by following the above steps, which gives the following expression.

$$\mathrm{A}_2 = \frac{1}{e^{(\mu\kappa)}} \sum_{n=0}^{\infty} \frac{\mu^{2n+\mu}\,\kappa^n\,\left(1+\kappa\right)^{n+\mu}\left(\alpha_2\right)^{-(n+\mu)}}{n!\,\Gamma(n+\mu)\,\bar{\gamma}_{\mathcal{I}}^{(n+\mu)}}$$
$$\mathrm{H}_{2,3}^{3,1}\left[\frac{\mu(1+\kappa)}{\alpha_2\bar{\gamma}_{\mathcal{I}}}\middle| \begin{matrix} (-(n+\mu),1),(1-(n+\mu),1) \\ (0,1),(-(n+\mu),1),(-(n+\mu),1) \end{matrix}\right]. \quad (5.36)$$

Ultimately, we substitute (5.35) and (5.36) into (5.32), which produces the final expression of EC of $\mathcal{I}$ as stated in Prop. 3, and the proof is complete. □

Proposition 9. The average channel capacity of the $\mathcal{O}$ NOMA user is given as

$$\bar{C}_{\mathcal{O}} = \frac{\mathrm{B}}{\ln(2)\, e^{(\mu\kappa)}} \sum_{n=0}^{\infty} \frac{\mu^{2n+\mu}\, \kappa^{n}\, (1+\kappa)^{n+\mu}}{n!\, \Gamma(n+\mu)\, \bar{\gamma}_{\mathcal{O}}^{(n+\mu)}} \times \left((\eta\alpha_1 + \alpha_2)^{-(n+\mu)} \times \mathrm{H}_{2,3}^{3,1} \left[\frac{\mu(1+\kappa)}{(\eta\alpha_1+\alpha_2)\,\bar{\gamma}_{\mathcal{O}}} \middle| \begin{matrix} (-(n+\mu),1),(1-(n+\mu),1) \\ (0,1),(-(n+\mu),1),(-(n+\mu),1) \end{matrix} \right] - (\eta\alpha_1)^{-(n+\mu)} \times \mathrm{H}_{2,3}^{3,1} \left[\frac{\mu(1+\kappa)}{\eta\alpha_1\bar{\gamma}_{\mathcal{O}}} \middle| \begin{matrix} (-(n+\mu),1),(1-(n+\mu),1) \\ (0,1),(-(n+\mu),1),(-(n+\mu),1) \end{matrix} \right] \right). \tag{5.37}$$

5.4.4 Throughput Analysis

The system throughput of each user in a delay-limited transmission mode can be evaluated by its probability of outage or EC. Therefore, the corresponding outage throughput of a two-user NOMA system is given as in [100] as follows.

$$\mathrm{T}_i^{\mathrm{OP}} = \left(1 - \mathrm{P}^{\mathrm{i}}\right) \times R_i \tag{5.38}$$

where $i \in \{\mathcal{I}, \mathcal{O}\}$, R is the user data target rate. Therefore, we substitute (5.19) and (5.25) in (5.38) to obtain the throughput of $\mathcal{I}$ and $\mathcal{O}$, respectively.

5.4.5 Energy Efficiency (EE)

The EE for a delay-limited system can be defined as the ratio of EC and the total power consumption of the system. Therefore, EE can be given as in [101]

$$EE = \frac{R_{\text{total}}}{\mathrm{P}_{\text{total}}} = \frac{\bar{C}_{\mathcal{I}} + \bar{C}_{\mathcal{O}}}{\delta(\alpha_1\mathcal{P}_{\mathrm{r}} + \alpha_2\mathcal{P}_{\mathrm{r}}) + \mathrm{P}_c - E_{\text{total}}} \tag{5.39}$$

where δ indicates the efficiency of the energy amplifier, $\tilde{C}_{\mathcal{I}}$ and $\tilde{C}_{\mathcal{O}}$ are given in (5.30) and (5.37), respectively. $\mathcal{P}_{\mathrm{c}}$ is known as the circuit power, and E_{total} is the overall power of the considered system, which can be expressed as

$$E_{\text{total}} = \delta \sum_{i} \left(\mathbb{E}[|h_i|^2] \sum_{j=1}^{2} \alpha_j \mathcal{P}_{\mathrm{r}} \right) \tag{5.40}$$

where $i \in \{\mathcal{I}, \mathcal{O}\}$ and $j \in \{1, 2\}$.

Table 5.1 Simulation Parameters.

Parameter	Value	Parameter	Value
Transmit power ($\mathcal{P}_{\rm s}$)	$(-40-40)$ dBm	Coordinates of the BS $(\mathring{x}_{\rm s}, \mathring{y}_{\rm s}, \mathring{z}_{\rm s})$	$(0, 0, 35)$m
Carrier Frequency (f)	900 MHz	Coordinates of the UAV-relay $(\mathring{x}_{\rm r}, \mathring{y}_{\rm r}, \mathring{z}_{\rm r})$	$(400, 20, 80)$m
System bandwidth (B)	1 MHz	Coordinates of the building$(\mathring{x}_{\rm b}, \mathring{y}_{\rm b}, \mathring{z}_{\rm b})$	$(1500, 98, 35)$m
Noise power (σ)	-174 dBm	Coordinates of $\mathcal{I}$ $(x_{\mathcal{I}}, y_{\mathcal{I}}, z_{\mathcal{I}})$	$(1502, 100, 3)$m
Target data rates ($R_{\mathcal{I}}$,$R_{\mathcal{O}}$)	(0.5,1.5) b/s/Hz	Coordinates of $\mathcal{O}$ $(x_{\mathcal{O}}, y_{\mathcal{O}}, z_{\mathcal{O}})$	$(1502, 50, 3)$m
Power allocation factor of $\mathcal{I}$ (α_1)	0.9	Indoor distance of $\mathcal{I}$ (d_{in})	2m
Indoor path loss parameter (χ)	0.6 dB/m	Perpendicular loss (L_{pc})	7 dB
Circuit power ($\mathcal{P}_{\rm c}$)	5 Watt	Loss of internal walls (L_i)	7 dB
Parallel penetration loss (L_{pt})	20 dB	Number of internal walls (n)	1
Energy amplifier efficiency (δ)	85%		

5.5 Results and Discussion

The parameters used in this section are presented in table 5.1. The channel coefficients have κ-μ distribution, which are generated as described in [102]. The channel is considered quasi-static where it remains fixed during the duration of one symbol, but changes randomly over consecutive symbol intervals. In each simulation run, we generate 10^6 symbols.

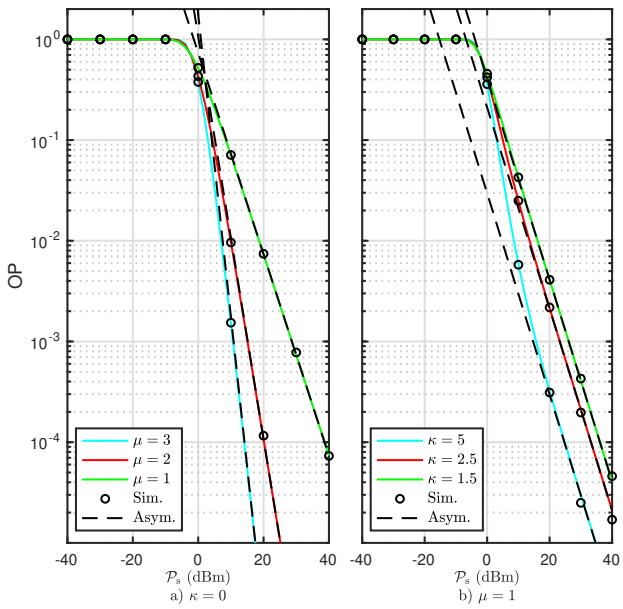

Fig. 5.2 OP of $\mathcal{I}$ in different fading conditions versus $\mathcal{P}_{\rm s}$.

Fig. 5.2 shows the OP of $\mathcal{I}$ over different channel fading parameters as a function of $\mathcal{P}_{\rm s}$. In Fig. 5.2a, the parameter μ is changed for a wide range of values, while $\kappa = 0$. As can be seen in the figure, OP of $\mathcal{I}$ improves slowly with $\mathcal{P}_{\rm s}$ for the case of $\mu = 1$. This performance is due to the severe attenuation caused by the walls of the building and the loss of paths over a long distance. For $\mu = 3$, OP improves significantly with $\mathcal{P}_{\rm s}$ because the channel gain is generally high for such values of μ. Similarly, Fig. 5.2b leads to

the same conclusion, but with less enhancements in OP. To illustrate, manipulating the fading parameter μ yields more effective results. Therefore, other parameters such as the distance between the walls, the number of internal walls, and the materials of the walls play an important role in obtaining a high OP. In general, $\mathcal{I}$ can experience various channel fading values for κ and μ. However, it is generally considered to be NLOS.

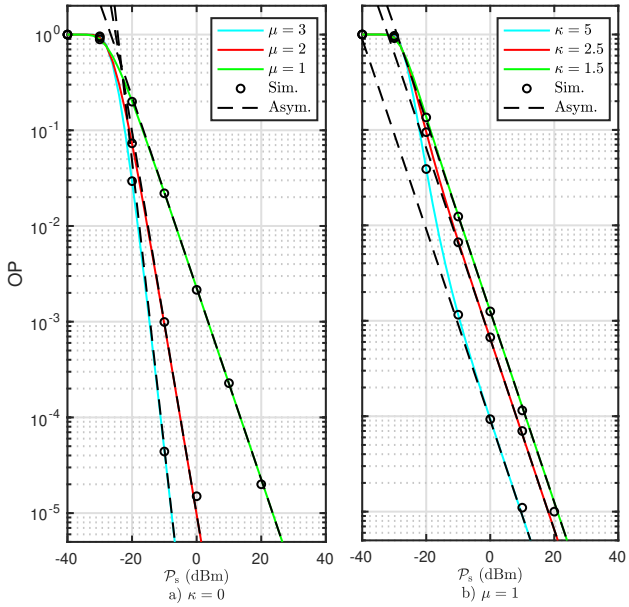

Fig. 5.3 OP of $\mathcal{O}$ under different fading conditions versus $\mathcal{P}_s$

Fig. 5.3 shows the OP of $\mathcal{O}$ on various values of κ and μ. Unlike the case of $\mathcal{I}$ in Fig. 5.2, this figure shows that OP of $\mathcal{O}$ outperforms OP of $\mathcal{I}$ in all ranges of channel fading components. This is due to the low path loss and the closer distance to the transmitter. It also shows the difference between the outdoor and indoor environment, where the challenges are more severe under indoor conditions. The channel fading parameter μ also has a greater effect on OP than on the κ component. For example, when $\kappa = 0$ and $\mu = 3$, OP of 10^{-4} can be easily reached using about 0 dBm of transmit power. However, when $\mu = 1$ and $\kappa = 5$, more than 0 dBm of transmit power is needed to reach the same value of OP. On the other hand, $\mathcal{I}$ requires about 20 dBm of $\mathcal{P}_s$ to achieve 10^{-4} of OP under the same channel conditions.

On the contrary, Fig. 5.4 illustrates the impact of the power allocation factor (α_i), where $i \in 1, 2$ within different transmit power values. This figure considers two scenarios of assigning different combinations of target data rate, i.e., when both users have a similar amount of target data rate and have different values. The significant impact of α_i on OP performance can be seen. Interestingly, $\mathcal{I}$ drops to full outage when $\alpha_{\mathcal{I}} = 0.74$ due to the direct impact of an equal amount of allocated target data rate, that is, $R_1 == R_2$. In fig. 5.4b, a similar approach with less suffering of OP occurs for $\mathcal{O}$

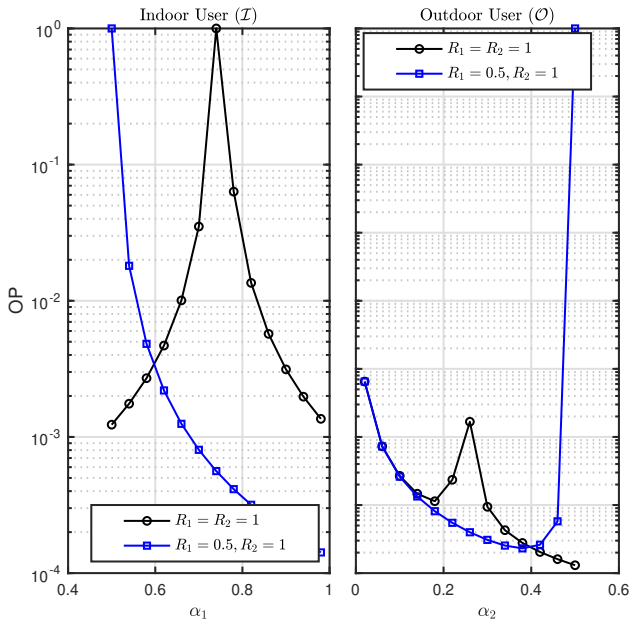

Fig. 5.4 OP of $\mathcal{I}$ and $\mathcal{O}$ versus their assigned power allocation α with $\eta = 0$.

when a corresponding $\alpha_{\mathcal{O}} = 0.26$ is applied. In general, the OP of $\mathcal{I}$ suffers more with a low selection of $\alpha_{\mathcal{I}}$ and vice versa for $\mathcal{O}$. In addition to that, the OP performance curve within various values of the data target rate is much better for being equal between two users. This figure also shows the most optimal power allocation that can improve the OP selection for each user. For example, when considering different target data rates, $\alpha_{\mathcal{O}} = 0.4$ becomes optimal for $\mathcal{O}$ and $\alpha_{\mathcal{I}} = 0.98$ for $\mathcal{O}$. In general, $\mathcal{I}$ and $\mathcal{O}$ achieve more improvements in terms of OP when α_1 increases in both scenarios.

Fig. 5.5 shows the impact of different combinations of channel fading parameters assigned to $\mathcal{I}$, where the target data rate R_1 is plotted over different values of $\mathcal{P}_{\text{s}}$. It indicates that increasing the amount of κ while μ remains fixed can potentially improve the OP performance over the total amount of $\mathcal{P}_{\text{s}}$. Therefore, the channel fading parameter has a major impact on the system performance of $\mathcal{I}$. In addition, one can observe that the increase in the amount of target data rate drives the OP performance dramatically to the lowest level at high and low values of $\mathcal{P}_{\text{s}}$.

Similarly, fig. 5.6 depicts the OP performance versus the target data rate R_2 over different values of $\mathcal{P}_{\text{s}}$. In contrast to the fig. 5.5, the OP of $\mathcal{O}$ is improved and the outage is reduced twice compared with the outage of $\mathcal{I}$. For example, a downtime of less than 10^{-1} is reached at $R_2 = 2$ in all allocated $\mathcal{P}_{\text{s}}$ ranges, while $\mathcal{I}$ achieves a complete downtime during the same level of the target data rate. It can be said that $\mathcal{I}$ shows more outages than $\mathcal{O}$ on the same given target data rate due to the difference in their channel conditions.

To obtain more information about the OP of $\mathcal{I}$, fig. 5.7 discusses the significant im-

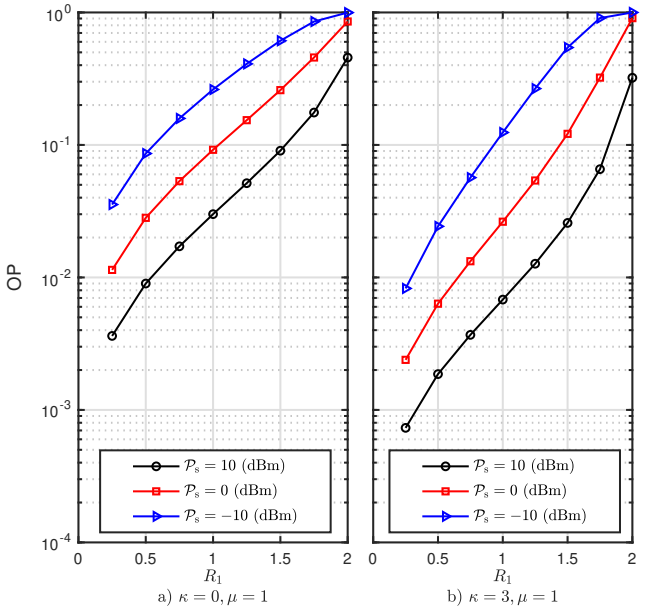

Fig. 5.5 OP of $\mathcal{I}$ versus its target data rate (R_1) with $\eta = 0$.

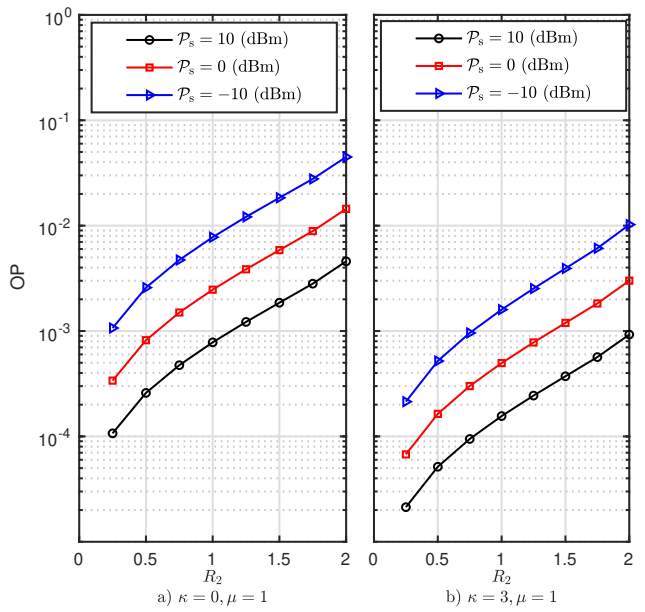

Fig. 5.6 Outage probability of $\mathcal{O}$ versus target data rate R_2.

pact of the number of internal walls on the OP performance. As can be seen, increasing the number of internal walls destructively affects the signal received from $\mathcal{I}$. This could increase the amount of outage even though more power is allocated. In addition to that, the channel fading parameters contribute adequately to improving the OP. For example, the OP of $\mathcal{I}$ is dramatically decreased when there are more than three internal walls (n). Moreover, when $\mu = 3$ and $\kappa = 0$, the outage is less than the selection of $\mu = 1$ and

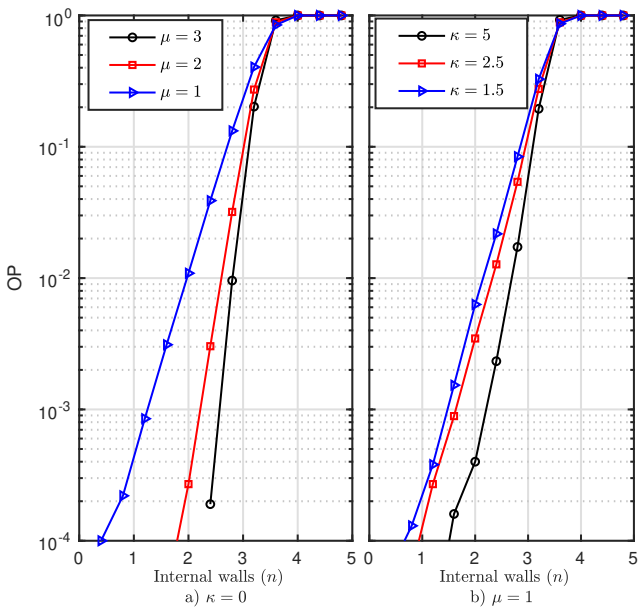

Fig. 5.7 Outage probability of $\mathcal{O}$ versus number of internal walls

$\kappa = 0$. Similarly, when $\mu = 1$ and $\kappa = 5$ the same conclusion is reached, but with a small high improvement.

Another important factor that plays an important role in the overall performance of the system of $\mathcal{I}$ is called the grazing angle (θ), which is the angle between the UAV and the wall of the building. In fig. 5.8 we plot the possible amount of θ versus OP. It indicates that the best OP can be achieved when θ is considered less than 1, and the floor outage is expected when theta exceeds that limit. Furthermore, manipulating channel fading parameters can inherently reduce floor outage.

Fig. 5.9 shows the performance of the throughput of $\mathcal{I}$ corresponding to $\mathcal{P}_{\text{s}}$. Two different scenarios are provided here. First, fig. 5.9a studies the case of different target data rates for both users, i.e., $R_1 = 0.5, R_2 = 1$ while fig. 5.9b provides the case of equal target data rates, that is, $R_1 = R_2 = 1$. Therefore, the throughput of $\mathcal{I}$ is almost zero at very low $\mathcal{P}_{\text{s}}$, i.e., ($\mathcal{P}_{\text{s}} < -25$), and it can reach the target rate of approximately ($\mathcal{P}_{\text{s}} = -15$). A little enhancement is gained by controlling the channel fading parameters, as can be seen in the same plot. However, when the second case is assumed, the throughput of $\mathcal{I}$ is completely changed to gain more enhancements. Overall, $\mathcal{O}$ outperforms $\mathcal{I}$ in terms of equall assigned target data rate. It is also observed that higher throughput is achieved at high $\mathcal{P}_{\text{s}}$ for $\mathcal{I}$ and at low $\mathcal{P}_{\text{s}}$ for $\mathcal{O}$. It also shows that different values of the fading parameters can significantly affect the system performance. The manipulation of μ provides more effective results than the parameter κ.

Fig. 5.10 shows the performance of the throughput of both users in different combinations of the target data rate. It can be seen that the most beneficial value of the target

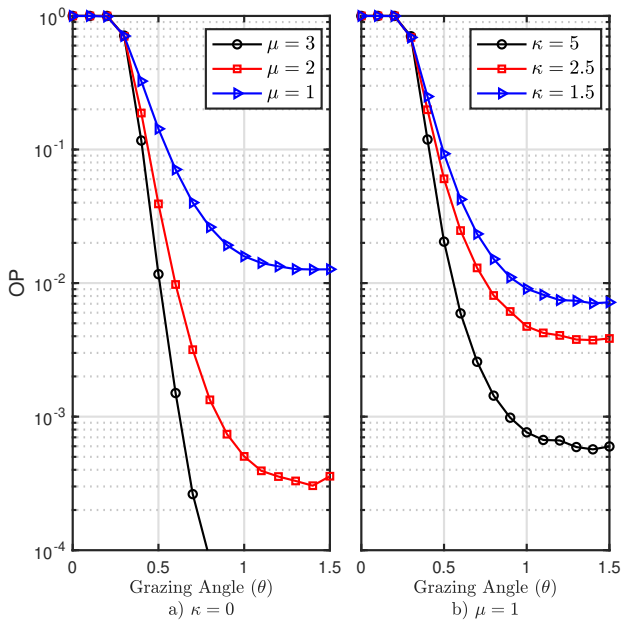

Fig. 5.8 Outage probability of $\mathcal{O}$ versus different values of θ

.

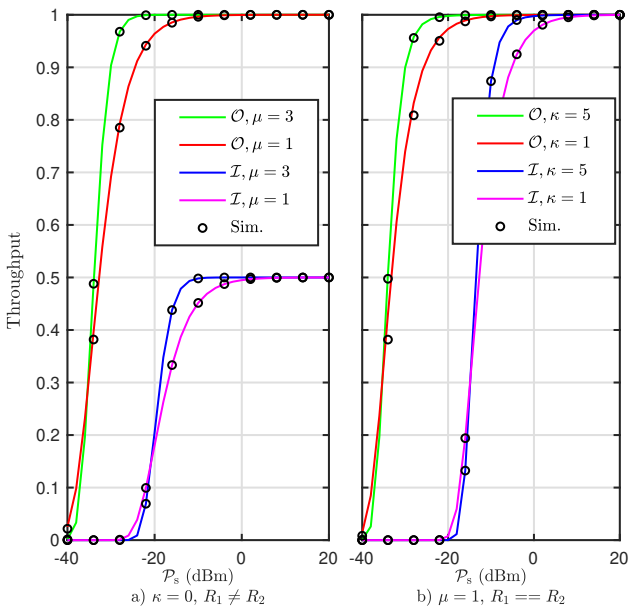

Fig. 5.9 Throughput of $\mathcal{I}$ versus $\mathcal{P}_s$.

rates for $\mathcal{I}$ and $\mathcal{O}$ can be presented, respectively, as in $R_1 = 0.75$ and $R_1 = 2.75$. The results obtained in these two optimal selections are varied according to the assigned channel fading components, as shown in the same figure.

Fig. 5.11 shows another crucial performance metric known as the average channel capacity. In particular, it plots the individual rates of both users versus $\mathcal{P}_s$. It can be observed from this figure that EC of $\mathcal{O}$ is manipulated by the impact factor of resid-

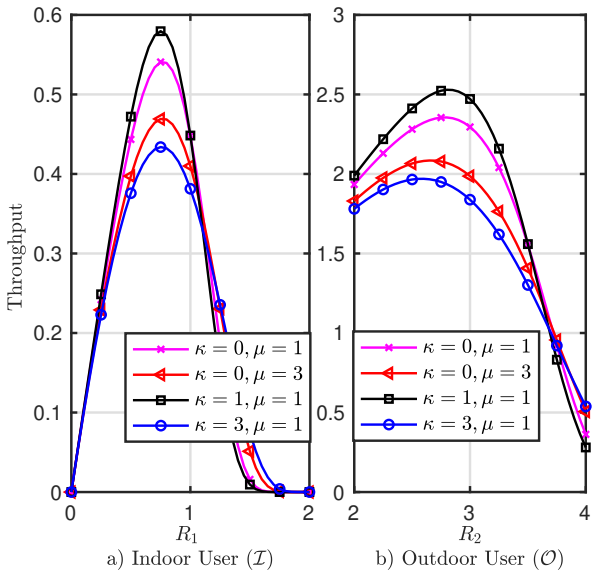

Fig. 5.10 Throughput of $\mathcal{O}$ versus $\mathcal{P}_{\mathrm{s}}$ with $\eta = 0$.

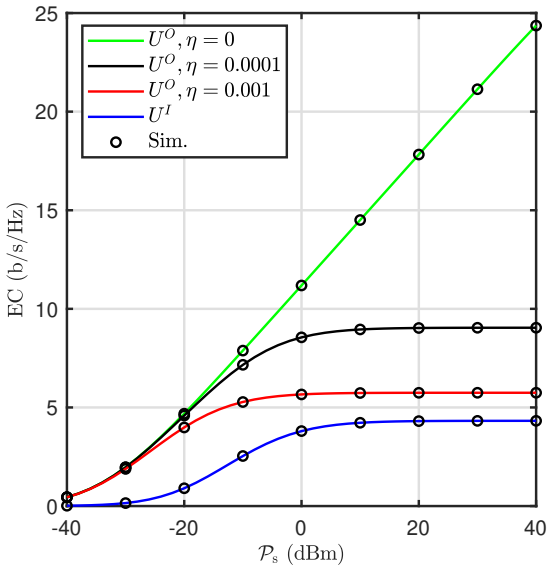

Fig. 5.11 Ergodic capacity of both users versus $\mathcal{P}_{\mathrm{s}}$ in different values of η where κ= 0,μ= 1 for all channels.

ual interference. It becomes worse than the ideal case, where η aims to be higher, but still performs better than $\mathcal{I}$ in all ranges of transmit power. However, $\mathcal{I}$ achieves approximately $0.5 - 4$ (b/s/Hz) on 0 dBm, while $\mathcal{O}$ gains between $11 - 25$ (b/s/ Hz) in the absence of residual interference, that is, $\eta = 0$. Ultimately, residual interference, path loss gain, and fading parameters have a significant influence on overall system performance.

Fig. 5.12 studies the overall efficiency of the energy system as a function of the transmit power under different conditions of SIC. It can be seen from Fig. 5.12 that EE

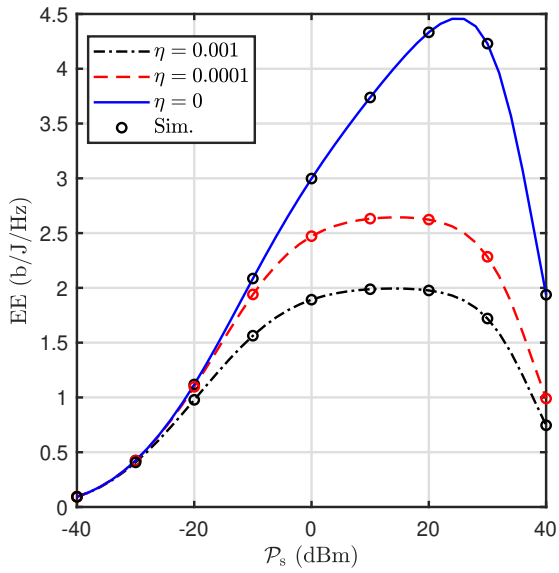

Fig. 5.12 Energy efficiency versus $\mathcal{P}_s$ with κ= 0,μ= 1.

increases as the transmit power increases, but gradually decreases at very large transmit power values due to the imperfect SIC phenomenon. In the best scenario of η, EE increases linearly over the entire transmit power range. However, when η intends to increase, EE exhibits almost floor performance at high transmit power. Therefore, different system parameters can play a major role in enhancing the overall system performance.

5.6 Chapter Summary

In this chapter, a performance analysis is performed for a mix of indoor and outdoor NOMA users, where both users can be served through outdoor-to-indoor and outdoor-to-outdoor channels. Different practical challenges are considered, including imperfect SIC and various fading conditions. Channel gains are sorted according to the product of instantaneous channel gains with their distance-dependent path loss, where $\mathcal{I}$ has different channel attributes than $\mathcal{O}$. We studied the path loss model of $\mathcal{I}$ in the generalised κ-μ fading distribution to better describe the channel gain when both scenarios of LOS and NLOS are present. Furthermore, we evaluated a variety of vital performance metrics such as OP and EC, as well as throughput and energy efficiency, and provided exact analytical expressions. The results obtained provide information on the impact of different key factors, such as power allocation, κ and μ fading, and residual interference, on the overall performance of the system. It is shown that the performance of $\mathcal{I}$ degrades more than $\mathcal{O}$ due to its environment defined by its different channel attributions, although it is located at the same distance from the base station. The analytical expres-

sions derived were validated by extensive simulations that confirmed the precision of our analysis.

CHAPTER 6

Low-Complexity Indoor-Outdoor User Pairing and Resource Optimisation in DL-NOMA Systems

A. Alqahtani, and E. Alsusa

Under process to be submitted in: IEEE Access

Abstract

This work proposes two algorithms to maximise the sum data rate and fairness in non-orthogonal multiple access (DL-NOMA) downlink systems with pairing of indoor-outdoor users. Specifically, one of the proposed algorithms is based on the streamlined simplex method (SSM), while the other utilises the least and most cost method (LMCM). The fairness rate in both cases is optimised using the Max-Min approach for the indoor device, which is assumed to have a lower channel gain due to its inherently more challenging environment. Various performance metrics such as the achievable data rate, fairness index, and energy efficiency are analysed to evaluate the effectiveness of the proposed algorithms relative to the random user-pairing benchmark method. The results show that the LMCM algorithm has a lower complexity and offers a better data rate and energy efficiency compared to the SSM algorithm and the random pairing method.

Keywords— Non-orthogonal multiple access (NOMA), User Pairing, Indoor-Outdoor NOMA, streamlined simplex method (SSM), least and most cost method (LMCM).

6.1 Chapter Introduction

The demand for wireless data delivery at massive rates and low latency has increased dramatically in recent years, prompting the need for new technologies, such as fifth generation (5G) and WiFi-6 systems, to meet such requirements. However, overcoming the limited radio frequency resource continues to be a major challenge in wireless environments. To this end, new radio access techniques, called non-orthogonal multiple access (NOMA), have been the subject of intensive investigation in a bid to provide better utilisation of the radio spectrum. To this end, NOMA is currently considered a potential candidate for future wireless generations, such as 6G and WiFi-7. In comparison to orthogonal frequency division multiple access (OFDMA), NOMA can double the utilisation of the radio resource, but at the cost of some interference and higher complexity. However, to minimise the impact of such drawbacks, NOMA receivers usually use successive interference cancellation (SIC) for data recovery. The basic principle of NOMA in the power domain is to differentiate between multiplexed users using unique power levels that are selected based on some optimisation criterion. Hence, to enhance the performance of such systems, power allocation and user grouping must be carefully addressed, [5, 76, 103].

6.2 Related Work

There is a large volume of published studies investigating NOMA systems. For example, the basic concept of NOMA is described in [104] and [5], while in [94] the probability of outage, the bit error rate, and the performance of ergodic capacity are presented, while in [105] cooperative NOMA systems are considered. Furthermore, in [106], Ding *et al.* showed that NOMA can achieve a better sum data rate performance than OFDMA. They also demonstrated that the allocated power and target data rate parameters can effectively manipulate the NOMA outage probability performance. In addition, similar work has been carried out that demonstrates the superiority of NOMA by Saito*et al.* in [107] and Benjebbovu*et al.* in [4]. In particular, the authors argue that NOMA can improve the capacity and throughput of the system over orthogonal multiple access (OMA) systems by applying different power allocation techniques such as full search power allocation (FSPA), fractional transmit power allocation (FTPA) and fixed power allocation (FPA). Their results showed that the FSPA technique outperforms the other techniques considered, though at the cost of higher complexity. In contrast, FTPA, which requires prior computations of specific parameters, outperforms the lower-complexity FPA.

User pairing and power allocation have also been shown to be key factors in improving the performance of NOMA systems, especially the sum of data rate. Conventional

user pairing and power allocation techniques have been shown to improve the capacity of NOMA systems, albeit to a limited extent. On the other hand, advanced algorithms that employ established optimisation techniques have been shown to achieve better performance, not surprisingly at the expense of high complexity, which can affect the efficiency of the system and the time for allocation decision [108–111]. For example, the authors of [111] proposed a real-time allocation technique based on a deep neural network, which is trained to estimate the interior point method (IPM) for power allocation, and it was shown to improve capacity and computational efficiency. In another corresponding investigation, [112], a joint dynamic user pairing and power allocation algorithm is introduced for hybrid OMA / NOMA systems. User pairing is performed based on being served by OMA or NOMA, where the proposed algorithm minimises the queueing delay and guarantees a minimum-time average data rate.

Furthermore, the authors in [113] proposed a new approach of vertical pairing that contributes to establishing user pairing based on their channel gains. They also examined the sum rate maximisation problem of NOMA over frequency-selective fading channels. Their results show that their approach is superior to other techniques and offers a performance comparable to that of the optimal solution. Zhu *et al.* [114] optimises user pairing and power allocation to improve the achievable sum rate. The results demonstrate that the proposed optimal user pairing significantly enhances the performance of NOMA compared to other methods, such as the random pairing method. A recent study on user pairing in NOMA with practical SIC is presented in [115]. The authors propose an adaptive user pairing (A-UP) algorithm to improve the sum-rate performance of the paired users. Furthermore, many recent research studies focus on identifying and evaluating user pairing and power allocation in single-input single-output (SISO) systems. On the other hand, Chen *et al.* [116] studied user pairing for massive multiple input multiple output (MIMO) NOMA, where the authors propose a user pairing and scheduling algorithm to ensure that paired users achieve a high sum data rate. Nguyen *et al.* [117] investigates the user pairing problem for multiple input, single output (MISO) NOMA networks with simultaneous wireless information and power transfer (SWIPT) to maximise overall energy efficiency (EE) and spectral efficiency (SE) restricted to some requirements of user quality of service (QoS). The authors propose a novel hybrid user pairing algorithm to solve the optimisation problem. The work in [118] investigates resource allocation in a NOMA system that deploys multiple antenna unmoored aerial vehicles (UAV) and tackles the maximisation of EE while satisfying various constraints related to user pairing, UAV positions, and satisfied QoS and SIC thresholds. The results indicate that the EE of NOMA can leverage the EE of OMA in most cases. The results also disclose the impact of applying an equal requirements rate in the EE, where the optimal performance is attained. In addition, the authors in [119] address some optimal solutions for user pairing, power allocation, to

Table 6.1 The list of symbols and notation used in this article.

Symbol	Definition
U	total number of users
S	total number of sub-carriers
K_s	total number of allocated users on sub-carrier s
$\mathcal{I}_{s,u}$	indoor user u on sub-carrier s
$\mathcal{O}_{s,u}$	outdoor user u on sub-carrier s
B	total bandwidth
B_{sc}	bandwidth for each sub-carrier
P_c	circuit power consumption
P_t	total transmitting power at BS
P_s	power allocation of sub-carrier s
$\mathrm{P}_{s,u}$	power allocation of user u on sub-carrier s
$h_{s,u}$	complex channel coefficient
$PL^{\mathcal{I}}_{s,u}$	path loss of indoor user
$PL^{\mathcal{O}}_{s,u}$	path loss of outdoor user

maximise the performance of the sum data rate and energy efficiency, where the Hungarian (HNG) algorithm is applied for pairing two NOMA users who are associated with different channel conditions. The authors attained closed-form solutions to maximise the sum data rate and EE by applying the Karush-Kuhn-Tucker (KKT) conditions and the Dinkelbach (DKL) algorithm, respectively.

6.3 System Model

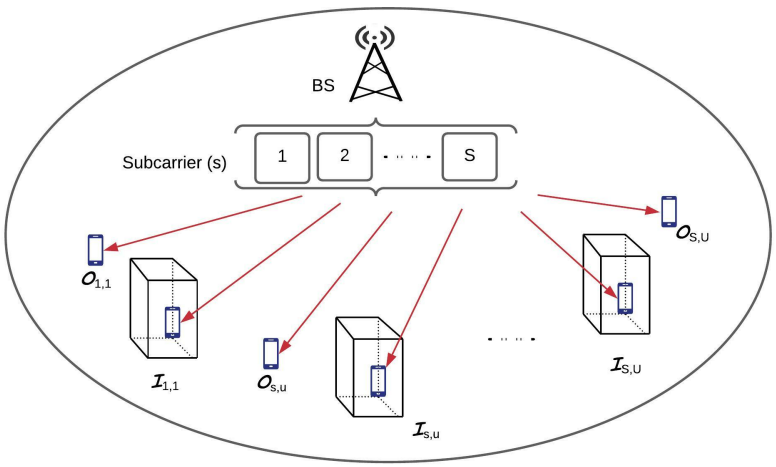

Fig. 6.1 System Model under consideration with indoor and outdoor user-pairing.

Consider a downlink NOMA system applied for multiplexing indoor and outdoor users served by a single base station (BS), in which all nodes communicate with the

BS through a single antenna. BS combines a set of transmitted signals and transmits them to a group of indoor-outdoor users $u = \{1, 2, ..., U\}$ using a group of subcarries $s = \{1, 2, ..., S\}$. Multiplexed signals are assigned different power levels, and the total bandwidth (B) is uniformly divided between the S subcarries to produce the dedicated bandwidth $(\mathrm{B_{sc}})$ for each subset of users, that is, $\mathrm{B_{sc}} = \frac{\mathrm{B}}{S}$. Furthermore, it is assumed that each sub-carrier s is assigned to certain (K_s) users. Therefore, the total number of users is $U = K_s \times S$. Furthermore, channel state information (CSI) of the links assigned between the BS and the users is considered available at BS. In NOMA-OFDM, each sub-carrier serves multiple users that employ SIC receivers. The BS can assign groups of users to different sub-carriers and assigns them different powers. The transmitted signal from BS to K_s users can be written as

$$X_s = \sum_{q=1}^{K_s} \sqrt{\mathrm{P}_{s,q}} x_{s,q} \tag{6.1}$$

where $x_{s,q}$ and $\mathrm{P}_{s,q}$ are the transmitted signal and allocated power to the qth user on sub-carrier s, respectively. The power constraints of the sth sub-carrier and BS are represented respectively as $\sum_{u=1}^{K_s} \mathrm{P}_{s,u} = \mathrm{P}_s$ and $\sum_{s=1}^{S} \mathrm{P}_s = \mathrm{P}_t$, where P_t is the total transmitted power, $\mathrm{P}_{s,u} = \beta_{s,u} \times \mathrm{P}_s$ and $\mathrm{P}_s = \eta_s \times \mathrm{P}_t$. Therefore, variables $\beta_{s,u}$ and η_s indicate the power allocation factor for user u on the sub-carrier s and the power allocation factor for sub-carrier s, respectively. In this chapter, it is assumed that $\eta = \frac{1}{S}$. Furthermore, the signal received at the user node can be given as [120],

$$y_{s,u} = h_{s,u} X_s + n_{s,u} = h_{s,u} \sqrt{\mathrm{P}_{s,u}} x_{s,u} + h_{s,u} \sum_{i=1 \neq u}^{K_s} \sqrt{\mathrm{P}_{s,i}} x_{s,i} + n_{s,u} \tag{6.2}$$

where $h_{s,u}$ indicates the complex channel gain between BS and user u on sub-carrier s, where the effect of path loss and small-scale fading is given as $h_{s,u} = \frac{|h_{s,u}|^2}{\sqrt{PL_{s,u}}}$ [121]. In particular, $PL_{s,u}$ indicates the path loss of user u on sub-carrier s, and $h_{s,u} \sim \mathcal{CN}(0, 1)$ defines the small-scale fading, and thus the envelope is Rayleigh. In addition, $n_{s,u} \sim \mathcal{CN}(0, \sigma^2)$ is the additive white Gaussian noise (AWGN) with zero mean and variance σ^2.

In downlink NOMA, the sub-carriers are shared by different groups of users, where the SIC technique is applied to eliminate the interference caused by the co-users of the same sub-carrier. Accordingly, any user assigned with better channel conditions is assigned a low power level, and vice versa. Therefore, high-power users treat signals from other users as noise, so they do not have to apply SIC. However, low power users apply SIC to successfully decode other users' signals that have high power levels. To illustrate, consider that K_s users transmit on sub-carrier s have the following ascending channel gain order $|h_{s,1}| \leq |h_{s,2}| \leq \cdots \leq |h_{s,u}|$, with a power allocation coefficient

order that ensures user fairness as $\mathrm{P}_{s,1} > \mathrm{P}_{s,2} > \cdots > \mathrm{P}_{s,u}$. Therefore, user u can correctly decode and eliminate the interference signals generated by user i under the constraints $i < u$ and $i \neq u$, where user i treats the interfering signal of user u as noise. Thus, the signal-to-interference noise ratio (SINR) received from user u on sub-carrier s is given as follows.

$$\gamma_{s,u} = \frac{\mathrm{P}_{s,u}|h_{s,u}|^2}{\sum_{i=1}^{u-1} \mathrm{P}_{s,i} h_{s,u} + \sigma^2}. \tag{6.3}$$

6.3.1 Path Loss Model

In the first scenario, communication between the BS and outdoor users occurs through air-to-ground channels. These links are affected by large-scale path loss, where the free space path loss model [96],

$$PL_{s,u}^{\mathcal{O}} = 32.45 + 20\log(d_{sr}) + 20\log(f) \tag{6.4}$$

where d_{sr} is the Euclidean distance between the BS and the outdoor nodes, and f is the frequency. However, the propagated signals from BS to indoor users are fulfilled over the outdoor-to-indoor channels, where the large-scale path loss and Loss of the indoor transmission path loss are included. Therefore, the empirical propagation model of COST 231 building penetration loss given in [96] is adopted. The indoor transmission path encompasses the loss of penetration of the building (PL_B) and the loss of the indoor path (PL_{in}). Thus, the total path loss for indoor users can be calculated as follows [122],

$$PL_{s,u}^{\mathcal{I}} = L_{fs} + L_t + L_{in} \tag{6.5}$$

where L_{fs} indicates the free space path loss, and L_t represents the transmission propagation path loss that includes the parallel penetration loss L_{pt} and the perpendicular loss L_{pc}, presented as follows:

$$L_t = L_{pc} + L_{pt}(1 - \sin(\theta))^2 \tag{6.6}$$

where θ is the grazing angle between BS and the exterior building wall. Moreover, the indoor propagation path loss, L_{in}, is identified by the mean path loss determined from the internal side of the exterior wall to the indoor user, given as

$$L_{in} = \max\{n\, L_i, \chi(d_{in} - 2)(1 - \sin(\theta))^2\} \tag{6.7}$$

where n is the total number of internal walls, L_i defines the internal wall loss, and χ is the indoor path loss factor. The standard values of the parameters of the indoor propagation model are shown in table 6.16.

6.3.2 Performance Analysis

6.3.2.1 Achievable Data Rate

In a wireless communication system, the effective rate of a successful transmission of a signal measured in bits per second (bps) is known as the achievable data rate. Therefore, to obtain the individual data rate of NOMA users, the following formula is applied, [123],

$$R_{s,u} = \mathrm{B}_{sc} \times \log_2 \left(1 + \frac{\mathrm{P}_{s,u} |h_{s,u}|^2}{\sum_{i=1}^{u-1} \mathrm{P}_{s,i} |h_{s,u}|^2 + \sigma^2} \right). \tag{6.8}$$

Thus, the total achievable data rate can be calculated as

$$R_{sum} = \sum_{s=1}^{S} \sum_{u=1}^{U} R_{s,u}. \tag{6.9}$$

6.3.2.2 Energy Efficiency (EE)

It is considered to be one of the main significant performance metrics in wireless communication. It can be obtained by the ratio of throughput to the total consumed power in the system. The mathematical expression of energy efficiency is given as [124]

$$EE_{s,u} = \frac{R_{s,u}}{\mathrm{P}_c + \sum_u^{K_s} \mathrm{P}_{s,u}} \tag{6.10}$$

where P_c is the power of the circuit.

6.3.2.3 Fairness Rate

The fairness metric shows the importance of power allocation and user pairing methods in overall system performance. It can be done by applying Jain's fairness index [125],

$$F = \frac{\left(\sum_u^{K_s} R_{s,u} \right)^2}{K_s \sum_u^{K_s} \left(R_{s,u} \right)^2}. \tag{6.11}$$

Jain's fairness has a value range of $0 \leq F \leq 1$. Thus, the fairness performance is considered high when F is close to 1.

6.4 Problem Formulation

In order to describe the pairing association between users and sub-carriers, a cost matrix (Z) of the sub-carrier-users assignment with the size of $(U \times S)$ is constructed to observe the best optimal user pairing, [119]. This can be formulated as

$$Z = \begin{bmatrix} c_{1,1} & \dots & c_{1,u} \\ \dots & \dots & \dots \\ c_{s,1} & \dots & c_{s,u} \end{bmatrix} \tag{6.12}$$

where $c_{s,u}$ illustrates the channel gain of each user over each sub-carrier. Decision variables can be expressed as

$$x_{s,u} = \begin{cases} 1, & \text{if user } u \text{ is assigned to sub-carrier s} \\ 0, & \text{otherwise.} \end{cases} \tag{6.13}$$

Hence, the main objective here is to maximise the achievable total data rate (R_{sum}) and to improve fairness among indoor and outdoor users. Therefore, the optimization problem can be written as

$$\max \quad R_{sum} \tag{6.14a}$$

$$\text{s.t.} \quad \sum_{s=1}^{S} \sum_{u=1}^{U} \mathrm{P}_{s,u} = \mathrm{P}_t \tag{6.14b}$$

$$\sum_{u=1}^{U} x_{s,u} = K_s, \forall s \tag{6.14c}$$

$$\sum_{s=1}^{S} x_{s.u} = 1, \forall u, x_{s.u} \in \{0, 1\}. \tag{6.14d}$$

The constraint of (6.14b) is applied to ensure that the power allocated to any paired users cannot exceed the total transmit power (P_t). In addition, constraint (6.14c) validates that each sub-carrier s is restricted to being used by certain K_s users. However, the constraint (6.14d) guarantees that each user can obtain its data from a single sub-carrier and shows the indicator value of the sub-carrier assignment.

6.4.1 Proposed User Pairing Algorithms

In this section, two proposed methods for user pairing, namely the Streamlined Simplex Method (SSM) and the Least and Most Cost Method (LMCM), are being proposed.

6.4.1.1 The SSM Algorithm

The SSM technique is typically used to solve linear programming problems such as transportation-type problems, where the assignment problem is considered a special case, [126]. This method includes two main phases. In the first phase, an initial basic

Algorithm 1: Streamlined Simplex Method (SSM) Algorithm

The SSM algorithm can be summarized into the following steps:

1. Formulate the problem and organize the data in the matrix form.
2. Achieve an initial basic feasible solution (IBFS):
   The initial solution can be found by applying **Algorithm2**, and it must satisfy the following conditions:
   (a) The obtained IBFS must be feasible, i.e. it must satisfy all the supply and demand constraints.
   (b) The number of positive allocations must be equal to m+n-1, where m is the number of rows and n is the number of columns.

   Any solution that meets the above conditions is called degenerate basic feasible solution, otherwise, non-degenerate solution.
3. Evaluate the initial solution for optimality by applying the Modified Distribution (MODI), also known as (u-v) method.
   This method is discussed to test the optimality of the solution attained in Step 2. If the current solution is optimal, then stop. Otherwise, calculate a new improved solution.
4. Updating the current solution:
   Repeat Step 3 until an optimal solution is accomplished.

feasible solution (IBFS) is obtained by common methods such as the least cost method (LCM), the North-West corner method (NWCM), or Vogel's Approximation Method (VAM). In the second phase, the first phase is optimised by applying one of the following techniques: the modified distribution method (MODI), which is also called the $u-v$ method, or the Stepping Stone method (SSTM). In this chapter, it is intended to apply LCM and MODI methods to achieve the best optimal user pairing for the discussed system model. It works by assigning an individual indoor or outdoor user to a particular sub-carrier with the aim of minimising or maximising the total cost assignment, which can be the channel gains. Furthermore, each user is assumed to be assigned only to a single sub-carrier, and each sub-carrier should only involve two users to form a pair of NOMA users. In this approach, the demand term can be defined as the total number of paired users in a single sub-carrier while the supply term is indicated for the user itself, i.e., supply always becomes unity for each user. Therefore, the optimisation problem in 6.14 can be rewritten as

Table 6.2 An example of the channel gain cost matrix.

s	$\mathcal{I}_{s,1}$	$\mathcal{I}_{s,2}$	$\mathcal{I}_{s,3}$	$\mathcal{O}_{s,4}$	$\mathcal{O}_{s,5}$	$\mathcal{O}_{s,6}$	**Supply**
1	0.02	0.01	0.06	0.12	1.7	0.09	2
2	0.05	0.11	0.08	0.05	0.6	0.11	2
3	0.07	0.15	0.04	0.06	0.2	1.5	2
Demand	1	1	1	1	1	1	

$$\max \quad z = \sum_{s=1}^{S} \sum_{u=1}^{U} c_{s,u} x_{s,u} \tag{6.15a}$$

$$\text{s.t.} \quad \sum_{s=1}^{S} x_{s,u} = 1, \; s = 1, 2, .., S \tag{6.15b}$$

$$\sum_{u=1}^{U} x_{s,u} = 2, \; u = 1, 2, .., U \tag{6.15c}$$

$$x_{s,u} = \{0, 1\}. \tag{6.15d}$$

In addition, SSM is proposed to solve the above problem according to Fig. 6.2, which is based on the original algorithm plotted in [126]. The following example is given to illustrate the procedures involved.

Table 6.2 shows an example of the cost matrix that has been randomly aggregated from simulating the average channel gains of three indoor users and three outdoor users over three different sub-carriers, that is, $S = 3$ and $U = 6$. Therefore, these values are captured by simulation of indoor and outdoor users according to the simulation parameters in table 6.16. It can be seen from Table 6.2 that our problem is categorised as a balanced problem due to the equivalent amount of the total summation between supply and demand. However, in the case of unbalanced problems, a dummy row or column should be considered to balance the problem. In this work, solving a problem such as a block chain, as given in Table 6.2, by following the entire procedures of the SSM algorithm, turns out to be inefficient. Therefore, to overcome this issue and obtain the optimal solution, it is proposed to consider each sub-carrier individually over all possible links between the BS and the assigned users to find the optimal pairing solution.

Now, the IBFS needs to be obtained to the above problem by performing the Least Cost Method (LCM), which is written in algorithm I. According to the flowchart presented in Fig. 6.2, one can start by solving the above problem by considering the first row at the first attempt. However, due to the unbalanced problem caused by the unequal

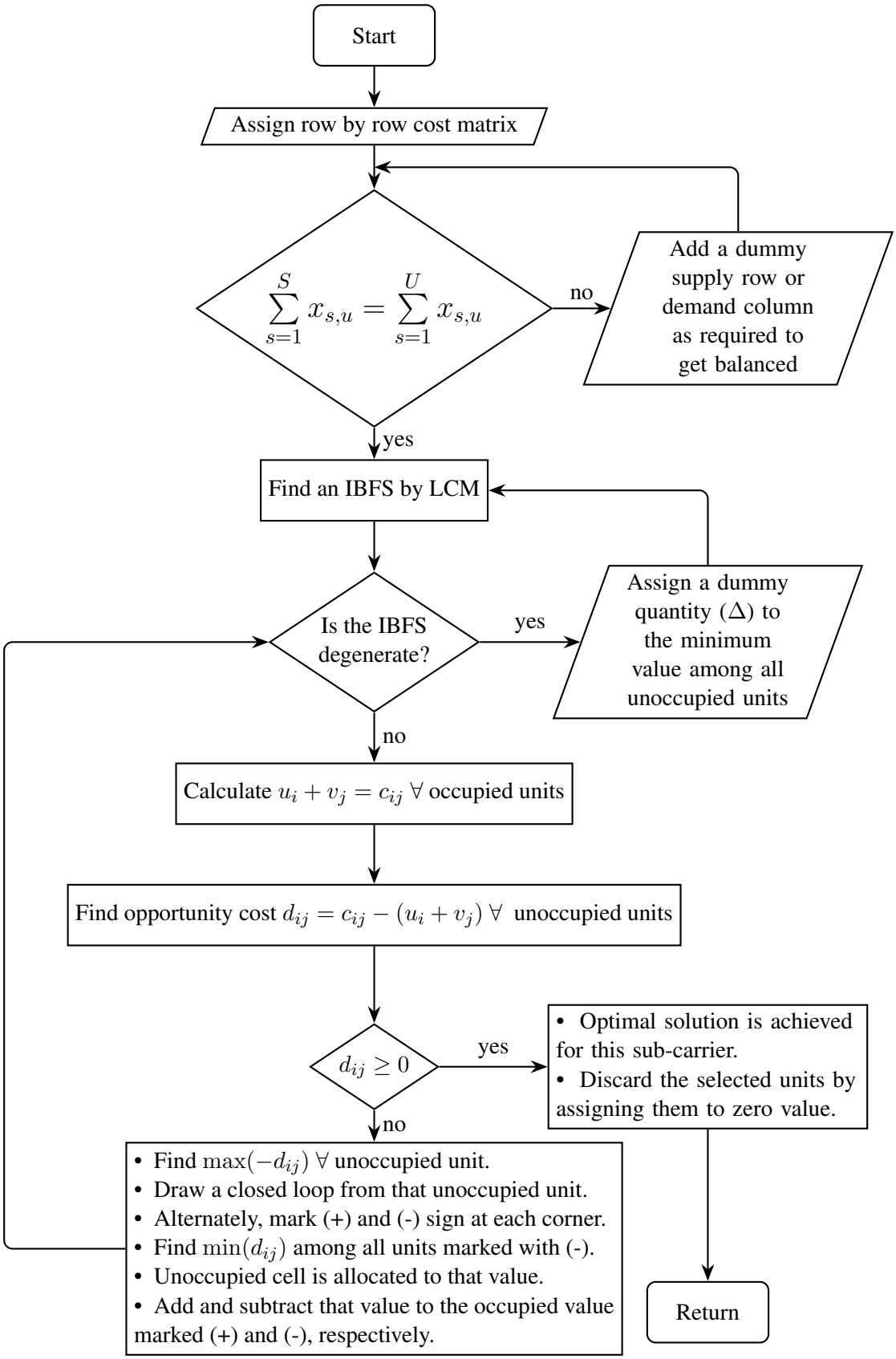

Fig. 6.2 Flowchart of the SSM Algorithm.

total amount between supply and demand, a dummy row filled with the (0) cost should be added for each unit and the (4) supply allocations. After that, the problem in (6.15a) should be converted to a minimisation scheme by finding the maximum units, which is (1.7), and subtracting it from all the remaining units in Table 6.2 to start with the lowest transportation cost. This yields the following update.

Table 6.3 First phase of the SSM algorithm: Problem balance

s	$\mathcal{I}_{s,1}$	$\mathcal{I}_{s,2}$	$\mathcal{I}_{s,3}$	$\mathcal{O}_{s,4}$	$\mathcal{O}_{s,5}$	$\mathcal{O}_{s,6}$	**Supply**
1	1.68	1.69	1.64	1.58	1.7	1.61	2
dummy	0	0	0	0	0	0	4
Demand	1	1	1	1	1	1	6

Now, allocate the selected unit by 1, which fulfils the entire demand of $\mathcal{O}_{1,5}$ and remains one unit with the first sub-carrier. Then the entire column is crossed because there is no demand left for $\mathcal{O}_{1,5}$. Similarly, repeat the same procedures for the remaining units until all supplies are consumed and all demands are satisfied. For example, the smallest transportation cost is now (0.2), and the allocation supply is one unit. Hence,

Table 6.4 First phase of the SSM algorithm: IBFS solution.

s	$\mathcal{I}_{s,1}$	$\mathcal{I}_{s,2}$	$\mathcal{I}_{s,3}$	$\mathcal{O}_{s,4}$	$\mathcal{O}_{s,5}$	$\mathcal{O}_{s,6}$	**Supply**
1	1.68	1.69	1.64	1.58	~~0~~ 1	1.61	~~2~~ 1
dummy	1.7	1.7	1.7	1.7	1.7	1.7	4
Demand	1	1	1	1	~~1~~ 0	1	

once all remaining units are treated similarly, then the following results can be obtained.

Table 6.5 First phase of the SSM algorithm: IBFS solution (cont.).

s	$\mathcal{I}_{s,1}$	$\mathcal{I}_{s,2}$	$\mathcal{I}_{s,3}$	$\mathcal{O}_{s,4}$	$\mathcal{O}_{s,5}$	$\mathcal{O}_{s,6}$	**Supply**
1	~~1.68~~	~~1.69~~	~~1.64~~	~~1.58~~ 1	~~0~~ 1	~~1.61~~	~~2~~ 0
dummy	~~1.7~~ 1	~~1.7~~ 1	~~1.7~~ 1	~~1.7~~	~~1.7~~	~~1.7~~ 1	~~4~~ 0
Demand	~~1~~ 0	~~1~~ 0	~~1~~ 0	~~1~~ 0	~~1~~ 0	~~1~~ 0	

As can be seen from Table 6.5 the current IBFS is degenerate since the condition of $(m + n - 1)$ is not satisfied, where m and n indicate the total number of columns and rows, respectively. As a consequence, the minimum transportation cost should be found

to be assigned as a dummy value (Δ), and repeat the optimality test until that condition is satisfied. As a result, the following IBFS, after satisfying the previous condition, can be represented in the following table.

Table 6.6 Second phase of the SSM algorithm: Degeneracy

s	$\mathcal{I}_{s,1}$	$\mathcal{I}_{s,2}$	$\mathcal{I}_{s,3}$	$\mathcal{O}_{s,4}$	$\mathcal{O}_{s,5}$	$\mathcal{O}_{s,6}$	**Supply**
1	1.68	1.69	1.64	$1.58^{(1)}$	$0^{(1)}$	$1.61^{(\Delta)}$	2
dummy	$1.7^{(1)}$	$1.7^{(1)}$	$1.7^{(1)}$	1.7	1.7	$1.7^{(1)}$	4
Demand	1	1	1	1	1	1	

The next step is to find the value of u_i and v_j for all occupied elements in table 6.6 by assigning an initial value of zero to one of them, where $c_{ij} = u_i + v_j$. Therefore, by assuming $u_2 = 0$, the result in Table 6.7 are attained.

Table 6.7 Second phase of the SSM algorithm: $(u - v)$ method.

s	$\mathcal{I}_{s,1}$	$\mathcal{I}_{s,2}$	$\mathcal{I}_{s,3}$	$\mathcal{O}_{s,4}$	$\mathcal{O}_{s,5}$	$\mathcal{O}_{s,6}$	**Supply**	$\mathbf{u_i}$
1	1.68	1.69	1.64	$1.58^{(1)}$	$0^{(1)}$	$1.61^{(\Delta)}$	2	-0.09
dummy	$1.7^{(1)}$	$1.7^{(1)}$	$1.7^{(1)}$	1.7	1.7	$1.7^{(1)}$	4	0
Demand	1	1	1	1	1	1		
$\mathbf{v_j}$	1.7	1.7	1.7	1.67	0.09	1.7		

Now, the opportunity cost for the unoccupied units is found by applying the relationship of $d_{ij} = c_{ij} - (u_i + v_j)$. Moreover, the optimal solution can be found at this stage if $d_{ij} \geq 0$, otherwise there exists an alternative solution. In that case, one can select the smallest opportunity cost among unoccupied units to draw a closed loop. After that, we mark each stop point with a plus or minus sign (+/-), alternately, starting with a plus sign (+) at the beginning of the loop. Thus, the following results are obtained as in Table 6.8.

Now, since all the opportunity cost values are greater than zero, i.e., $(d_{ij} \geq 0)$, then the optimal solution is found and the final allocations in our problem for the first sub-carrier is given as below.

The dummy row values can be discarded, since the maximum profit will not be affected. Therefore, U_4 and U_5 are assigned as the optimal pairing of users for $\mathcal{S}_1$. Consequently, these selected users are reserved in the next step, and one can start with the same procedures for all the remaining sub-carriers. Ultimately, the final optimal user pairing for the above problem, after applying the SSM algorithm, can be given as

Table 6.8 Second phase of the SSM algorithm: $u - v$ method (cont.).

s	$\mathcal{I}_{s,1}$	$\mathcal{I}_{s,2}$	$\mathcal{I}_{s,3}$	$\mathcal{O}_{s,4}$	$\mathcal{O}_{s,5}$	$\mathcal{O}_{s,6}$	**Supply**	$\mathbf{u_i}$
1	~~1.68~~ (0.07)	~~1.69~~ (0.08)	~~1.64~~ (0.03)	$1.58^{(1)}$	$0^{(1)}$	$1.61^{(\Delta)}$	2	-0.09
dummy	$1.7^{(1)}$	$1.7^{(1)}$	$1.7^{(1)}$	~~1.7~~ (0.03)	~~1.7~~ (1.61)	$1.7^{(1)}$	4	0
Demand	1	1	1	1	1	1		
$\mathbf{v_j}$	1.7	1.7	1.7	1.67	0.09	1.7		

Table 6.9 Second phase of the SSM algorithm: optimal solution of the first sub-carrier.

s	$\mathcal{I}_{s,1}$	$\mathcal{I}_{s,2}$	$\mathcal{I}_{s,3}$	$\mathcal{O}_{s,4}$	$\mathcal{O}_{s,5}$	$\mathcal{O}_{s,6}$	**Supply**
1	1.68	1.69	1.64	$1.58^{(1)}$	$1.7^{(1)}$	$1.61^{(\Delta)}$	2
dummy	$0^{(1)}$	$0^{(1)}$	$0^{(1)}$	0	0	$0^{(1)}$	4
Demand	1	1	1	1	1	1	

Table 6.10 Second phase of the SSM algorithm: optimal solutions of all sub-carriers.

s	$\mathcal{I}_{s,1}$	$\mathcal{I}_{s,2}$	$\mathcal{I}_{s,3}$	$\mathcal{O}_{s,4}$	$\mathcal{O}_{s,5}$	$\mathcal{O}_{s,6}$	**Supply**
1	0.02	0.01	0.06	0.12	1.7	0.09	2
2	0.05	0.11	0.08	0.05	0.6	0.11	2
3	0.07	0.15	0.04	0.06	0.2	1.5	2
Demand	1	1	1	1	1	1	

6.4.1.2 Least and Most Cost Method (LMCM)

In this approach, it is assumed that each $\mathcal{I}_{s,u}$ is paired with an $\mathcal{O}_{s,u}$. Since indoor users mostly suffer from path loss and non-line of sight (NLOS) impacts, their channel gains may become insignificant. However, in the ideal scenario, outdoor users are supposed to exhibit less of the limitations effects mentioned above, so their channel gains are considered to be better than the channel gains of indoor users. Therefore, a conventional NOMA system user pairing approach is applied, in which the weak user is paired with the strong user, i.e., a subset of indoor users are paired with a subset of outdoor users in each particular sub-carrier. The algorithm proposed for this method is mentioned in the algorithm 3. To illustrate, an example of applying this algorithm is given as $K_s = 2$ and $S = 3$, where the total number of users can be calculated as $U = K_s \times S = 6$ users. Therefore, the same cost matrix (cost function) given in Table

Algorithm 2: Least-cost method (LCM)

```
initialization;
Find max(c_{s,u}) and allocate it;
Subtract max(c_{s,u}) from its supply (s_i) and demand (d_j);
while max(c_{s,u}) is unique do
    if (s_i = 0) and (d_j ≠ 0) then
        Eliminate (cross off) the row of that unit;
    else
        if (s_i ≠ 0) and (d_j = 0) then
            Eliminate (cross off) the column of that unit;
        else
            if (s_i = 0) and (d_j = 0) then
                Eliminate the row and column of that unit;
            end
        end
    end
end
repeat
    ∀ remaining (uncrossed) units
until All demands and supplies are consumed, i.e., (s_i = 0, ∀i) and
  (d_j = 0, ∀j);
```

6.2 is reused, where indoor and outdoor users are highlighted in light red and light blue colours, respectively. Hence, this algorithm is valid when the condition in algorithm 3 is satisfied.

Table 6.11 is divided between $\mathcal{I}_{s,u}$, of light red colour, and $\mathcal{O}_{s,u}$, of light blue colour. Each cell value indicates the average channel gain between BS and a designated user u over a particular sub-carrier s .

According to algorithm 3, the least cost value of the first three columns among all gains in the channel of all indoor users will be selected as an initial starting point, as in table 6.12. Similarly, the most cost-value of the remaining three columns is also chosen to start the second iteration's loop. Once both selected points are found, they become reserved cells for user pairing, and their rows and columns are reset to zero.

The previous procedures are repeated until all possible pairs are selected. Therefore, in Table 6.14, the last applicable choices of the maximum and minimum cost values are lifted with no more rows and columns. Therefore, the iteration is hold and one can assign them as allocated cells for user pairing purposes.

Finally, the optimal selections of the cost matrix for both indoor and outdoor users are indicated by ones, which means that these users can be paired on the same sub-carrier s, and the algorithm ends here.

Algorithm 3: Least and Most Cost Method (LMCM)

input : channel gain matrix with size of $(U \times S)$
output: Paired users of $\mathcal{I}_{s,i}$ and $\mathcal{O}_{s,i}$

```
i : Total number of indoor users;
j : Total number of outdoor users;
𝕌^I ← {c_{1,1}, ..., c_{s,i}}, ∀s, i;
𝕌^O ← {c_{1,i+1}, ..., c_{s,j}}, ∀s, j;
while (i==j) do
    foreach element in 𝕌^I do
        for s ← 1 to S do
            Find min(𝕌^I);
            Strike its row and column values;
        end
    end
    foreach element in 𝕌^O do
        for s ← 1 to S do
            Find max(𝕌^O);
            Strike its row and column values;
        end
    end
    Apply eq. 6.13 to show the paired users status
end
```

Table 6.11 First phase of LMCM: arranging $\mathcal{I}_{s,u}$ and $\mathcal{O}_{s,u}$.

s	$\mathcal{I}_{s,1}$	$\mathcal{I}_{s,2}$	$\mathcal{I}_{s,3}$	$\mathcal{O}_{s,4}$	$\mathcal{O}_{s,5}$	$\mathcal{O}_{s,6}$
1	0.016	0.006	0.006	0.12	1.7	0.06
2	0.048	0.11	0.046	0.05	0.6	0.11
3	0.05	0.15	0.04	0.06	0.2	1.5

Table 6.12 second phase of LMCM: finding the least and the most cost value.

s	$\mathcal{I}_{s,1}$	$\mathcal{I}_{s,2}$	$\mathcal{I}_{s,3}$	$\mathcal{O}_{s,4}$	$\mathcal{O}_{s,5}$	$\mathcal{O}_{s,6}$
1	~~0.016~~	0.006	~~0.006~~	~~0.12~~	1.7	~~0.06~~
2	0.048	0.11	0.046	0.05	0.6	0.11
3	0.05	0.15	0.04	0.06	0.2	1.5

6.4.2 Computational Complexity

SSM algorithm has different phases to eventually provide the optimal solution, which means that time consumption may become critical. In contrast, LMCM algorithm has less time consumption and low complexity comparing to SSM.

Table 6.13 second phase of LMCM: finding the least and the most cost value (cont.).

s	$\mathcal{I}_{s,1}$	$\mathcal{I}_{s,2}$	$\mathcal{I}_{s,3}$	$\mathcal{O}_{s,4}$	$\mathcal{O}_{s,5}$	$\mathcal{O}_{s,6}$
1	0	1	0	0	1	0
2	0.048	0	0.046	0.05	0	0.11
3	~~0.05~~	~~0~~	~~0.04~~	~~0.06~~	~~0~~	~~1.5~~

Table 6.14 second phase of LMCM: finding the least and most cost value (cont.).

s	$\mathcal{I}_{s,1}$	$\mathcal{I}_{s,2}$	$\mathcal{I}_{s,3}$	$\mathcal{O}_{s,4}$	$\mathcal{O}_{s,5}$	$\mathcal{O}_{s,6}$
1	0	1	0	0	1	0
2	0.048	0	0	0.05	0	0
3	0	0	1	0	0	1

Table 6.15 last phase of LMCM: optimal solutions

s	$\mathcal{I}_{s,1}$	$\mathcal{I}_{s,2}$	$\mathcal{I}_{s,3}$	$\mathcal{O}_{s,4}$	$\mathcal{O}_{s,5}$	$\mathcal{O}_{s,6}$
1	0	1	0	0	1	0
2	1	0	0	1	0	0
3	0	0	1	0	0	1

6.4.2.1 Complexity Analysis of SSM Algorithm

The computational complexity analysis for each procedure of Algorithm 1 can be given as below:

- The first step of the Algorithm 1 is about finding the initial basic feasible solution (IBFS), which can be provided by Algorithm 2. The worst-case time is the slowest of the two possibilities: max(time(first if-condition),time(second if-condition)) which can be given as in total complexity of $\mathcal{O}(n)$. Hence, the total process is repeated for all units in the outer loop, which consumes another time complexity of $\mathcal{O}(n)$. Ultimately, the total time complexity for the two loops of Algorithm 2 is $\mathcal{O}(n^2)$.

- The second step of the Algorithm 1 is applied to testing the solution for the optimility, which can be found by searching the whole cost matrix and the time complexity is $\mathcal{O}(n)$.

- In the third step of the Algorithm 1, the attained IBFS is aimed to be improved to overcome the degeneracy. This step consumes time of $\mathcal{O}(n)$ since the calculation

of u-v and the opportunity cost are applied for all occupied and unoccupied cells. That means different loops and the total complexity is $\mathcal{O}(n)$+$\mathcal{O}(n)$.

- In the last steps of the Algorithm 1, outer loops for the second and third steps are applied to obtain the optimal solution where the total complexity in this step is considered as $\mathcal{O}(n^2)$.
- According to the aforementioned discussions, the total time complexity of Algorithm 1 can be straightforwardly expressed as $\mathcal{O}(n^4)$, where different inner and outer loops are applied for the given cost matrix to find the most optimal solution.

6.4.2.2 Complexity Analysis of LCMC Algorithm

In contrast with SSM, LCMC algorithm has less time complexity. To illustrate, the total time complexity of Algorithm 3 is $\mathcal{O}(n^2)$. It has two different independent inner and outer loops that consume time complexity of $\mathcal{O}(n^2)$+$\mathcal{O}(n^2)$.

6.5 Maximizing The Indoor User's Achievable Data Rate

In this section, our aim is to optimise the minimum achievable data rate of indoor users, since they practise low channel gains due to their environmental nature. Therefore, power allocation is applied to improve the minimum data rate of the indoor user. The optimisation problem can be formulated as follows.

$$\max \quad \min\left(R_{s,1}, R_{s,2}\right) \tag{6.16a}$$

$$\text{s.t.} \quad \sum_{s=1}^{S} \mathrm{P}_{s,1} + \sum_{s=1}^{S} \mathrm{P}_{s,2} \leq \mathrm{P}_t \tag{6.16b}$$

$$\mathrm{P}_{s,1} \geq 0, \mathrm{P}_{s,2} \geq 0, \forall s \tag{6.16c}$$

where the constraints of (6.16b) and (6.16c) are used to verify that both users are less than or equal to the total power and are considered positive values. It can be observed that the objective function in (6.16) is considered as a non-convex problem, thus the optimisation problem can be treated as a quasi-concave problem since all of its super-level set is convex and linear. Furthermore, all related constraints are considered convex because of their linearity. In order to solve the above optimisation problem, we need to find its corresponding series of convex feasibility, as in [127]. Therefore, the optimisation problem in (6.16) becomes as follows.

$$\text{find} \quad (\mathrm{P}_{s,1}, \mathrm{P}_{s,2}) \tag{6.17a}$$

$$\text{s.t.} \quad \sum_{s=1}^{S} \mathrm{P}_{s,1} + \sum_{s=1}^{S} \mathrm{P}_{s,2} \leq \mathrm{P}_t, \tag{6.17b}$$

$$\mathrm{P}_{s,1} \geq 0, \mathrm{P}_{s,2} \geq 0, \forall s \tag{6.17c}$$

$$R_{s,1} \geq \alpha, R_{s,2} \geq \alpha. \tag{6.17d}$$

The problem in (6.17a) is feasible when the optimal solutions of $\hat{R}_{s,1} > \alpha$ and $\hat{R}_{s,2} > \alpha$, where $\alpha > 0$, [128]. Consequently, problem (6.17a) can be written as follows.

$$\min \quad \left(\sum_{s=1}^{S} P_{s,1} + \sum_{s=1}^{S} P_{s,2} \right) \tag{6.18a}$$

$$\text{s.t.} \quad \sum_{s=1}^{S} \mathrm{P}_{s,1} + \sum_{s=1}^{S} \mathrm{P}_{s,2} \leq \mathrm{P}_t \tag{6.18b}$$

$$\mathrm{P}_{s,1} \geq 0, \mathrm{P}_{s,2} \geq 0, \forall s \tag{6.18c}$$

$$R_{s,1} \geq \alpha, R_{s,2} \geq \alpha. \tag{6.18d}$$

It is worth noting that the objective function in (6.18a) and all its constraints are convex due to its linearity. Thus, the Lagrangian function of (6.18a) after solving the constraint in (6.18d) is given as

$$\begin{aligned} L(\mathrm{P}_{s,1}, \mathrm{P}_{s,2}, \lambda_1, \lambda_2, \lambda_3) = \sum_{s=1}^{S} \mathrm{P}_{s,1} + \sum_{s=1}^{S} \mathrm{P}_{s,2} + \lambda_1 (\sum_{s=1}^{S} \mathrm{P}_{s,1} + \sum_{s=1}^{S} \mathrm{P}_{s,2} - \mathrm{P}_t) \\ + \lambda_2 (\epsilon \mathrm{P}_{s,2} \Gamma_{s,1} + \epsilon - \mathrm{P}_{s,1} \Gamma_{s,1}) + \lambda_3 (\epsilon - \mathrm{P}_{s,2} \Gamma_{s,2}) \end{aligned} \tag{6.19}$$

where $\Gamma_{s,u} \triangleq \frac{h_{s,u}}{\sigma^2}$, $\epsilon \triangleq 2^{\alpha/B_{sc}} - 1$, and $(\lambda_1, \lambda_2, \lambda_3)$ are the Lagrange multipliers. The optimal solution to the convex problem in (17) can be obtained using the following Karush-Kuhn-Tucker (KKT) equation.

$$\frac{\partial l}{\partial \mathrm{P}_{s,1}} = 1 + \lambda_1 - \lambda_2 \Gamma_{s,1} = 0 \tag{6.20}$$

$$\frac{\partial l}{\partial \mathrm{P}_{s,2}} = 1 + \lambda_1 - \lambda_2 \epsilon \Gamma_{s,1} - \lambda_3 \Gamma_{s,2} = 0 \tag{6.21}$$

$$\frac{\partial l}{\partial \lambda_1} = \mathrm{P}_{s,1} + \mathrm{P}_{s,2} - P_t = 0 \tag{6.22}$$

$$\frac{\partial l}{\partial \lambda_2} = \epsilon \mathrm{P}_{s,2}\Gamma_{s,1} + \epsilon - \mathrm{P}_{s,1}\Gamma_{s,1} = 0 \tag{6.23}$$

$$\frac{\partial l}{\partial \lambda_3} = \epsilon - \mathrm{P}_{s,2}\Gamma_{s,2} = 0 \tag{6.24}$$

Rearranging (6.23) and (6.24), the following expressions of optimal power allocation solutions are obtained;

$$\begin{cases} \mathrm{P}_{s,1} = \frac{\epsilon}{\Gamma_{s,1}}\left(\frac{\epsilon}{\Gamma_{s,2}}\Gamma_{s,1} + 1\right) \\ \mathrm{P}_{s,2} = \frac{\epsilon}{\Gamma_{s,2}} \end{cases}. \tag{6.25}$$

Since the above optimal solutions depend on α and ϵ, we need to recalculate them with respect to ϵ considering (6.22). Therefore, the optimal solution for (6.25) can be found by considering (6.22) as follows:

$$\begin{aligned} \mathrm{P_t} &= \sum_{s=1}^{S} \mathrm{P}_{s,1} + \sum_{s=1}^{S} \mathrm{P}_{s,2} \\ &= \sum_{s=1}^{S} \epsilon \frac{\left(\frac{\epsilon}{\Gamma_{s,2}}\right)\Gamma_{s,1} + 1}{\Gamma_{s,1}} + \sum_{s=1}^{S} \frac{\epsilon}{\Gamma_{s,2}}. \end{aligned} \tag{6.26}$$

To obtain a closed-form for the optimal solution in (6.25), one can solve (6.26) for ϵ and substitute the result in (6.25). Thus, (6.26) is rewritten as

$$\epsilon = \sqrt{\Gamma_{s,2}\mathrm{P}_t} \tag{6.27}$$

Finally, substitute (6.27) into (6.25) to obtain the following expressions.

$$\begin{cases} \mathrm{P}_{s,1} = \frac{\sqrt{\Gamma_{s,2}\mathrm{P}_t}\left(\sqrt{\frac{\mathrm{P}_t}{\Gamma_{s,2}}}\Gamma_{s,1}+1\right)}{\Gamma_{s,1}} \\ \mathrm{P}_{s,2} = \sqrt{\frac{\mathrm{P}_t}{\Gamma_{s,2}}} \end{cases}. \tag{6.28}$$

6.6 Results and Discussion

In this section, the performance of the proposed resource allocation algorithms is evaluated through a number of extensive simulations. The system parameters applied in the simulations are given in table 6.16. For this work, a fixed power allocation technique is applied as $\beta_{s,1} = 0.85$ and $\beta_{s,2} = 0.15$, unless otherwise stated.

Fig. 6.3 shows the data rate achievable by the sum of multiple indoor and outdoor users paired differently using the SSM, LMCM, and random pairing algorithms. The result indicates that the LMCM algorithm outperforms the other two methods, particu-

Table 6.16 Simulation Parameters

Description	Value
Transmit power(P_t)	[-40−40] dBm
Frequency(f)	900 MHz
System bandwidth(BW)	1 MHz
Noise power(σ_j^2)	-174 dBm
indoor distance(d_{in}) in meters	$[1, 2, 3]$ m
Perpendicular loss (L_{pc})	7 dB
The loss in the internal walls (L_i)	7 dB
Number of internal walls in meters (n)	$[1, 2, 3]$
Indoor path loss parameter (χ)	0.6 dB/m
Parallel penetration loss(L_{pt})	20 dB

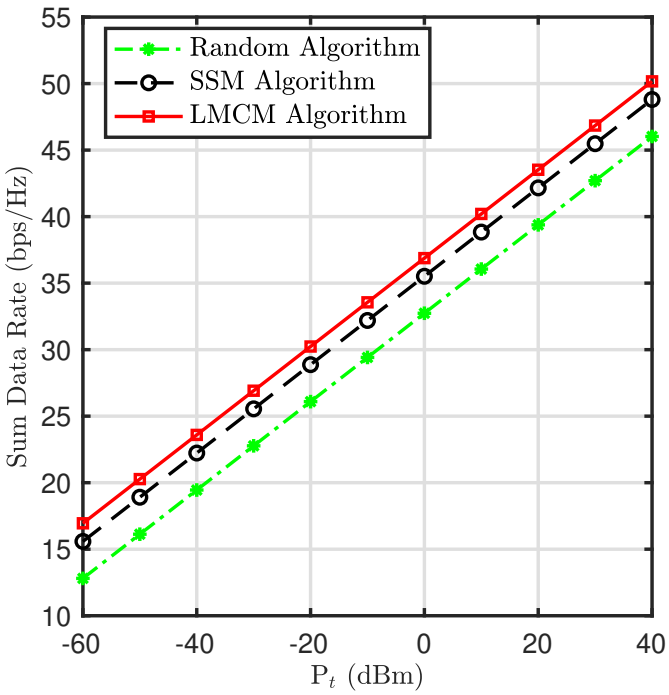

Fig. 6.3 Sum data rate versus transmitted power in dBm.

larly with a significant improvement compared to the random pairing. To illustrate, the LMCM algorithm consistently shows a steady improvement in the sum data rate over the other applied methods. Moreover, the performance difference gained between the LMCM and SSM algorithms is almost half the amount between the LMCM and the random algorithm. This also indicates that the SSM algorithm can provide more enhancements of the sum data rate of all paired users than the random method. Generally speaking, this figure shows some competitive results produced by the aforementioned methods given that the different user pairing techniques can significantly impact the overall system performance.

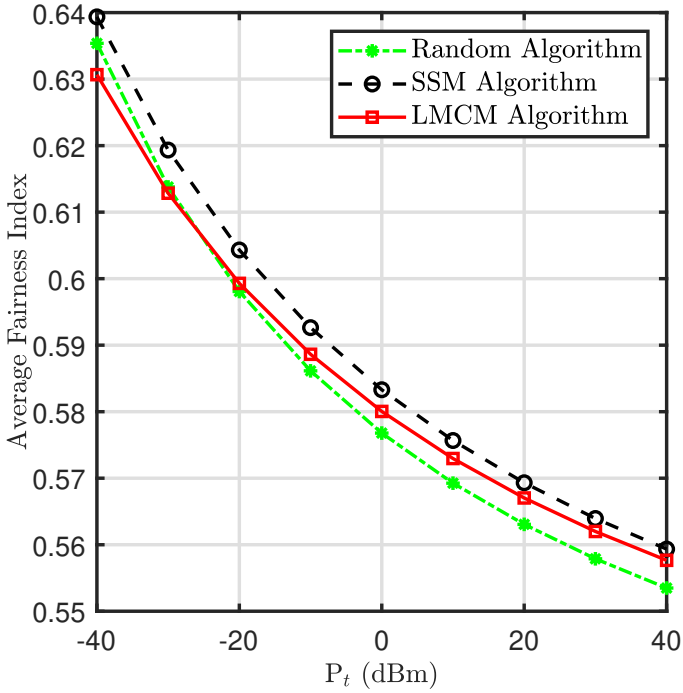

Fig. 6.4 Average fairness index rate of indoor-outdoor users versus transmitted power in dBm over different types of algorithms.

Fig. 6.4 represents one of the main vital performance measures known as the fairness index. It mainly determines whether a user is allocated a fair share of resources relative to the other users. Therefore, this figure explains the average fairness of all sub-carriers presented over the entire range of transmitted power. As can be seen from that figure, all considered algorithms are fluctuated in their fairness performance among all sub-carriers. As a result, SSM provides better fairness among other algorithms where random pairing appears to be the worst among the others, particularly when the transmitted signal exceeds (-20) dbm. A notable difference between LMCM and random algorithms can be achieved at low transmitted power, that is, $(\mathrm{P}_t < -30)$ dBm. In addition to that, random pairing can achieve a very close result to the SSM algorithm but with overlapping at approximately (-30) dBm. In general, the fairness index is degraded when the transmitted power is increased, while both the SSM and the LMCM algorithms can beat the random pairing method. Furthermore, all algorithms employed behave mostly similarly in their fluent curves from low to high transmitting power.

Table 6.17 depicts the values of the fairness index for each individual sub-carrier over some distinct values of the transmitting power. One can notice the difference of the fairness rate among all considered algorithms at various levels of transmit power. For instance, random pairing provides the highest value of the fairness rate on the first sub-carrier at (-40) dBm, whereas it becomes the lowest among the others on the third sub-carrier for the same transmitting powers. In contrast, the SSM algorithm has gained

TABLE 6.17 FAIRNESS INDEX RATE OVER DIFFERENT ALGORITHMS

Algorithm	Sub-carrier	Transmit Power (dBm)				
		-40	-20	0	20	40
Random	1	0.67	0.62	0.60	0.58	0.57
	2	0.65	0.61	0.59	0.57	0.56
	3	0.58	0.56	0.55	0.54	0.53
SSM	1	0.62	0.59	0.58	0.56	0.56
	2	0.64	0.61	0.59	0.57	0.56
	3	0.66	0.61	0.59	0.57	0.56
LMCM	1	0.62	0.59	0.58	0.56	0.56
	2	0.65	0.61	0.59	0.57	0.56
	3	0.62	0.59	0.58	0.56	0.56

the highest value of fairness index on the third sub-carrier over all applied transmitting powers. Finally, as the transmit power increases, the fairness rate among all algorithms decreases.

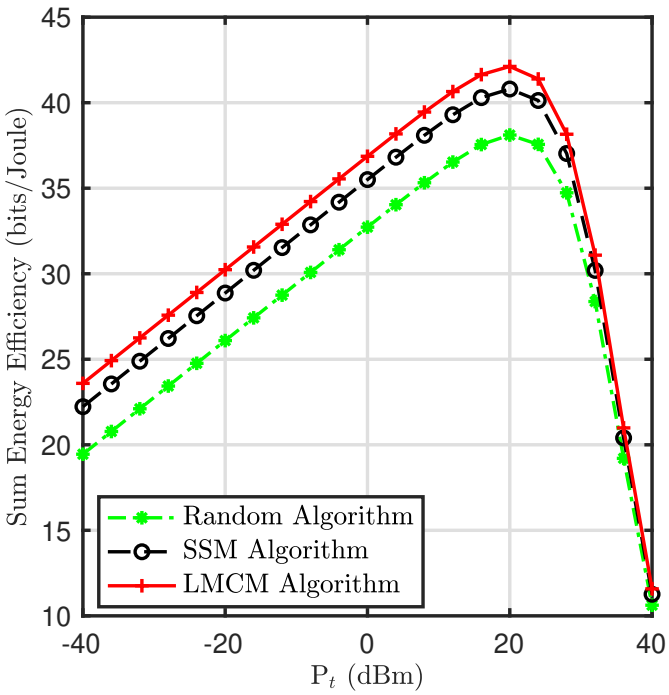

Fig. 6.5 Average energy efficiency versus transmitted power in dBm.

Fig. 6.5 shows the significant impact of different user pairing algorithms on the performance metric of average energy efficiency. Because energy efficiency is inversely

proportional to transmit power, the results show a fast and distinct decrease in energy efficiency at high transmitting power. In contrast, the results gradually increase at low transmission power, where the LMCM algorithm outperforms the SSM and random pairing algorithms. The LMCM algorithm can achieve a maximum value of approximately (7) Mbits / joule at (20) dbm of transmit power. Furthermore, the energy efficiency of the SSM algorithm is about (0.7) Mbits/joule more than that of the random method, while the SSM algorithm achieves (0.2) less than the LMCM algorithm. This indicates that the LMCM is superior to all the other user pairing algorithms considered in this chapter.

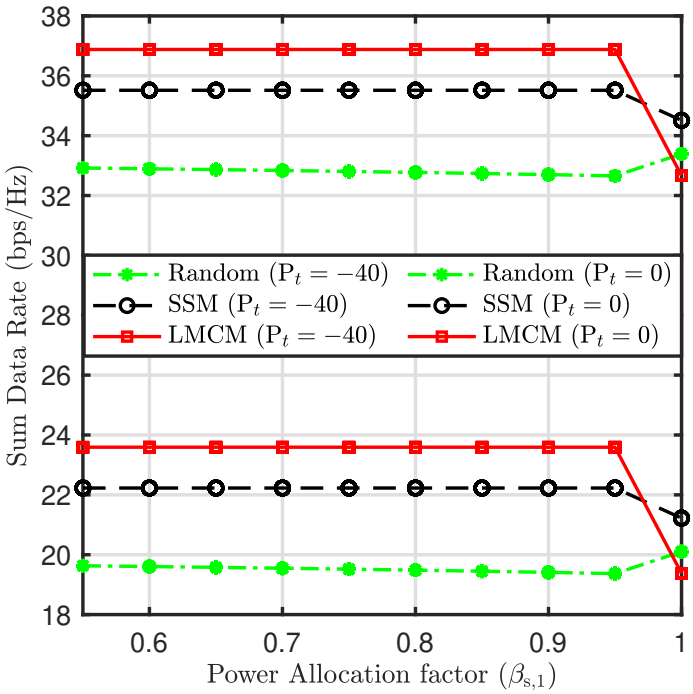

Fig. 6.6 Sum data rate versus power allocation factor of $\beta_{s,1}$.

Fig.6.6 shows the significant role of the power allocation factor $\beta_{s,1}$ in a particular amount of transmit power, that is, $P_t \in \{-40, 0\}$ dBm. It can be seen that the LMCM algorithm achieves the highest data rate assigned among the other methods. In particular, the promising amount of sum data rate gained by LMCM is greater than the SSM algorithm with about (1) Mbps when ($\beta_{s,1} < 0.9$) and ($P_t = 0$) dBm. Similarly, the random algorithm achieves about (2) Mbps less than the LMCM algorithm on the same givens, which indicates that LMCM outperforms all the pairing methods considered. However, when the power allocation factor $\beta_{s,1}$ belongs to the range of (0.9 - 1), the performance of the LMCM and SSM algorithms rapidly decrease below their achieved sum data rate levels. However, the random method increases dramatically by about (0.5) Mbps in the same scenario of exceeding (0.9).

Another important key performance is called the outage probability, where the user

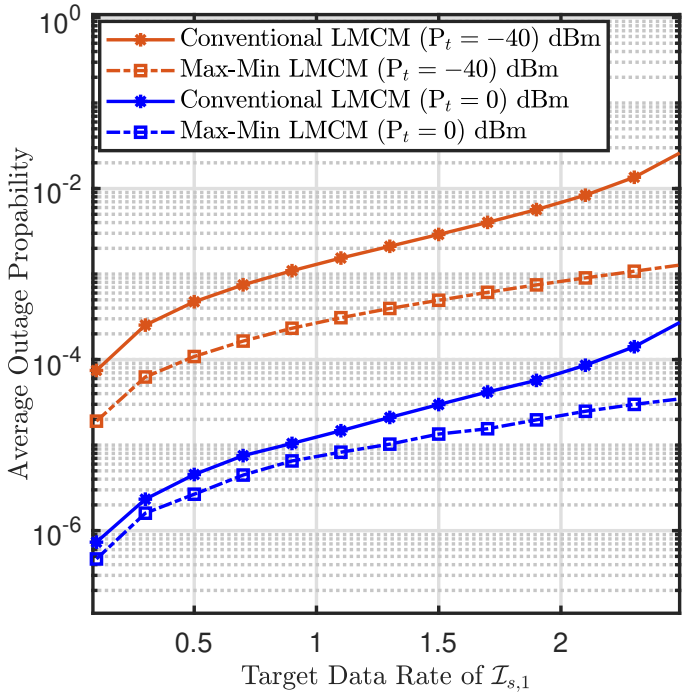

Fig. 6.7 Average outage probability versus target data rate in the conventional and optimised LMCM algorithm.

can achieve lower data rates than the required threshold. Thus, figure 6.7 attempts to show the average outage probability of the indoor and outdoor paired users in all assigned sub-carriers obtained by the LMCM algorithm versus some particular target data rates of indoor users over different values of P_t. In this particular figure, the outage probability performance of the conventional and optimised LMCM algorithm over a fixed range of target data rates of $\mathcal{I}_{s,1}$ is being studied. As can be seen, the optimised method of the LMCM algorithm obtains a low outage compared with the conventional method, as expected. The optimised method improves outage performance, particularly with lower target data rates for indoor users. For example, the system can approach a high outage level when the target data rates of $\mathcal{I}_{s,1}$ are increased, where the optimised method can reduce this outage for further target data rates up to about 2.5 BPCH.

Furthermore, Fig. 6.8 shows the sum data rate of indoor and outdoor users on all sub-carriers versus a range of transmitting power. It involves both conventional and optimised LMCM algorithms. From that figure, it can be seen that a significant improvement in the sum data rate for indoor users is achieved when the optimised method is applied. However, by applying the Max-Min optimisation technique of LMCM, the sum data rate of the outdoor users is decreased by the same amount gained by the indoor users. The main objective of the optimisation is to maximise the minimum data rate for indoor users, and the result shows high potential for indoor users. Therefore, fairness in terms of sum data rate between indoor and outdoor users can be achieved

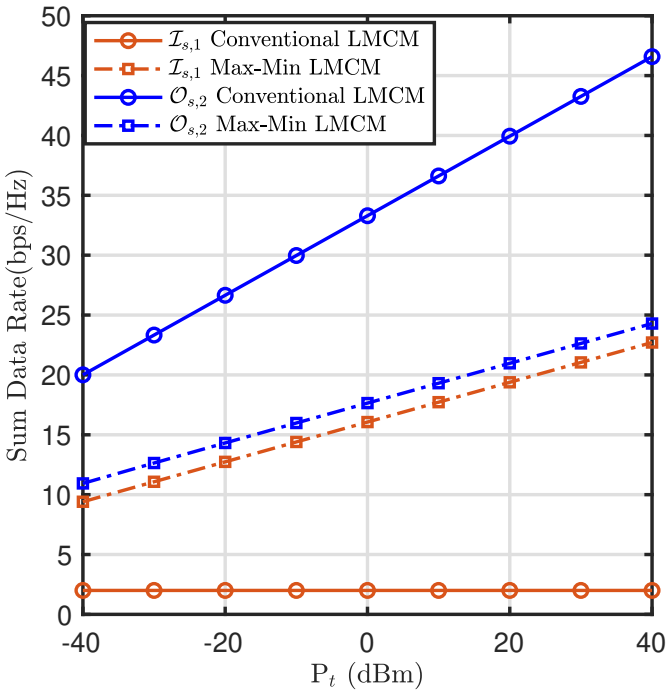

Fig. 6.8 Sum data rate of paired indoor and outdoor users versus transmitted power in dBm.

when considering such an optimisation technique.

6.7 Chapter Summary

In this chapter, the pairing of indoor and outdoor users in NOMA downlink systems have been studied and two different algorithms known as the streamlined simplex method (SSM) and the least and most cost method (LMCM) have been proposed. The proposed algorithms were shown to be able to improve the sum data rate performance by various degrees when a group of users from different environments are paired on the same sub-carrier. Moreover, to obtain more insights, the performance of these algorithms is compared to a random pairing benchmark. To maximise the minimum achievable data rate, which is associated with indoor users in this chapter, the Max-Min optimisation method has been employed. The results demonstrated that the proposed LMCM and SSM algorithms offer superior performance to the random algorithm, where the LMCM algorithm outperforms the SSM algorithm in most cases. The results also show a significantly improved level of fairness rate of the indoor user compared to the conventional method. In future work, our aim is to investigate other advanced optimisation techniques for resource allocations for indoor-outdoor NOMA users with cooperative relay networks and multiple input, multiple output (MIMO) systems.

CHAPTER 7

QoS and QoE in IRS-assisted Indoor NOMA System over κ-μ Fading Channels

A. Alqahtani, and E. Alsusa

Under process to be submitted in: IEEE Transactions on Communications

Abstract

Quality of service (QoS) and quality of experience (QoE) are considered vital indicators in fifth-generation (5G) and beyond cellular systems. This article presents an analytical study on indoor non-orthogonal multiple access (NOMA) systems based on intelligent reflecting surfaces (IRS) over composite $\kappa - \mu$ fading channels. In particular, the QoS of the network has been studied through different performance metrics such as outage probability (OP), ergodic capacity (EC), average bit error rate (BER), and system throughput, for which exact and asymptotic closed-form expressions are derived. In contrast, to measure a user's QoE, it is proposed to use the mean score opinion (MOS) factor to mutate the objective technical criterion into subjective user-recognised quality. Therefore, in this work, an MOS-based QoE evaluation model is applied to the interactive web browsing service. The results indicate that IRS plays an important role in improving the QoS and QoE of indoor NOMA users. Additionally, manipulating channel fading components, power allocation coefficients, and path loss factors enhances overall system performance. Monte Carlo simulations are performed to validate the accuracy of the derived results.

Keywords— non-orthogonal multiple access (NOMA), quality of experience (QoE), intelligent reflecting surface (IRS).

7.1 Chapter Introduction

Driven by the dramatic demands for higher data rates and lower latency beyond 5G wireless networks, non-orthogonal multiple access (NOMA) has been considered a potential multiple access technology, [129]. The key concept of NOMA is to provide multiple users in each orthogonal bandwidth resource block. Traditional orthogonal multiple access (OMA) serves one user in each space direction, while NOMA uses multiple users simultaneously in each space direction. In addition to the fact that NOMA offers high spectral efficiency compared to traditional OMA [37], it can also be combined with other wireless communication technologies, such as intelligent reflecting surfaces (IRS), to actively manage the wireless communication environment to improve reception reliability at a minimal cost. This results in improved throughput, energy efficiency, and communication coverage [130]-[131].

7.2 Related Work

An IRS can change the mobile user's propagation environment, causing tremendous increases in data throughput and reception reliability [132]-[133]. In addition, the potential improvements recognised by IRS such as energy and spectral efficiency and low cost are caused by the main reasons of having no additional spectrum needs, which provide favourable radio propagation conditions. On the contrary, NOMA can also introduce some potentials, such as an effective increase in spectral efficiency, user fairness, massive connectivity, and low latency, by allowing dynamic spectrum sharing among users and achieving their quality of service (QoS) requirements [134]. In essence, these two enabling technologies are complementary, where NOMA can enhance the spectral efficiency and connectivity of IRS systems, and IRS establishes customised constructive propagation environments for NOMA application [135].

Several studies investigate the possibilities of combining NOMA with an intelligent reflecting surface (IRS). For example, Ding *et al.* in [130] proposed a new type of NOMA transmission consisting of IRS, which offers a low-cost antenna array involving a large number of IRS elements. This is done to ensure that multiple users can be served in each orthogonal spatial direction, compared to SDMA. They also studied hardware impairments on the IRS-NOMA design, as well as practical transmission performance. In [136], the authors integrated IRS with NOMA and OMA system and improved IRS reflection with discrete phase shifts for designated systems in order to decrease the transmit power with specified user rates. The results reveal that NOMA may be considered worse than TDMA for near-IRS users with symmetric rates. Thus, they proposed pairing the user with asymmetric rates to overcome this problem. IRS has been used with various wireless communication technologies in a variety of sce-

narios due to its low power consumption and channel manoeuvrability [137]. When an IRS-aided wireless power transfer (WPT) system was deployed to a WPT system in [137], the asymptotic closed expressions of the probability of outage (OP) and the probability of the average symbol error of the system were determined, demonstrating the strong performance of the IRS-supported system. Several research studies have recently been conducted on the combination of IRS and NOMA [138–141]. Ding*et al.* in [138] investigated the impact of two types of IRS phase change (coherent phase shift and random discrete phase shift) on the performance of a NOMA network under various conditions. In [139], the authors analysed an IRS-assisted NOMA system and evaluated OP and average channel capacity in exact closed-form expressions. The findings indicate that the performance of an IRS-supported NOMA network is superior to that of an OMA system. Taking into account numerous antennas, Zhu*et al.* in [140] evaluated an IRS-aided downlink multiple input single output (MISO) system by optimising the beam formation vector and IRS phase change matrix simultaneously to decrease transmission power. Furthermore, Fang *et al.* in [141], studied an IRS-assisted wireless power NOMA network where energy efficiency is optimised under the constraints of minimising the power consumption and maximising the sum data rate.

In NOMA networks, different performance indicators have been investigated to measure the quality of service level (QoS), such as outage probability (OP), throughput, energy efficiency (EE), latency, etc. For example, ElHalawany *et al.* in [142] studied the performance analysis of the NOMA downlink system and derived closed-form expressions of different QoS metrics such as ergodic capacity (EC), average bit error rate (BER), and OP, in which the shadowed fading model $\kappa - \mu$ is applied. Furthermore, Alqahtani*et al.* in [94] studied the QoS of multiple NOMA users by analysing OP, the average bit error rate (BER) and the ergodic capacity (EC). The study shows that channel fading components, power allocation factors, and target data rates have significant impacts on QoS. However, users may experience different levels of QoE even with the same throughput due to considerable variances in application types and user preferences. The mean opinion score (MOS) is often used to assess customer satisfaction with services such as video streaming, file download, and online browsing [143]. Sun *et al.* in [144] investigated the resource allocation problem for NOMA by applying the MOS to evaluate the user's QoE and maximise it. Furthermore, the authors in [145] proposed a QoE-assisted resource allocation algorithm for the multi-cell MC-NOMA network.

7.3 System Model

In this chapter, an IRS-NOMA downlink system is considered, which consists of a single base station (BS), an IRS, equipped with passive reflective elements N, and three

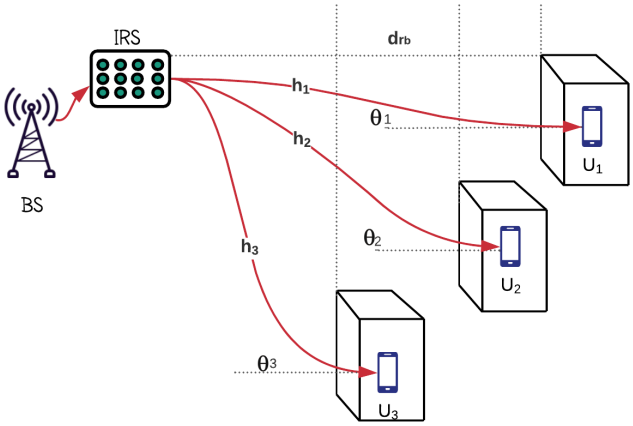

Fig. 7.1 System model

legitimate indoor users. The communications between BS and legitimate users are done through the IRS which is considered to be deployed very close to the BS. Henceforth, the channel attenuation between the BS and IRS is neglected. In addition to that, the IRS is assumed to be aware of the channel information, so the induced phase of a reflected element is manipulated to maximise the instantaneous signal-to-noise ratio (SNR) on the receiver side. It should be noticed that CSI considered in this work is not practical, but is assumed to provide technical performance.

7.3.1 Path Loss Model

In this article, all active wireless channels are assumed to be independent and identically distributed (i.i.d.) and follow the composite $\kappa - \mu$ fading model, where all channel state information (CSI) is assumed to be fully available in the BS. Furthermore, legitimate nodes can detect the NOMA signal over a single hop established between outdoor-to-indoor channels, where they are affected by the outdoor-to-indoor path loss. Therefore, the path loss model of the indoor NOMA environment, discussed in [122], is used. Therefore, the total path loss for U_i can be calculated as follows.

$$PL_i = L_{fs} + L_t + L_{in} \tag{7.1}$$

where L_{fs} represents the loss of the free space path, which can be given as $32.45 + 20\log_{10}((d_{rb} + d_{in})) + 20\log_{10}(f)$, where d_{in} is the distance between the wall of the building and U^I, and d_{rb} is the distance between the UAV and the wall of the external building. Furthermore, L_t is known as the loss of the propagation transition path that involves the perpendicular loss L_{pc} and the parallel penetration loss L_{pt}. It can be given as

$$L_t = L_{pc} + L_{pt} \times (1 - \sin(\theta))^2 \tag{7.2}$$

where θ indicates the grazing angle between the BS and the exterior wall of the building, given as $\theta = \cos^{-1}(d_{rb}/d_{out})$. Furthermore, the loss of the indoor propagation path, L_{in}, is obtained by the mean loss of the path selected from the interior side of the exterior wall, which can be calculated as

$$L_{in} = \max\{n\, L_i, \chi(d_{in} - 2)(1 - \sin(\theta))^2\} \tag{7.3}$$

where χ is the parameter of loss of the indoor path, n is the number of internal walls, and L_i is the loss of internal walls.

7.4 Performance Analysis

7.4.1 Signal to Interference and Noise Ratio (SINR)

The signal received by each user can be mathematically described as

$$y_i = \left(\sum_{n=1}^{N} h_{i,n} e^{j\phi_{i,n}}\right) \times \underbrace{\left(\sum_{i} \sqrt{a_i \mathrm{P}_s} x_i\right)}_{x_{sc}} + n_i. \tag{7.4}$$

where $i \in \{U_1, U_2, U_3\}$, P_s is the total transmission power in BS, and x_{sc} defines the superimposed signal, in which x_1, x_2 and x_3 represent the data symbols of U_1, U_2 and U_3, respectively. Furthermore, α_i represents the power allocation factor of the user i, and is given accordingly as $\sum_i^3 a_i = 1$ and $a_3 \leq a_2 \leq a_1$. $h_{i,n} = \alpha_{i,n} e^{j\theta_{i,n}}$ illustrates the channel gain between the ith user and the nth passive reflector of IRS, $n \in \{1, 2, ..., N\}$, where α_n and θ_n define its magnitude and phase, respectively. It is assumed that each induced phase of the IRS passive reflector is given as $(\phi_{i,n} = -\theta_{i,n})$, which leads to the maximum SNR. Without loss of generality, the channel coefficients between the BS and all indoor users are considered to be in ascending order as $|\sum_{n=1}^{N} h_{1,n}|^2 \leq |\sum_{n=1}^{N} h_{2,n}|^2 \leq |\sum_{n=1}^{N} h_{3,n}|^2$, where the effects of path loss (PL) and small-scale fading (g_i) are given as $|h_{i,n}| = \frac{g_{i,n}}{\sqrt{PL_{i,n}}}$. In particular, $g_{i,n}$ is modelled as the sum of N independent and identically distributed (i.i.d.) $\kappa - \mu$ random variables (RV) in this work. Furthermore, n_i indicates the additive white Gaussian noise (AWGN), where $n_i \sim \mathcal{CN}(0, \sigma_i^2)$. Thereafter, the noise powers of all users are assumed to be identical in this work. Therefore, the signal-to-interference noise ratio (SINR) received at U_1 is given below.

$$\gamma_{U_1}^{x_1} = \frac{a_1 \mathrm{P}_s \zeta_1}{a_2 \mathrm{P}_s \zeta_1 + a_3 \mathrm{P}_s \zeta_1 + \sigma^2} = \frac{a_1 \gamma_1}{a_2 \gamma_1 + a_3 \gamma_1 + 1}, \tag{7.5}$$

where $\zeta_1 = |\sum_{n=1}^{N} h_{1,n}|^2$, $\rho = \frac{\mathrm{P_s}}{\sigma^2}$ and $\gamma_1 \triangleq \rho\zeta_1$, which is the instantaneous SNR at U_1.

According to the NOMA principle, U_2 can detect U_1's signal and treat it as interference to be eliminated, and then decode its own signal while U_3's signal is treated as noise. This infers the successive interference cancellation (SIC) technique. Subsequently, the SINR at U_2 is given to detect the symbols x_1 and x_2, respectively, as follows.

$$\gamma_{U_2}^{x_1 \to x_2} = \frac{a_1 \mathrm{P}_s \zeta_2}{a_2 \mathrm{P}_s \zeta_2 + a_3 \mathrm{P}_s \zeta_2 + \sigma^2} = \frac{a_1 \gamma_2}{a_2 \gamma_2 + a_3 \gamma_2 + 1} \tag{7.6}$$

$$\gamma_{U_2}^{x_2} = \frac{a_2 \mathrm{P}_s \zeta_2}{a_3 \mathrm{P}_s \zeta_2 + \sigma^2} = \frac{a_2 \gamma_2}{a_3 \gamma_2 + 1}, \tag{7.7}$$

where $\zeta_2 = |\sum_{n=1}^{N} h_{2,n}|^2$ and $\gamma_2 \triangleq \rho \zeta_2$, which is the instantaneous SNR at U_2. Similarly, U_3 treats the signals of other users as interference and applies SIC to decode and eliminate them to obtain its own signal. Therefore, the SINR at U_3 to detect the symbols x_1, x_2, and x_3 are given, respectively, as follows.

$$\gamma_{U_3}^{x_1 \to x_2} = \frac{a_1 \mathrm{P}_s \zeta_3}{a_2 \mathrm{P}_s \zeta_3 + a_3 \mathrm{P}_s \zeta_3 + \sigma^2} = \frac{a_1 \gamma_3}{a_2 \gamma_3 + a_3 \gamma_3 + 1} \tag{7.8}$$

$$\gamma_{U_3}^{x_2 \to x_3} = \frac{a_2 \mathrm{P}_s \zeta_3}{a_3 \mathrm{P}_s \zeta_3 + \sigma^2} = \frac{a_2 \gamma_3}{a_3 \gamma_3 + 1} \tag{7.9}$$

$$\gamma_{U_3}^{x_3} = \frac{a_3 \mathrm{P}_s \zeta_3}{\sigma^2} = a_3 \gamma_3, \tag{7.10}$$

where $\zeta_3 = |\sum_{n=1}^{N} h_{3,n}|^2$ and $\gamma_3 \triangleq \rho \zeta_3$, which is the instantaneous SNR at U_3.

7.4.2 Outage Probability (OP):

Essentially, the OP analysis involves the scenario in which the individual user's data rate is demanded to satisfy a certain quality of service (QoS). Therefore, the outage event of U_1 appears when its SINR or data rate is less than a threshold or a predefined data rate, and it can be expressed as

$$\mathrm{P}_{U_1}^{out} = 1 - \mathrm{P}_r\left(\gamma_{U_1}^{x_1} > \gamma_{th_1}\right) = 1 - \left[1 - \underbrace{\mathrm{P}_r\left(\gamma_{U_1}^{x_1} < \gamma_{th_1}\right)}_{E_{11}}\right], \tag{7.11}$$

where $\gamma_{th_1} = 2^{R_1} - 1$, and R_1 is the target data rate of U_1. Now, submitting (7.5) into E_{11} yields the following expression.

$$E_{11} = \mathrm{P}_r\left(\gamma_1 < \frac{\gamma_{th_1}}{(a_1 - a_2\gamma_{th_1} - a_3\gamma_{th_1})} \triangleq \varepsilon_1\right) = F_\gamma\left(\varepsilon_1\right). \tag{7.12}$$

Now, (2.14) is substituted into (7.12), and then the result is resubmitted into (7.11), resulting in

$$\begin{aligned}\mathrm{P}_{U_1}^{out} = 1 - \Bigg(1 - \frac{1}{\mathrm{e}^{(N\mu\kappa)}} \sum_{c=0}^{\infty} \frac{(N\kappa\mu)^c}{c!\,\Gamma(c+N\mu)} \\ \times \mathrm{H}_{1,2}^{1,1}\left[\frac{N\mu(1+\kappa)\varepsilon_1}{\bar{\gamma}_1}\middle| \begin{matrix}(1,1)\\(c+N\mu,1),(0,1)\end{matrix}\right]\Bigg).\end{aligned} \tag{7.13}$$

Similarly, U_2 can be out of service if its SINR or U_1's SINR are below certain thresholds. In other words, outage events of U_2 are considered when the U_1' s signal is incorrectly decoded at U_2 during the SIC process or if its own signal (x_2) is also improperly decoded. As a result, the OP of U_2 can be obtained as follows.

$$\begin{aligned}\mathrm{P}_{U_2}^{out} &= 1 - \mathrm{P}_r\left(\gamma_{U_2}^{x_1\to x_2} > \gamma_{th_1}, \gamma_{U_2}^{x_2} > \gamma_{th_2}\right) \\ &= 1 - \left[\left(1 - \mathrm{P}_r\left(\gamma_{U_2}^{x_1\to x_2} < \gamma_{th_1}\right)\right)\left(1 - \mathrm{P}_r\left(\gamma_{U_2}^{x_2} < \gamma_{th_2}\right)\right)\right].\end{aligned} \tag{7.14}$$

By substituting (7.7) and (7.8) into (7.14), and following the same procedures as (7.11)-(7.13), the OP of U_2 can be given in the following form as follows.

$$\begin{aligned}\mathrm{P}_{U_2}^{out} = 1 - \prod_{i=1}^{2}\Bigg(1 - \frac{1}{\mathrm{e}^{(N\mu\kappa)}} \sum_{c=0}^{\infty} \frac{(N\kappa\mu)^c}{c!\,\Gamma(c+N\mu)} \\ \mathrm{H}_{1,2}^{1,1}\left[\frac{N\mu(1+\kappa)\varepsilon_{2,i}}{\bar{\gamma}_2}\middle| \begin{matrix}(1,1)\\(c+N\mu,1),(0,1)\end{matrix}\right]\Bigg).\end{aligned} \tag{7.15}$$

where $\varepsilon_{2,1} = \varepsilon_1$ and $\varepsilon_{2,2} = \frac{\gamma_{th_2}}{(a2 - a3\gamma_{th_2})}$.

In a similar fashion, U_3 can experience an outage if its own SINR or U_1's SINR or U_2's SINR are below certain thresholds. Consequently, the outage events of U_3 are presented when the U_1's or U_2's signals are imprecisely decoded in U_3 during the SIC process or if its own signal (x_3) is also incorrectly decoded. Thereafter, the OP of U_3 can be illustrated as follows.

$$\begin{aligned}\mathrm{P}_{U_3}^{out} &= 1 - \mathrm{P}_r\left(\gamma_{U_3}^{x_1\to x_2} > \gamma_{th_1}, \gamma_{U_3}^{x_2\to x_3} > \gamma_{th_2}, \gamma_{U_3}^{x_3} > \gamma_{th_3}\right) \\ &= 1 - \Big[\left(1 - \mathrm{P}_r\left(\gamma_{U_3}^{x_1\to x_2} < \gamma_{th_1}\right)\right) \\ &\quad \left(1 - \mathrm{P}_r\left(\gamma_{U_3}^{x_2\to x_3} < \gamma_{th_2}\right)\right)\left(1 - \mathrm{P}_r\left(\gamma_{U_3}^{x_3} < \gamma_{th_3}\right)\right)\Big].\end{aligned} \tag{7.16}$$

$$\mathrm{P}_{U_1}^{out}(\infty) = 1 - \left(1 - \frac{1}{\mathrm{e}^{(N\mu\kappa)}} \sum_{c=0}^{\infty} \frac{(N\kappa\mu)^c}{c!\,\Gamma(1+c+N\mu)} \times \left(\frac{N\mu(1+\kappa)\varepsilon_1}{\bar{\gamma}_1}\right)^{c+N\mu}\right). \tag{7.18}$$

$$\mathrm{P}_{U_2}^{out}(\infty) = 1 - \prod_{i=1}^{2}\left(1 - \frac{1}{\mathrm{e}^{(N\mu\kappa)}} \sum_{c=0}^{\infty} \frac{(N\kappa\mu)^c}{c!\,\Gamma(1+c+N\mu)} \times \left(\frac{N\mu(1+\kappa)\varepsilon_{2,i}}{\bar{\gamma}_2}\right)^{c+N\mu}\right). \tag{7.19}$$

$$\mathrm{P}_{U_3}^{out}(\infty) = 1 - \prod_{i=1}^{3}\left(1 - \frac{1}{\mathrm{e}^{(N\mu\kappa)}} \sum_{c=0}^{\infty} \frac{(N\kappa\mu)^c}{c!\,\Gamma(1+c+N\mu)} \times \left(\frac{N\mu(1+\kappa)\varepsilon_{3,i}}{\bar{\gamma}_3}\right)^{c+N\mu}\right). \tag{7.20}$$

Follow the same previous steps to find the final format of OP of U_3 as follows.

$$\begin{aligned}\mathrm{P}_{U_3}^{out} = 1 - \prod_{i=1}^{3}\Bigg(1 - \frac{1}{\mathrm{e}^{(N\mu\kappa)}} \sum_{c=0}^{\infty} \frac{(N\kappa\mu)^c}{c!\,\Gamma(c+N\mu)} \\ \times \mathrm{H}_{1,1}^{1,2}\left[\frac{N\mu(1+\kappa)\varepsilon_{3,i}}{\bar{\gamma}_3}\middle| \begin{matrix}(1,1)\\(c+N\mu,1),(0,1)\end{matrix}\right]\Bigg),\end{aligned} \tag{7.17}$$

where $\varepsilon_{3,1} = \varepsilon_1$, $\varepsilon_{3,2} = \varepsilon_{2,2}$ and $\varepsilon_{3,3} = \frac{\gamma_{th_3}}{a3}$.

To seek further insight, the asymptotic OP at high SNR, i.e., ($\bar{\gamma} \to \infty$) has been studied. Therefore, apply the following asymptotic expression of the Fox H function given in [146] as follows.

$$\lim_{z\to 0} \mathrm{H}_{p,q}^{m,n} \cong \sum_{j=1}^{m}\left[h_i z^{\frac{b_j}{\beta_j}} + \mathcal{O}(z\frac{b_j+1}{\beta_j})\right], \tag{7.21}$$

where $\mathcal{O}$ indicates the high order and h_j is defined as follows.

$$h_j = \frac{\prod_{i=1,i\neq j}^{m}\Gamma(b_i - \frac{b_j\beta_i}{\beta_j})\prod_{i=1}^{n}\Gamma(1-a_i+\frac{b_j a_i}{\beta_j})}{\beta_j\,\prod_{i=1+n}^{p}\Gamma(a_i - \frac{b_j a_i}{\beta_j})\prod_{i=1+m}^{q}\Gamma(1-b_i+\frac{b_j\beta_i}{\beta_j})}. \tag{7.22}$$

Now, the asymptotic OP expressions of all users are achieved by applying the above identity to (7.13), (7.15) and (7.17), and they are stated at the top of the next page.

7.4.3 Throughput Analysis

The system throughput of each user in a delay-limited transmission mode can be evaluated by its OP or ergodic capacity. Therefore, the corresponding outage throughput of a two-user NOMA system is given as follows.

$$\mathrm{T}_i^{\mathrm{OP}} = \left(1 - \mathrm{P}_i^{out}\right) \times R_i, \tag{7.23}$$

where R_i is the individual data rate of user i, in which $i \in \{U_1, U_2 U_3\}$. Hence, R_i can be calculated as: $\mathrm{R}_i = BW \times \log_2(1 + \gamma_i)$. Therefore, (7.13) and (7.15) and (7.17) are substituted in (7.23), separately, to obtain the throughput of all legitimate users.

7.4.4 Average Bit Error Rate (BER)

It is common practise to assess the quality of communication links in the presence of fading by characterising the conditional function of (BER) over the probability density function of the instantaneous signal-to-noise ratio (SNR) of the fading channel. For a wide range of wireless systems, the expressions for BER can be given as in [6] as follows.

$$\bar{P}_l^e = \int_0^\infty P_l^e \, f_{\gamma_l}(\gamma) d\gamma, \tag{7.24}$$

where $l \in \{1, 2, 3\}$. In this subsection, three different indoor NOMA users with similar modulation orders using QAM, i.e., $M_l = 4 \; \forall l$, $l \in$ 1,2,3 are being proposed, and the average BER performance is investigated in the κ -μ fading model. The conditional BER (P_l^e) of the three users can be given, respectively, in terms of $\mathrm{Q}(.)$ as in [94].

$$P_1^e = \frac{1}{4} \sum_{i=1}^{4} \mathrm{Q}\left(\sqrt{\lambda_{3,i} \gamma_1}\right) \tag{7.25}$$

$$P_2^e = \frac{1}{4} \sum_{i=5}^{14} c_i \times \mathrm{Q}\left(\sqrt{\lambda_{3,i} \gamma_1}\right) \tag{7.26}$$

$$P_3^e = \frac{1}{4} \sum_{i=15}^{33} d_i \times \mathrm{Q}\left(\sqrt{\lambda_{3,i} \gamma_1}\right) \tag{7.27}$$

where $d_i = [4, -2, 2, 1, -1, 1, -2, 2, -2, 1, 1, -1, 1, -1, 2, -1, -1, 1, -1]$, $c_i = [1, -1, 2, 1, -1, 2, 1, -1, 1, -1]$, and $\gamma_{3,i}$ can be found in [94]. Now, submit (7.25)

in (7.24). Thus, the following expression is obtained.

$$P_1^e = \frac{1}{4}\sum_{i=1}^{4}\left[\mathcal{D}_1\int_0^\infty {\gamma_1}^{c+N\mu-1}\exp\left(-\frac{N\mu(1+\kappa)\gamma}{\bar{\gamma}}\right)\mathrm{Q}\left(\sqrt{\lambda_{3,i}\gamma_1}\right)d\gamma\right]. \quad (7.28)$$

where $\mathcal{D}_1 = \frac{1}{\mathrm{e}^{(N\mu\kappa)}}\sum_{c=0}^{\infty}\frac{(N\mu)^{2c+N\mu}\kappa^c(1+\kappa)^{c+N\mu}}{c!\ \Gamma(c+N\mu)\bar{\gamma}_1^{(c+N\mu)}}$. With the aid of [99, pp. 8.4.3.1, 8.4.14.2, 8.4.16.1], [13, p. 6.2.8], and the identity of $\mathrm{Q}(x) = \frac{1}{2}\mathrm{erfc}\left(\frac{x}{\sqrt{2}}\right)$, the integral in (7.25) can be evaluated as follows.

$$I_1 = \frac{1}{\sqrt{\pi}}\int_0^\infty \gamma_1^{(c+N\mu-1)}\ \mathrm{G}_{0,1}^{1,0}\left[\frac{N\mu(1+\kappa)\gamma}{\bar{\gamma}}\middle|\begin{matrix}-\\0\end{matrix}\right]\times\mathrm{G}_{1,2}^{2,0}\left[\frac{\lambda_{3,i}\gamma_1}{2}\middle|\begin{matrix}1\\0,\frac{1}{2}\end{matrix}\right]d\gamma_1. \quad (7.29)$$

The integral above in (7.29) can be solved by using the Mellin transform of the two-fox H function, given as [71].

$$I_1 = \frac{1}{\sqrt{\pi}}\left(\frac{\lambda_{3,i}}{2}\right)^{-(c+N\mu)} \times \mathrm{H}_{2,2}^{1,2}\left[\frac{N\mu(1+\kappa)}{\bar{\gamma}_1}\delta^{-1}\middle|\begin{matrix}(1-c-N\mu,1) & \left(\frac{1}{2}-c-N\mu,1\right)\\(0,1) & (-c-N\mu,1)\end{matrix}\right], \quad (7.30)$$

where $\delta = \left(\frac{\lambda_{3,i}}{2}\right)$. Substituting (7.30) into (7.28), the average BER of U_1 is given at the top of the next page. Likewise, follow the same procedures as applied for U_1 to obtain the average BER of the remaining users. As a result, (7.32) and (7.33), given at the top of the next page, express the average BER of U_2 and U_3, respectively.

At high SNR, the asymptotic expression of the average BER can be achieved for all users using the identity of (7.17) in (7.31)-(7.33). Therefore, the closed asymptotic expressions of all users are given at the top of the next page in (7.34)-(7.36).

7.4.5 Average Channel Capacity

The Shannon channel fading capacity, which is also known as the ergodic capacity in (bits/s/Hz), is defined in [6] as

$$\bar{C}_l = B\int_0^\infty \log_2(1+\gamma_l)f_{\gamma_l}(\gamma_l)d\gamma_l. \quad (7.37)$$

where $l \in \{1,2,3\}$.

For the case of $l = 1$, substitute (7.5) in (7.37) and recall the identity of $\log_e(x) = \ln(x)/\ln(e)$. Thus, after some algebraic manipulations, one can obtain the following

$$\bar{P}_1^e = \frac{1}{4}\sum_{i=1}^{4}\left(\frac{1}{\sqrt{\pi}}\mathcal{D}_1\left(\delta\right)^{-(c+N\mu)}\right.$$
$$\left.\times\ \mathrm{H}_{2,2}^{1,2}\left[\frac{N\mu(1+\kappa)}{\bar{\gamma}_1}\left(\delta\right)^{-1}\middle|\begin{matrix}(1-c-N\mu,1) & \left(\frac{1}{2}-c-N\mu,1\right)\\ (0,1) & (-c-N\mu,1)\end{matrix}\right]\right). \tag{7.31}$$

$$\bar{P}_2^e = \frac{1}{4}\sum_{i=5}^{14}\left(\frac{1}{\sqrt{\pi}}\mathcal{D}_2\ c_i\left(\delta\right)^{-(c+N\mu)}\right.$$
$$\left.\times\ \mathrm{H}_{2,2}^{1,2}\left[\frac{N\mu(1+\kappa)}{\bar{\gamma}_2}\left(\delta\right)^{-1}\middle|\begin{matrix}(1-c-N\mu,1) & \left(\frac{1}{2}-c-N\mu,1\right)\\ (0,1) & (-c-N\mu,1)\end{matrix}\right]\right). \tag{7.32}$$

$$\bar{P}_3^e = \frac{1}{4}\sum_{i=15}^{33}\left(\frac{1}{\sqrt{\pi}}\mathcal{D}_3\ d_i\left(\delta\right)^{-(c+N\mu)}\right.$$
$$\left.\times\ \mathrm{H}_{2,2}^{1,2}\left[\frac{N\mu(1+\kappa)}{\bar{\gamma}_3}\left(\delta\right)^{-1}\middle|\begin{matrix}(1-c-N\mu,1) & \left(\frac{1}{2}-c-N\mu,1\right)\\ (0,1) & (-c-N\mu,1)\end{matrix}\right]\right). \tag{7.33}$$

$$\bar{P}_1^{e(\infty)} = \frac{1}{4}\sum_{i=1}^{4}\left[\frac{1}{\sqrt{\pi}}\mathcal{D}_1\left(\delta\right)^{-(c+N\mu)}\times\frac{\Gamma(c+N\mu)\Gamma(\frac{1}{2}+c+N\mu)}{\Gamma(1+c+N\mu)}\right]. \tag{7.34}$$

$$\bar{P}_2^{e(\infty)} = \frac{1}{4}\sum_{i=5}^{14}\left(\frac{1}{\sqrt{\pi}}\mathcal{D}_2\ c_i\left(\delta\right)^{-(c+N\mu)}\times\frac{\Gamma(c+N\mu)\Gamma(\frac{1}{2}+c+N\mu)}{\Gamma(1+c+N\mu)}\right]. \tag{7.35}$$

$$\bar{P}_3^{e(\infty)} = \frac{1}{4}\sum_{i=15}^{33}\left(\frac{1}{\sqrt{\pi}}\mathcal{D}_3\ d_i\left(\delta\right)^{-(c+N\mu)}\times\frac{\Gamma(c+N\mu)\Gamma(\frac{1}{2}+c+N\mu)}{\Gamma(1+c+N\mu)}\right]. \tag{7.36}$$

Table 7.1 Definitions for The Symbols Used in Formulations.

Symbol	Definition	Symbol	Definition
$\lambda_{3,1}$,$\lambda_{3,6}$,$\lambda_{3,33}$	$A_1 + A_2 + A_3$	$\lambda_{3,2}$,$\lambda_{3,11}$,$\lambda_{3,30}$	$A_1 - A_2 + A_3$
$\lambda_{3,3}$,$\lambda_{3,14}$,$\lambda_{3,24}$	$A_1 + A_2 - A_3$	$\lambda_{3,4}$,$\lambda_{3,8}$,$\lambda_{3,18}$	$A_1 - A_2 - A_3$
$\lambda_{3,5}$,$\lambda_{3,31}$	$2A_1 + A_2 + A_3$	$\lambda_{3,7}$	$A_2 + A_3$
$\lambda_{3,9}$,$\lambda_{3,20}$	$2A_1 - A_2 - A_3$	$\lambda_{3,10}$,$\lambda_{3,22}$	$A_2 - A_3$
$\lambda_{3,12}$,$\lambda_{3,28}$	$2A_1 - A_2 + A_3$	$\lambda_{3,13}$,$\lambda_{3,25}$	$2A_1 + A_2 - A_3$
$\lambda_{3,15}$	A_3	$\lambda_{3,16}$	$A_2 + A_3$
$\lambda_{3,17}$	$2A_2 + A_3$	$\lambda_{3,19}$	$2A_1 - 2A_2 - A_3$
$\lambda_{3,21}$	$2A_1 - A_3$	$\lambda_{3,23}$	$2A_2 - A_3$
$\lambda_{3,26}$	$2A_1 + 2A_2 - A_3$	$\lambda_{3,29}$	$2A_1 + A_3$
$\lambda_{3,32}$	$2A_1 + 2A_2 + A_3$	$\lambda_{3,27}$	$2A_1 - 2A_2 + A_3$
$A_1 = \sqrt{a_1}$, $A_2 = \sqrt{a_2}$, $A_3 = \sqrt{a_3}$			

expression.

$$\bar{C}_1 = \frac{\mathrm{B}}{\ln(2)} \left[\underbrace{\int_0^\infty \ln\left(1+\gamma_1\right) f_{\gamma_1}(\gamma_1) d\gamma_1}_{\mathcal{I}_1} - \underbrace{\int_0^\infty \ln\left(1+\Psi\gamma_1\right) f_{\gamma_1}(\gamma_1) d\gamma_1}_{\mathcal{I}_2} \right], \quad (7.38)$$

where $\Psi = (1 - a_1)$. Substituting (2.13) and (7.5) into the integral of $\mathcal{I}_1$, and applying further manipulations, the following is obtained.

$$\mathcal{I}_1 = \int_0^\infty {\gamma_1}^{c+N\mu-1} \exp\left(-\frac{N\mu(1+\kappa)\gamma_1}{\bar{\gamma}_1}\right) \times \ln\left(1+\gamma_1\right) d\gamma_1 \times \mathcal{D}_1, \quad (7.39)$$

where $\mathcal{D}_1$ is defined in (7.28). The above integral can be expressed in a compact form by rewriting exponential and logarithmic functions in their alternative Meijer G function formats defined in [99, pp. 8.4.3.1, 8.4.6.5]. Thus,

$$\mathcal{I}_1 = \mathcal{D}_1 \times \int_0^\infty \gamma_1^{(C+N\mu-1)} \; \mathrm{G}_{0,1}^{1,0} \left[\frac{\gamma_1 N\mu(1+\kappa)}{\bar{\gamma}_1} \middle| \begin{matrix} - \\ 0 \end{matrix} \right] \times \mathrm{G}_{2,2}^{1,2} \left[\gamma_1 \middle| \begin{matrix} 1,1 \\ 1,0 \end{matrix} \right] d\gamma_1. \quad (7.40)$$

To solve the above integral in a closed form, the identity in [147] is applied. Thus, the following expression is obtained.

$$\mathcal{I}_1 = \mathcal{D}_1 \Upsilon_1 \times \mathrm{G}_{3,2}^{1,3} \left[\left(\frac{N\mu(1+\kappa)}{\bar{\gamma}_1} \right)^{-1} \middle| \begin{matrix} 1,1,1-(c+N\mu) \\ 1,0 \end{matrix} \right], \quad (7.41)$$

where $\Upsilon_1 = \left(\frac{N\mu(1+\kappa)}{\bar{\gamma}_1} \right)^{-(c+N\mu)}$. Now, follow the same derivation from (7.38)-(7.40) to

$$\bar{C}_1 = \frac{\mathrm{B}}{\ln(2)}\mathcal{D}_1\Upsilon_1 \times \left(\mathrm{G}_{3,2}^{1,3}\left[\left(\frac{N\mu(1+\kappa)}{\bar{\gamma}_1}\right)^{-1}\middle| \begin{matrix}1,1,1-(c+N\mu)\\ 1,0\end{matrix}\right] - \mathrm{G}_{3,2}^{1,3}\left[\Psi\left(\frac{N\mu(1+\kappa)}{\bar{\gamma}_1}\right)^{-1}\middle| \begin{matrix}1,1,1-(c+N\mu)\\ 1,0\end{matrix}\right]\right) \tag{7.43}$$

$$\bar{C}_2 = \frac{\mathrm{B}}{\ln(2)}\mathcal{D}_2\Upsilon_2 \times \left(\mathrm{G}_{3,2}^{1,3}\left[\Psi\left(\frac{N\mu(1+\kappa)}{\bar{\gamma}_2}\right)^{-1}\middle| \begin{matrix}1,1,1-(c+N\mu)\\ 1,0\end{matrix}\right] - \mathrm{G}_{3,2}^{1,3}\left[a_3\left(\frac{N\mu(1+\kappa)}{\bar{\gamma}_2}\right)^{-1}\middle| \begin{matrix}1,1,1-(c+N\mu)\\ 1,0\end{matrix}\right]\right) \tag{7.44}$$

$$\bar{C}_3 = \frac{\mathrm{B}}{\ln(2)}\mathcal{D}_3\Upsilon_3 \times \left(\mathrm{G}_{3,2}^{1,3}\left[a_3\left(\frac{N\mu(1+\kappa)}{\bar{\gamma}_3}\right)^{-1}\middle| \begin{matrix}1,1,1-(c+N\mu)\\ 1,0\end{matrix}\right]\right) \tag{7.45}$$

solve the integral of $\mathcal{I}_2$. Thus, the following result is achieved.

$$\mathcal{I}_2 = \mathcal{D}_1\Upsilon_1 \times \mathrm{G}_{3,2}^{1,3}\left[\Psi\left(\frac{N\mu(1+\kappa)}{\bar{\gamma}_1}\right)^{-1}\middle| \begin{matrix}1,1,1-(c+N\mu)\\ 1,0\end{matrix}\right]. \tag{7.42}$$

Now, submit the results obtained in (7.41) and (7.42) to (7.38). Thus, the final exact expression of the average channel capacity of U_1 is expressed in (7.43) at the top of the next page. To reach the remaining achievable average capacity of U_2 and U_3, a similar derivation approach from (7.38)-(7.43) is applied for both users. Therefore, (7.44) and (7.45) represent closed-form expressions of the ergodic capacity for U_2 and U_3, respectively. Therefore, $\Upsilon_l = \left(\frac{N\mu(1+\kappa)}{\bar{\gamma}_l}\right)^{-(c+N\mu)}$ and $\mathcal{D}_l = \frac{1}{\mathrm{e}^{(N\mu\kappa)}}\sum_{c=0}^{\infty}\frac{N(\mu)^{2c+N\mu}\kappa^c(1+\kappa)^{c+N\mu}}{c!\,\Gamma(c+N\mu)(\bar{\gamma}_l)^{(c+N\mu)}}$, where $l \in \{1,2,3\}$.

7.5 MOS-Based QoE Evaluation Model for Web Browsing

MOS is employed to measure the user's QoE for the provided services, such as web browsing, video streaming, and file download. As one of the widely used applications in wireless networks, in this work, it has been concentrated on web browsing applications. It delineates the subjective human awareness of quality for the purpose of web browsing applications to the objective metrics. According to [148], the appropriate model that described the MOS for web browsing applications is defined as follows:

$$\mathrm{MOS}_{web} = -\xi_1 \ln\left(d(\mathrm{R}_i)\right) + \xi_2, \tag{7.46}$$

where ξ_1 and ξ_2 are obtained by analysing the experimental results of the web browsing applications, which are constant and set to become 1.120 and 4.6746, respectively, as in [149]. $d(\mathrm{R}_i)$ indicates the delay time that is consumed between a request, made by a user, for a web page and the display of the web contents. It mainly relies on different components such as the web page size, known as the round-trip time (RTT), and the effects of the applied transfer of data protocols. Therefore, the Hypertext Transfer Protocol (HTTP) and the Transmission Control Protocol (TCP) are considered in this work. Therefore, $d(\mathrm{R}_i)$ can be given accordingly to [149] as follows.

$$d\left(\mathrm{R}_i\right) = 3\mathrm{RTT} + \frac{\mathrm{FS}}{\mathrm{R}_i} + \mathcal{L}\left(\frac{\mathrm{MSS}}{\mathrm{R}_i} + \mathrm{RTT}\right) - \frac{2\mathrm{MSS}(2^{\mathcal{L}} - 1)}{\mathrm{R}_i} \tag{7.47}$$

where RTT stands for the round-trip time in seconds, MSS defines the maximum segment size in bits, and FS is the web page size in bits. However, the number of slow begin cycles with idle duration can be represented by $\mathcal{L} = \min\{\mathcal{L}_1, \mathcal{L}_2\}$, where $\mathcal{L}_1$ indicates the number of cycles required for the congestion window to achieve the bandwidth-delay product and $\mathcal{L}_2$ represents the amount of slow begin cycles required until the entire web page size is successfully transmitted. Both factors can be given as follows.

$$\mathcal{L}_1 = \log_2\left(\frac{\mathrm{R}_i \times \mathrm{RTT}}{\mathrm{MSS}} + 1\right) - 1 \tag{7.48}$$

$$\mathcal{L}_2 = \log_2\left(\frac{\mathrm{FS}}{2 \times \mathrm{MSS}} + 1\right) - 1. \tag{7.49}$$

According to [145], RTT has an insignificant impact on MOS compared to the other factors of the data rate, web page, etc. Beside, RTT is expected to drop to less than 10 ms in 5G and beyond, therefore, $\mathrm{RTT} \approx 0ms$ is assumed. As a consequence, (7.47) can be rewritten accordingly to $d\left(\mathrm{R}_i\right) = \frac{\mathrm{FS}}{\mathrm{R}_i}$. Thus, the MOS function of each assigned user can be expressed as follows.

$$\mathrm{MOS}_{web} = \xi_1 \ln\left(d(\mathrm{R}_i)\right) + \chi, \tag{7.50}$$

where $\chi = \xi_2 + \xi_1 \ln\left(\frac{\mathrm{BW}}{\mathrm{FS}}\right)$.

7.6 Results and Discussion

In this part, different numerical and Monte Carlo simulation results are obtained to validate analytical closed-form expressions. In particular, the simulation parameters applied for this work are chosen at random. The channel is classified as quasi-static when it remains constant for the period of one symbol, but varies randomly across successive symbol intervals. 10^6 symbols in each simulation run is produce for the

simulation.

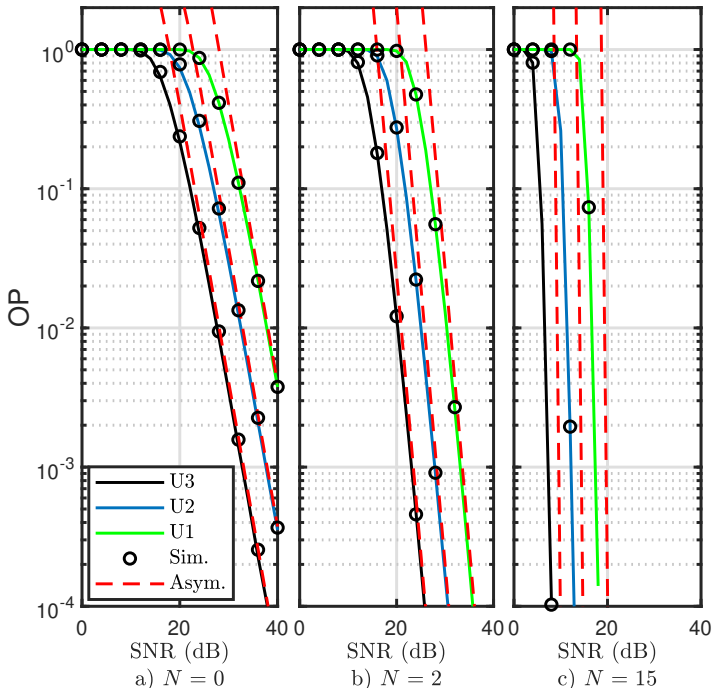

Fig. 7.2 OP of three users versus SNR, where $\kappa = 0$ and $\mu = 2$.

Fig. 7.2 illustrates the OP of three NOMA users on different amounts of N passive reflectors of IRS versus SNR in dB. It can be seen that IRS has a significant impact on outage performance. Therefore, as the passive reflector N of IRS increases, the OP of all users increases. Therefore, the OP for each user is investigated on 2 and 10 IRS elements, as depicted in that figure. For example, an improvement of about 20 dB is achieved for U_3 to achieve 10^-3 of OP when N increases to 10 units.

Fig. 7.3 shows the BER performance versus SNR for the three users considering the exist and the absence of IRS reflectors, that is $N = \{1, 5, 15\}$. As can be seen from this figure that increasing the number of IRS reflectors can lead to reducing the BER. For example, when $N = 1$, U_1 requires more than 40 dB to reach 10^{-2} of the target BER, however, if N increases by 15, then U_1 needs about 25 dB less to achieve the similar BER target. This analysis can be repeated to all remaining users over different aspect of BER targets. Furthermore, this figure shows the performance of BER at high average SNR, where an accurate match of the exact and asymptotic curves is achieved at high SNR.

Fig. 7.4 demonstrates the significant improvement in total throughput for each user when considering a different number of N reflectors. It can be observed that a low SNR is required to meet the predefined data rate for each user at a high value of N, that is, $N = 15$. For instance, in fig. 7.4b, U_3 requires about 15 dB less than in the case of $N = 2$ to satisfy its target data rate. It indicates the advantages of increasing the

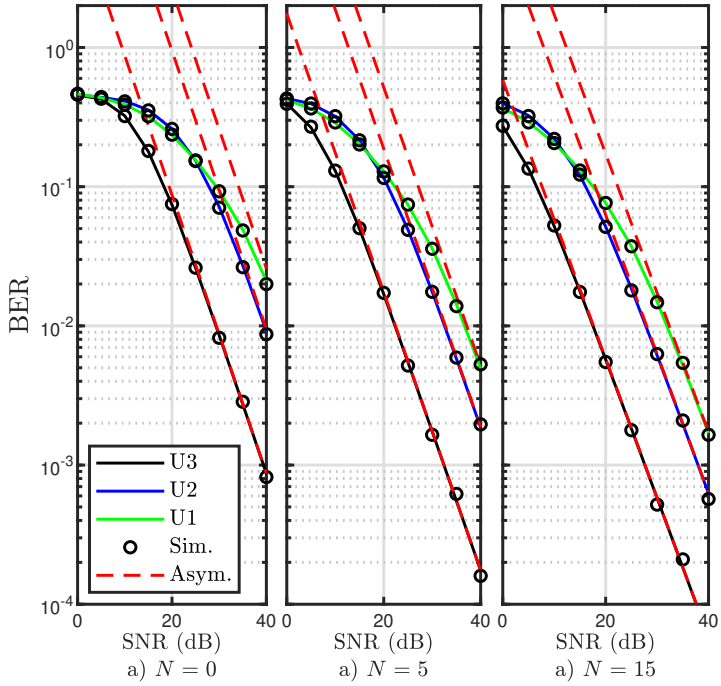

Fig. 7.3 BER of three users versus SNR.

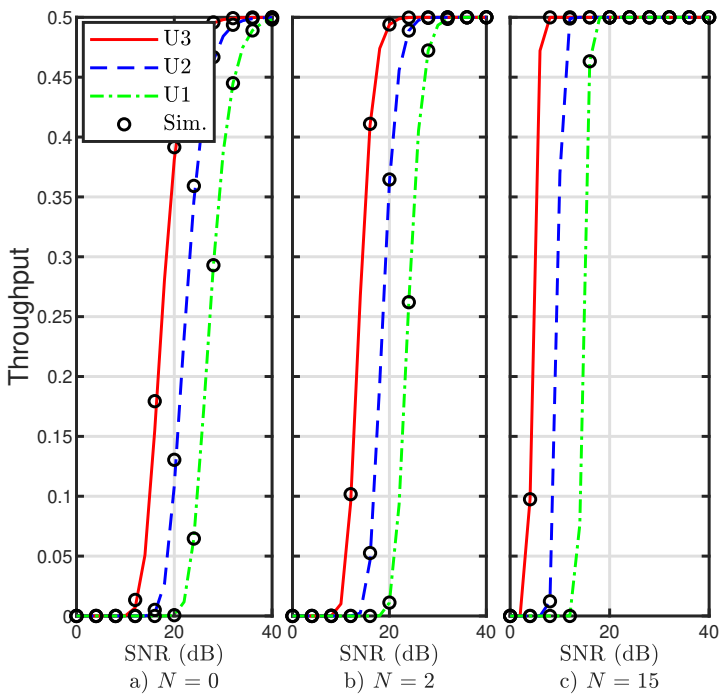

Fig. 7.4 Performance of three users throughput versus SNR, $R_1 = 0.5, R_2 = 1, R_3 = 2$.

number of passive reflectors in IRS. On the other hand, Fig. 7.5 represents the MOS of each user with different values of N, where MOS measures QoE. At low SNR, MOS behaves differently when $N = 0$. In the case of $N = 2$, it is observed that the MOS of U_3 overlaps with U_2 at about 22 dB and with U_1 at very low SNR. However, a critical

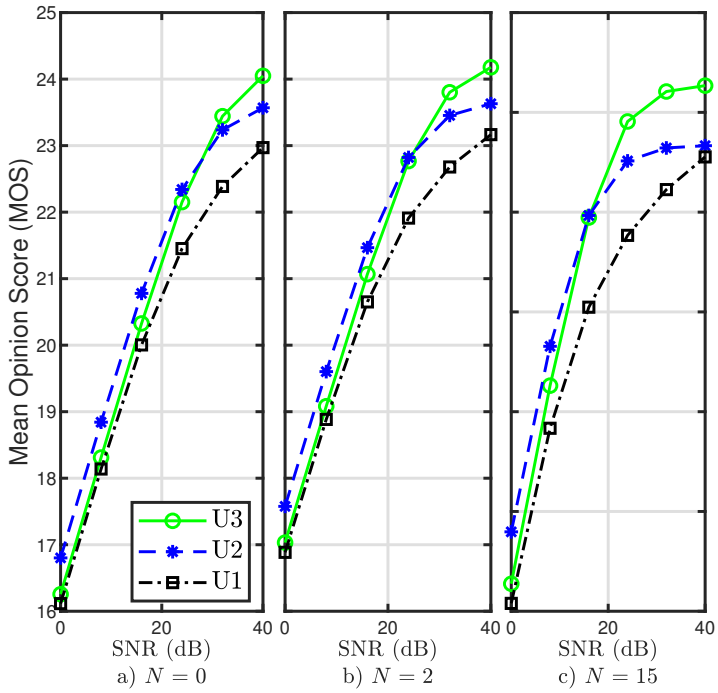

Fig. 7.5 Mean opinion score (MOS) of three users versus SNR.

overlap point is sketched at about 18 dB between both users in fig. 7.5b, where $N = 15$. This is due to the different impacts caused by different factors, such as amount of IRS reflector channel gains, power allocation coefficients, intra-cell interference, distance from the BS, etc. Therefore, manipulating these factors can lead to different outcomes for MOS. Furthermore, noticeable improvements in MOS can be gained by increasing the total number of IRS passive reflectors.

Fig. 7.6 shows the sum MOS of all users versus web page size within certain values of P_t and N. The results show that a large improvement in MOS can be achieved with a low web page size. The larger the size of the web page, the lower the MOS. Moreover, the increase of N reflectors in IRS improves the sum of MOS, particularly above the high value P_t. Furthermore, the difference in the sum improvement in MOS obtained by increasing N at low P_t is approximately 8 times the enhancement obtained at high P_t. The reasons behind this phenomenon are reflected in the different factors mentioned in the previous figure.

Fig. 7.7 illustrates the impact of IRS on EC of all three NOMA users, where the absence of IRS has been considered. As it can be seen from that figure that increases of the number of IRS reflectors manipulates with the overall EC performance. Moreover, u_3 has the most significant performance improvement with the increment of N while other users behave significantly when $N = 15$. It is expected that U_3 outperforms other users due to its channel conditions. Overall, once can notice the essential manipulation of IRS on the system performance.

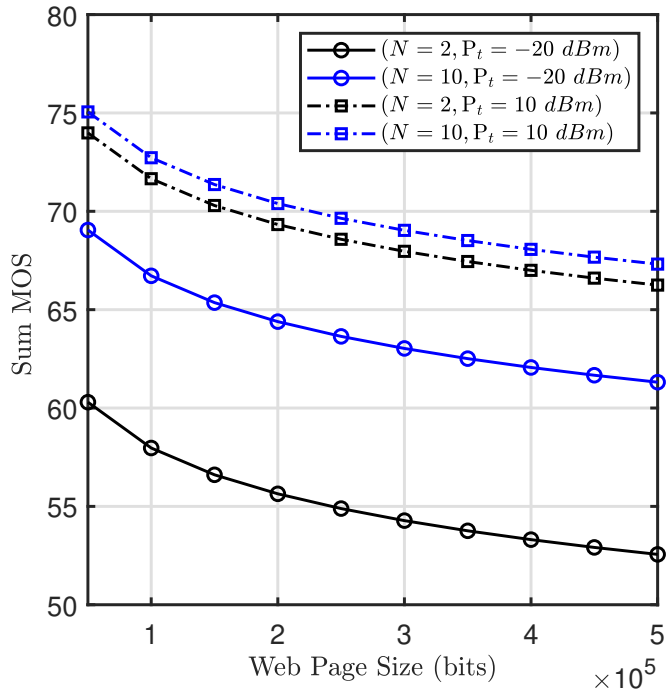

Fig. 7.6 sum Mean opinion score (MOS) of three users versus web page size.

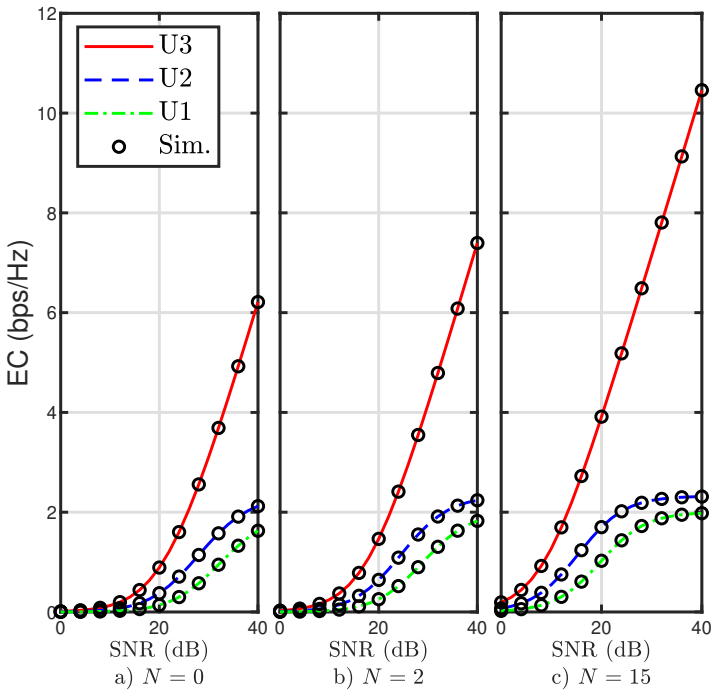

Fig. 7.7 EC of three users versus SNR, where $\kappa = 0$ and $\mu = 2$.

7.7 Chapter Summary

This chapter considered the QoS and QoE of IRS-assisted indoor NOMA systems in $\kappa - \mu$ fading channels. Specifically, the OP, EC, BER, and throughput of the considered

system model and the MOS-based QoE have been investigated. The results reveal that increasing the number of IRS reflectors plays an important role in enhancing the overall user experience and service. Furthermore, the results show that a large improvement in MOS can be achieved with a small web page size. Furthermore, other important factors, such as the fading components κ and μ, the power allocation factors, the predefined data rates, the distance from the BS and the components of indoor environments, have a significant influence on the overall performance of the system. Future work will focus on studying more performance metrics of both QoS and QoE in different channel fading and antenna deployments of the IRS-NOMA system.

CHAPTER 8

Conclusions and Future Work

8.1 Conclusion

The main objective of this thesis is to analyse the performance of NOMA system in different channel configurations and composite fading distributions, as well as to optimise user pairing. In particular, various performance matrices have been analysed, such as ergodic capacity (EC), outage probability (OP), bit error rate (BER), throughput, and energy efficiency (EE), to investigate the effectiveness of the proposed system models. In addition to that, different optimisation techniques, such as streamlined simplex method (SSM) and least- and most-cost method (LMCM) are primarily designed to address user pairing issue in mixed distribution environments. Furthermore, an analytical work is carried out to address the potential combining of NOMA with IRS by discussing a variety of performance measurements.

In Chapter 4, order statistics and the advanced Fox H function are used to produce accurate closed-form analytical expressions of OP, BER, and EC for various NOMA users in α-μ fading channels. To begin, we tested the OP in two scenarios: when predetermined target data rates are chosen for all users based on their QoS needs and when the OMA rate surpasses the NOMA rate in the same instance. The error probability for two NOMA users using M-QAM higher modulation is then calculated analytically by averaging their conditional BER probabilities across the PDFs of their instantaneous SNRs. The EC of NOMA is next investigated, and additional specific examples of comparable fading models are used to obtain more enlightening conclusions. Surprisingly, the findings show that for all users, OP with the OMA rate beats OP with the prepared data rate. Furthermore, power allocation variables, channel fading parameters, and target rates have been shown to have a considerable influence on the overall performance of NOMA systems.

In Chapter 5, a performance study is carried out for a mix of indoor and outdoor NOMA customers, where both can be supplied via an outdoor-to-indoor and outdoor-

to-outdoor channel. Variable practical obstacles, such as faulty SIC and various fading situations, are taken into account. Channel gains are sorted according to the product of instantaneous channel gains and their distance-dependent path loss, where $\mathcal{I}$ has different channel attributes than $\mathcal{O}$. We investigated the path-loss model of $\mathcal{I}$ in a generalised $\kappa - \mu$ fading distribution to better characterise the channel gain when both LOS and NLOS situations are present. Furthermore, we evaluated and supplied accurate analytical expressions for a range of critical performance measures such as OP and EC, as well as throughput and energy efficiency. The acquired results give information on the influence of many major aspects on the performance of the total system, such as power allocation, time splitting, κ and μ fading, and residual interference. It is shown that the performance of $\mathcal{I}$ decreases faster than that of $\mathcal{O}$ due to the environment provided by its different channel attributions.

In Chapter 6, we investigated the pairing of indoor and outdoor users in the NOMA downlink system and proposed two distinct methods based on the streamlined simplex technique and the least- and most-cost method. When a group of users from diverse settings are paired with the same subcarrier, the suggested methods are utilised to significantly increase the cumulative data rate performance. Additionally, the performance of these algorithms is compared to a random user pairing as a benchmark to provide additional insights. In this research, we also performed the Max-Min optimisation approach to maximise the minimum achievable data rate for indoor users. The findings indicate that the suggested LMCM and SSM algorithms outperform the random algorithm in most circumstances, with the LMCM method outperforming the SSM algorithm in the majority of cases. Furthermore, the findings indicate a much higher degree of fairness when applying these techniques to the indoor user compared to the usual technique.

Chapter 7 examines the quality of service (QoS) and the quality of experience (QoE) of the IRS-assisted indoor NOMA system in $\kappa - \mu$ fading channels. In particular, we examine different QoS and QoE indicators such as OP, EC, BER, and web browsing of the suggested system model. The findings indicate that increasing the number of IRS reflectors significantly improves overall customer service and experience. Additionally, the findings demonstrate that a significant increase in MOS is achieved with a small web page size. Furthermore, several critical elements such as the fading components of κ and μ, power allocation factors, predetermined data rate, distance from the base station, and components of the indoor atmosphere all have a substantial impact on overall system performance.

8.2 Future Work

This thesis discusses various critical strategies to analyse and optimise downlink NOMA in single-input single-output (SISO) networks. However, this thesis does not cover all characteristics and uses of NOMA in different antenna and channel deployments. The work included in this thesis may be expanded in the future in light of the following proposals.

- **Analyse a hybrid OMA and NOMA system over different advanced fading channels in multiple antenna and cell deployment systems.**

  Chapter 4 describes the analysis performance of the NOMA system with a single cell and limited transmitting and receiving antennas. Therefore, the study may be extended to the combination of NOMA and OMA systems on multiple cells and MIMO systems. This may lead to more sustainable, reliable and competitive communication systems. Moreover, while the fading channel in different environments plays an important role in overall system performance, advanced composite fading channel models such as $\alpha - \eta - \kappa$, $\alpha - \eta - \mu$, fisher-snedecor $\mathcal{F}$, etc., can be investigated to better characterise the wireless channel between the BS and legitimate users.

- **Evaluate different Cooperative scheme of NOMA-based multiple antenna system over indoor environments.**

  Chapter 5 can be extended to cover different cooperative schemes such as amplify-and-forward (AF), relay selection, full duplex mode, etc. Indoor environments can be described by different path loss models and compared with the current model to obtain more information. MIMO system can also be considered here to enhance the overall system performance.

- **Resource allocation optimisation by applying machine learning.**

  It is interesting to extend the work in Chapter 6 to include more advanced machine learning techniques to optimise resource allocation, including the problem of user pairing of multiple indoor-outdoor users.

- **Analyse and maximising intelligent reflecting surfaces (IRS) based NOMA system in uplink and downlink scenarios with direct and indirect communication links.**

  In Chapter 7, we apply IRS as an access point, where the channel gain between BS and IRS can be neglected, which compensates for a less complex analysis. Therefore, we aim to extend that work to include the effect of IRS when it is considered away from the BS and having a direct link as well. Thus, the random

variables of the channel gain between the source and the destination become more challenging to be accurately modelled over the advanced fading channels, particularly when considering a MIMO based NOMA system. In addition to that, the IRS reflecting phase has to be optimised since the idle assumption is not practical. Thus, it is aimed to optimized the IRS phase to enhance the practical scenario.

Bibliography

[1] A. Goldsmith. *Wireless Communications*. Cambridge University Press, 2005.

[2] J. G. Andrews et al. "What Will 5G Be?" In: *IEEE J. Select. Areas Commun.* 32.6 (2014), pp. 1065–1082.

[3] T. Rappaport. *Wireless communications: Principles and practice*. English (US). Prentice Hall, 1996. ISBN: 0133755363.

[4] A. Benjebbovu et al. "System-level performance of downlink NOMA for future LTE enhancements". In: *2013 IEEE Globecom Workshops (GC Wkshps)*. 2013, pp. 66–70.

[5] L. Dai et al. "A Survey of Non-Orthogonal Multiple Access for 5G". In: *IEEE Commun. Surveys Tuts.* 20.3 (2018), pp. 2294–2323.

[6] M. K. Simon and M.-S. Alouini. *Digital Communication Over Fading Channels*. 2nd ed. New York, US: Wiley, 2004.

[7] M. D. Yacoub. "The α-μ Distribution: A Physical Fading Model for the Stacy Distribution". In: *IEEE Trans. Veh. Technol.* 56.1 (Jan. 2007), pp. 27–34.

[8] A. M. Magableh and M. M. Matalgah. "Channel characteristics of the generalized α-μ multipath fading model". In: *Int.Wireless Commun. and Mobile Compu. Conf.* July 2011, pp. 1535–1538.

[9] A. Jeffrey and D. Zwillinger. *Table of Integrals, Series, and Products*. 7th ed. Academic Pr, 2007.

[10] D. B. Da Costa and M. D. Yacoub. "Average channel capacity for generalized fading scenarios". In: *IEEE Commun. Lett.* 11.12 (Dec. 2007), pp. 949–951.

[11] M. Hamza and M. Hadzialic. "BEP/SEP and Outage Performance Analysis of L-Branch Maximal-Ratio Combiner for $\kappa - \mu$ fading". In: *Int. J. Digit. Multimed.* (2019).

[12] A. Prudnikov, Y. Brychkov, and O. Marichev. *Integrals and Series. Volume 3: More Special Functions.* London, UK: Godron and Breach Science, 1990.

[13] M. Springer and K. M. R. Collection. *The Algebra of Random Variables*. New York, US: Wiley, 1979.

[14] K. J. R. Liu et al. *Cooperative Communications and Networking*. Cambridge University Press, 2008.

[15] M. Basharat et al. "A survey and taxonomy on non-orthogonal multiple-access schemes for 5G networks". In: *Trans. Emerg. Telecommun. Technol.* 29 (June 2017), e3202.

[16] Y. Cai et al. "Modulation and Multiple Access for 5G Networks". In: *IEEE Commun. Surveys Tuts.* 20.1 (2018), pp. 629–646.

[17] R. Steele and L. Hanzo. *Mobile Radio Communications: Second and Third Generation Cellular and WATM Systems: 2nd*. Address: Chichester, UK. IEEE Press - John Wiley, May 1999.

[18] K. S. Gilhousen et al. "On the capacity of a cellular CDMA system". In: *IEEE Trans. Veh. Technol.* 40.2 (1991), pp. 303–312.

[19] W. Shin et al. "Non-Orthogonal Multiple Access in Multi-Cell Networks: Theory, Performance, and Practical Challenges". In: *IEEE Commun. Mag.* 55.10 (2017), pp. 176–183.

[20] M. S. Ali, E. Hossain, and D. I. Kim. "Coordinated Multipoint Transmission in Downlink Multi-Cell NOMA Systems: Models and Spectral Efficiency Performance". In: *IEEE Wireless Commun.* 25.2 (2018), pp. 24–31.

[21] S. M. R. Islam et al. "Power-Domain Non-Orthogonal Multiple Access (NOMA". In: *IEEE Commun. Surveys Tuts.* ().

[22] H. Tabassum et al. "Non-Orthogonal Multiple Access (NOMA) in Cellular Uplink and Downlink: Challenges and Enabling Techniques". In: *TechRxiv* (Aug. 2016).

[23] A. Benjebbour et al. "Concept and practical considerations of non-orthogonal multiple access (NOMA) for future radio access". In: *2013 Int. Symp. Intell. Signal Process.* 2013, pp. 770–774.

[24] N. Nonaka, Y. Kishiyama, and K. Higuchi. "Non-Orthogonal Multiple Access Using Intra-Beam Superposition Coding and SIC in Base Station Cooperative MIMO Cellular Downlink". In: *2014 IEEE 80th Veh. Technol. Conf. (VTC)*. 2014, pp. 1–5.

[25] D. Tse and P. Viswanath. *Fundamentals of Wireless Communication*. Cambridge University Press, 2005.

[26] K. Higuchi and Y. Kishiyama. "Non-Orthogonal Access with Random Beamforming and Intra-Beam SIC for Cellular MIMO Downlink". In: *2013 IEEE 78th Veh. Technol. Conf. (VTC)*. 2013, pp. 1–5.

[27] M. Zeng et al. "Capacity Comparison Between MIMO-NOMA and MIMO-OMA With Multiple Users in a Cluster". In: *IEEE J. Select. Areas Commun.* 35.10 (2017), pp. 2413–2424.

[28] Z. Ding, F. Adachi, and H. V. Poor. "The Application of MIMO to Non-Orthogonal Multiple Access". In: *IEEE Wireless Commun.* 15.1 (2016), pp. 537–552.

[29] M. Zeng et al. "On the Sum Rate of MIMO-NOMA and MIMO-OMA Systems". In: *IEEE Wireless Commun. Lett.* 6.4 (2017), pp. 534–537.

[30] Y. Saito et al. "System-level performance evaluation of downlink non-orthogonal multiple access (NOMA)". In: *2013 IEEE 24th Annual Int. Symposium on Personal, Indoor, and Mobile Radio Commun. (PIMRC)*. 2013, pp. 611–615.

[31] P. Sedtheetorn and T. Chulajata. "Spectral efficiency evaluation for non-orthogonal multiple access in Rayleigh fading". In: *2016 18th In. Conf. on Advanced Commun. Techn. (ICACT)*. 2016, pp. 747–750.

[32] A. Li, A. Benjebbour, and A. Harada. "Performance Evaluation of Non-Orthogonal Multiple Access Combined with Opportunistic Beamforming". In: *2014 IEEE 79th Veh. Technol. Conf. (VTC)*. 2014, pp. 1–5.

[33] R. Hoshyar, F. P. Wathan, and R. Tafazolli. "Novel Low-Density Signature for Synchronous CDMA Systems Over AWGN Channel". In: *IEEE Trans. Signal Processing* 56.4 (2008), pp. 1616–1626.

[34] M. AL-Imari, M. A. Imran, and R. Tafazolli. "Low Density Spreading for next generation multicarrier cellular systems". In: *2012 International Conference on Future Communication Networks*. 2012, pp. 52–57.

[35] H. Nikopour and H. Baligh. "Sparse code multiple access". In: *2013 IEEE 24th Annual Int. Symposium on Personal, Indoor, and Mobile Radio Commun. (PIMRC)*. 2013, pp. 332–336.

[36] F. Fang et al. "Energy efficiency of resource scheduling for non-orthogonal multiple access (NOMA) wireless network". In: *2016 IEEE Int. Conf. Commun. (ICC)*. 2016, pp. 1–5.

[37] Z. Ding et al. "On the Performance of Non-Orthogonal Multiple Access in 5G Systems with Randomly Deployed Users". In: *IEEE Signal Processing Lett.* 21.12 (2014), pp. 1501–1505.

[38] Z. Ding, M. Peng, and H. V. Poor. "Cooperative Non-Orthogonal Multiple Access in 5G Systems". In: *IEEE Wireless Commun. Lett.* 19.8 (2015), pp. 1462–1465.

[39] A. Mohamad, R. Visoz, and A. O. Berthet. "Outage achievable rate analysis for the Non Orthogonal Multiple Access Multiple Relay Channel". In: *2013 IEEE Wireless Communications and Networking Conference Workshops (WCNCW)*. 2013, pp. 160–165.

[40] L. Yang et al. "Cooperative Non-Orthogonal Layered Multicast Multiple Access for Heterogeneous Networks". In: *IEEE Trans. Commun.* 67.2 (2019), pp. 1148–1165.

[41] A. Mohamad, R. Visoz, and A. O. Berthet. "Code design for multiple-access multiple-relay wireless channels with non-orthogonal transmission". In: *2015 IEEE Int. Conf. on Commun. (ICC)*. 2015, pp. 2318–2324.

[42] Z. Zhang et al. "Full-Duplex Device-to-Device-Aided Cooperative Non-orthogonal Multiple Access". In: *IEEE Trans. Veh. Technol.* 66.5 (2017), pp. 4467–4471.

[43] A. Shahini and N. Ansari. "NOMA Aided Narrowband IoT for Machine Type Communications With User Clustering". In: *IEEE Internet of Things Journal* 6.4 (2019), pp. 7183–7191.

[44] Y. Liu et al. "Non-orthogonal Multiple Access for 5G and Beyond". In: *Proc. of the IEEE* 105.12 (2017), pp. 2347–2381.

[45] J. A. Oviedo and H. R. Sadjadpour. "A new NOMA approach for fair power allocation". In: *2016 IEEE Conf. Compu. Commun. Workshops (INFOCOM WKSHPS)*. 2016, pp. 843–847.

[46] R. C. Kizilirmak. "Non-Orthogonal Multiple Access (NOMA) for 5G Networks". In: *Towards 5G Wireless Networks*. Ed. by H. K. Bizaki. Rijeka: IntechOpen, 2016. Chap. 4.

[47] F. Liu, P. Mähönen, and M. Petrova. "Proportional fairness-based user pairing and power allocation for non-orthogonal multiple access". In: *2015 IEEE 26th Annual Int. Symposium on Personal, Indoor, and Mobile Radio Commun. (PIMRC)*. 2015, pp. 1127–1131.

[48] N. Otao, Y. Kishiyama, and K. Higuchi. "Performance of non-orthogonal access with SIC in cellular downlink using proportional fair-based resource allocation". In: *2012 Int. Symposium on Wireless Commun. Sys. (ISWCS)*. 2012, pp. 476–480.

[49] Z. Al-Abbasi and D. K. C. So. "Resource Allocation in Non-Orthogonal and Hybrid Multiple Access System With Proportional Rate Constraint". In: *IEEE Wireless Commun.* 16.10 (2017), pp. 6309–6320.

[50] M. W. Baidas, E. Alsusa, and K. A. Hamdi. "Performance analysis of downlink NOMA networks over Rayleigh fading channels". In: *Proc. IEEE Wireless Commun. and Networking Conf. (WCNC)*. June 2018, pp. 1–6.

[51] P. Sharma, A. Kumar, and M. Bansal. "Performance Analysis of Downlink NOMA over η-μ and κ-μ Fading Channels". In: *IET Commun.* 14.3 (Feb. 2020), pp. 522–531.

[52] T. Hou, X. Sun, and Z. Song. "Outage Performance for Non-Orthogonal Multiple Access With Fixed Power Allocation Over Nakagami-m Fading Channels". In: *IEEE Commun. Lett.* 22.4 (Jan. 2018), pp. 744–747.

[53] A. Agarwal et al. "Outage Probability Analysis for NOMA Downlink and Uplink Communication Systems With Generalized Fading Channels". In: *IEEE Access* 8 (Dec. 2020), pp. 220461–220481.

[54] X. Xie et al. "Ergodic Capacity and Outage Performance Analysis of Uplink Full-Duplex Cooperative NOMA System". In: *IEEE Access* 8 (Sept. 2020).

[55] B. M. ElHalawany et al. "Performance Analysis of Downlink NOMA Systems Over κ-μ Shadowed Fading Channels". In: *IEEE Trans. Veh. Technol.* 69.1 (Jan. 2020), pp. 1046–1050.

[56] W. Yu, L. Musavian, and Q. Ni. "Link-Layer Capacity of NOMA Under Statistical Delay QoS Guarantees". In: *IEEE Trans. Commun.* 66.10 (Oct. 2018), pp. 4907–4922.

[57] F. Kara and H. Kaya. "BER performances of downlink and uplink NOMA in the presence of SIC errors over fading channels". In: *IEEE Commun. Lett.* 12.15 (Sept. 2018), pp. 1834–1844.

[58] M. Aldababsa et al. "Bit Error Rate for NOMA Network". In: *IEEE Commun. Lett.* 24.6 (Mar. 2020), pp. 1188–1191.

[59] F. Wei et al. "BER Analysis for Uplink NOMA in Asymmetric Channels". In: *IEEE Commun. Lett.* 24.11 (June 2020), pp. 2435–2439.

[60] J. Yeom et al. "BER Performance of Uplink NOMA With Joint Maximum-Likelihood Detector". In: *IEEE Trans. Veh. Technol.* 68.10 (Aug. 2019), pp. 10295–10300.

[61] I. Lee and J. Kim. "Average Symbol Error Rate Analysis for Non-Orthogonal Multiple Access With M-Ary QAM Signals in Rayleigh Fading Channels". In: *IEEE Commun. Lett.* 23.8 (Aug. 2019), pp. 1328–1331.

[62] T. Assaf et al. "Exact BER Performance Analysis for Downlink NOMA Systems Over Nakagami- m Fading Channels". In: *IEEE Access* 7 (Sept. 2019), pp. 134539–134555.

[63] L. Bariah, S. Muhaidat, and A. Al-Dweik. "Error Performance of NOMA-Based Cognitive Radio Networks With Partial Relay Selection and Interference Power Constraints". In: *IEEE Trans. Commun.* 68.2 (Feb. 2020), pp. 765–777.

[64] A. S. Alqahtani and E. Alsusa. "Performance Analysis of Downlink NOMA System over α-η-μ Generalized Fading Channel". In: *Proc. IEEE Veh. Technol. Conf. (VTC)*. June 2020, pp. 1–5.

[65] V. Kumar, B. Cardiff, and M. F. Flanagan. "Performance Analysis of NOMA-Based Cooperative Relaying in α-μ Fading Channels". In: *IEEE Int. Conf. on Commun. (ICC)*. Shanghai, China, May 2019, pp. 1–7.

[66] A. Al-Dweik and Y. Iraqi. "Power Allocation for Reliable SIC Detection of Rectangular QAM-based NOMA Systems". In: (Jan. 2021).

[67] T. Assaf et al. "NOMA Receiver Design for Delay-Sensitive Systems". doi: 10.1109/JSYST.2020.3032878.

[68] Z. Ding et al. "On the Performance of Non-Orthogonal Multiple Access in 5G Systems with Randomly Deployed Users". In: *IEEE Signal Processing Lett.* 21.12 (Dec. 2014), pp. 1501–1505.

[69] H. A. (A. David. *Order statistics*. 3rd ed. Hoboken, N.J: Wiley, 2003.

[70] T. Assaf et al. "Exact Bit Error-Rate Analysis of Two-User NOMA Using QAM with Arbitrary Modulation Orders". In: *IEEE Commun. Lett.* (Aug. 2020), pp. 1–5.

[71] A. Mathai, R. Saxena, and H. Haubold. *The H-function: Theory and Applications*. New York, US: Springer, 2009.

[72] A. Prudnikov, Y. Brychkov, and O. Marichev. *Integrals and Series. Volume 3: More Special Functions.* London, UK: Godron and Breach Science, 1990.

[73] K. Peppas et al. "Simple, accurate formula for the average bit error probability of multiple-input multiple-output free-space optical links over negative exponential turbulence channels". In: *Opt. Lett.* 37 (Aug. 2012), pp. 3243–3245.

[74] Q. Li et al. "5G network capacity: Key elements and technologies". In: *IEEE Veh. Technol. Mag.* 9.1 (Mar. 2014), pp. 71–78.

[75] M. Agiwal, A. Roy, and N. Saxena. "Next generation 5G wireless networks: A comprehensive survey". In: *IEEE Commun. Surveys Tuts.* 18.3 (June 2016), pp. 1617–1655.

[76] Z. Ding et al. “Application of Non-Orthogonal Multiple Access in LTE and 5G Networks”. In: *IEEE Commun. Mag.* 55.2 (2017), pp. 185–191.

[77] S. R. Islam et al. “Power-domain non-orthogonal multiple access (NOMA) in 5G systems: Potentials and challenges”. In: *IEEE Commun. Surveys Tuts.* 19.2 (Feb. 2016), pp. 721–742.

[78] Z. Ding et al. “On the Performance of Non-Orthogonal Multiple Access in 5G Systems with Randomly Deployed Users”. In: *IEEE Signal Process. Lett.* 21.12 (Dec. 2014), pp. 1501–1505.

[79] Z. Yang et al. “On the Performance of Non-orthogonal Multiple Access Systems With Partial Channel Information”. In: *IEEE Trans. Commun.* 64.2 (Dec. 2016), pp. 654–667.

[80] Z. Ding, M. Peng, and H. V. Poor. “Cooperative Non-Orthogonal Multiple Access in 5G Systems”. In: *IEEE Commun. Lett.* 19.8 (June 2015), pp. 1462–1465.

[81] Q. Y. Liau and C. Y. Leow. “Successive User Relaying in Cooperative NOMA System”. In: *IEEE Commun. Lett.* 8.3 (Feb. 2019), pp. 921–924.

[82] H. Liu et al. “Decode-and-Forward Relaying for Cooperative NOMA Systems With Direct Links”. In: *IEEE Wireless Commun.* 17.12 (Oct. 2018), pp. 8077–8093.

[83] L. Bariah, S. Muhaidat, and A. Al-Dweik. “Error Probability Analysis of NOMA-Based Relay Networks With SWIPT”. In: *IEEE Commun. Lett.* 23.7 (May 2019), pp. 1223–1226.

[84] L. Bariah, S. Muhaidat, and A. Al-Dweik. “Error Performance of NOMA-Based Cognitive Radio Networks With Partial Relay Selection and Interference Power Constraints”. In: *IEEE Trans. Commun.* 68.2 (May 2020), pp. 765–777.

[85] M. Guangchen. “Joint beamforming and power allocation for wireless powered UAV-assisted cooperative NOMA systems”. In: *EURASIP J. Wirel. Commun. Netw.* 55 (Mar. 2020), pp. 1–14.

[86] X. Liang et al. “Outage Performance for Cooperative NOMA Transmission with an AF Relay”. In: *IEEE Commun. Lett.* 21.11 (Mar. 2017), pp. 2428–2431.

[87] S. K. Zaidi, S. F. Hasan, and X. Gui. “Outage Analysis of Ground-Aerial NOMA With Distinct Instantaneous Channel Gain Ranking”. In: *IEEE Trans. Veh. Technol.* 68.11 (Aug. 2019), pp. 10775–10790.

[88] Z. Ding, P. Fan, and H. V. Poor. “Impact of User Pairing on 5G Nonorthogonal Multiple-Access Downlink Transmissions”. In: *IEEE Trans. Veh. Technol.* 65.8 (Aug. 2016), pp. 6010–6023.

[89] R. C. Kizilirmak, C. R. Rowell, and M. Uysal. "Non-orthogonal multiple access (NOMA) for indoor visible light communications". In: *Int. Workshop on Opt. Wirel. Commun. (IWOW)* (Sept. 2015), pp. 98–101.

[90] Y. Liu et al. "Cooperative Non-orthogonal Multiple Access With Simultaneous Wireless Information and Power Transfer". In: *IEEE J. Sel. Areas Commun.* 34.4 (Mar. 2016), pp. 938–953.

[91] Y. Ma et al. "User Pairing Schemes in Cooperative Downlink NOMA System with SWIPT". In: *Comp., Commun. and IoT App.* Oct. 2019, pp. 82–87.

[92] M. Abd-Elnaby, G. G. Sedhom, and M. Elwekeil. "Subcarrier-User Assignment in Downlink NOMA for Improving Spectral Efficiency and Fairness". In: *IEEE Access* 9 (Dec. 2020), pp. 5273–5284.

[93] M. T. Nguyen and L. B. Le. "NOMA User Pairing and UAV Placement in UAV-Based Wireless Networks". In: *IEEE Int. Conf. on Commun. (ICC)*. May 2019, pp. 1–6.

[94] A. Alqahtani et al. "Performance Analysis for Downlink NOMA over α - μ Generalized Fading Channels". In: *IEEE Trans. Veh. Technol.* 70.7 (May 2021), pp. 6814–6825.

[95] Z. Wei et al. "Optimal Resource Allocation for Power-Efficient MC-NOMA With Imperfect Channel State Information". In: *IEEE Trans. Commun.* 65.9 (May 2017), pp. 3944–3961.

[96] A. A. Zavala. *Indoor Wireless Communications: from Theory to Implementation*. John Wiley and Sons, Ltd, 2017.

[97] M. Narasimman et al. "Outage Probability Analysis of Multi-relay Cooperative Decode-and-Forward System Over Generalized $\eta - \mu$ and $\kappa - \mu$ Fading Channels". In: *Wireless Personal Commun.* 119 (Aug. 2021), pp. 1–21.

[98] L. Yingting et al. "Ergodic Capacity and Throughput Analysis of Two-Way Wireless Energy Harvesting Network with Decode-and-Forward Relay". In: *Communications and Networking*. Ed. by X. Liu, D. Cheng, and L. Jinfeng. Cham: Springer Int. Publishing, 2019, pp. 729–739.

[99] A. Jeffrey and D. Zwillinger. *Table of Integrals, Series, and Products*. 7th ed. Academic Pr, 2007.

[100] X. Yue et al. "Performance Analysis of NOMA With Fixed Gain Relaying Over Nakagami- m Fading Channels". In: *IEEE Access* 5 (Mar. 2017), pp. 5445–5454.

[101] J. Tang et al. "Energy Efficiency Optimization for NOMA With SWIPT". In: *IEEE J. Select. Topics in Signal Processing* 13.3 (Feb. 2019), pp. 452–466.

[102] B. Kumbhani and R. S. Kshetrimayum. *MIMO Wireless Communications over Generalized Fading Channels*. USA: CRC Press, Inc., 2017.

[103] L. Dai et al. "Non-orthogonal multiple access for 5G: solutions, challenges, opportunities, and future research trends". In: *IEEE Commun. Mag.* 53.9 (2015), pp. 74–81.

[104] S. M. R. Islam et al. "Power-Domain Non-Orthogonal Multiple Access (NOMA) in 5G Systems: Potentials and Challenges". In: *IEEE Commun. Surveys Tuts.* 19.2 (2017), pp. 721–742.

[105] Q. Y. Liau and C. Y. Leow. "Successive User Relaying in Cooperative NOMA System". In: *IEEE Wireless Commun. Lett.* 8.3 (2019), pp. 921–924.

[106] Z. Ding et al. "On the Performance of Non-Orthogonal Multiple Access in 5G Systems with Randomly Deployed Users". In: *IEEE Signal Processing Lett.* 21.12 (2014), pp. 1501–1505.

[107] Y. Saito et al. "Non-Orthogonal Multiple Access (NOMA) for Cellular Future Radio Access". In: *2013 IEEE 77th Vehicular Technology Conference (VTC Spring)*. 2013, pp. 1–5.

[108] J. Liu et al. "Efficient Power Allocation in Downlink Multi-Cell Multi-User NOMA Networks". In: *IET Commun.* 13 (Feb. 2019), pp. 396–402.

[109] J. Cui et al. "QoE-Based Resource Allocation for Multi-Cell NOMA Networks". In: *IEEE Wireless Commun.* 17.9 (2018), pp. 6160–6176.

[110] M. Abd-Elnaby. "Capacity and Fairness Maximization-Based Resource Allocation for Downlink NOMA Networks". In: *Comput. Mater. and Contin.* 69.1 (2021), pp. 521–537.

[111] N. Yang et al. "Deep Neural Network for Resource Management in NOMA Networks". In: *IEEE Trans. Veh. Technol.* 69.1 (2020), pp. 876–886.

[112] M. Choi, J. Kim, and J. Moon. "Dynamic Power Allocation and User Scheduling for Power-Efficient and Delay-Constrained Multiple Access Networks". In: *IEEE Wireless Commun.* 18.10 (2019), pp. 4846–4858.

[113] Z. Al-Abbasi and D. K. C. So. "User-Pairing Based Non-Orthogonal Multiple Access (NOMA) System". In: *2016 IEEE 83rd Vehicular Technology Conference (VTC Spring)*. May 2016, pp. 1–5.

[114] L. Zhu et al. "Optimal User Pairing for Downlink Non-Orthogonal Multiple Access (NOMA)". In: *IEEE Commun. Lett.* 8.2 (2019), pp. 328–331.

[115] N. S. Mouni, A. Kumar, and P. K. Upadhyay. "Adaptive User Pairing for NOMA Systems With Imperfect SIC". In: *IEEE Commun. Lett.* 10.7 (2021), pp. 1547–1551.

[116] X. Chen et al. "User Pairing and Pair Scheduling in Massive MIMO-NOMA Systems". In: *IEEE Commun. Lett.* 22.4 (2018), pp. 788–791.

[117] T.-V. Nguyen et al. "Hybrid User Pairing for Spectral and Energy Efficiencies in Multiuser MISO-NOMA Networks With SWIPT". In: *IEEE Trans. Commun.* 68.8 (2020), pp. 4874–4890.

[118] S. Najmeddin, S. Aissa, and S. Tahar. "Energy-Efficient Resource Allocation in Multi-UAV Networks With NOMA". In: *IEEE Trans. Green Commun.* 5.4 (2021), pp. 1906–1917.

[119] Z. J. Ali et al. "Novel Resource Allocation Techniques for Downlink Non-Orthogonal Multiple Access Systems". In: *Appl. Sci.* 10.17 (2020).

[120] F. Fang et al. "Energy-Efficient Resource Allocation for Downlink Non-Orthogonal Multiple Access Network". In: *IEEE Trans. Commun.* 64.9 (2016), pp. 3722–3732.

[121] Z. Wei et al. "Optimal Resource Allocation for Power-Efficient MC-NOMA With Imperfect Channel State Information". In: *IEEE Trans. Commun.* 65.9 (2017), pp. 3944–3961.

[122] a. A. E. Alqahtani Adel and A.-D. Arafat. "UAV-Enabled Cooperative NOMA with Indoor- Outdoor User-Paring and SWIPT in κ-μ Channels". In: *TechRxiv* (2021).

[123] Z. Al-Abbasi and D. K. C. So. "Power allocation for sum rate maximization in non-orthogonal multiple access system". In: *IEEE 26th Annual International Symposium on Personal, Indoor, and Mobile Radio Communications (PIMRC).* 2015, pp. 1649–1653.

[124] T. Zewde and M. C. Gursoy. "NOMA-Based Energy-Efficient Wireless Powered Communications". In: *IEEE Trans. Green Commun.* 2.3 (2018), pp. 679–692.

[125] R. Jain, D. M. Chiu, and H. WR. "A Quantitative Measure Of Fairness And Discrimination For Resource Allocation In Shared Computer Systems". In: *DEC Research Report TR-301* (Sept. 1984).

[126] J. K. SHARMA. *Operations Research:Theory and Applications*. Macmillan Publishers India Limited, 2009.

[127] L. Boyd S.and Vandenberghe. *Convex Optimization*. Cambridge University Press, 2004.

[128] T. E. A. Alharbi and D. K. C. So. "Power Allocation for Full-Duplex Cooperative Non-Orthogonal Multiple Access System". PhD thesis. Dept. Elect. Eng., Univ. of Manch., 2021.

[129] L. Dai et al. "Non-orthogonal multiple access for 5G: solutions, challenges, opportunities, and future research trends". In: *IEEE Commun. Mag.* 53.9 (2015), pp. 74–81.

[130] Z. Ding and H. Vincent Poor. "A Simple Design of IRS-NOMA Transmission". In: *IEEE Commun. Lett.* 24.5 (2020), pp. 1119–1123.

[131] M. Fu, Y. Zhou, and Y. Shi. "Intelligent Reflecting Surface for Downlink Non-Orthogonal Multiple Access Networks". In: *2019 IEEE Globecom Workshops (GC Wkshps)*. 2019, pp. 1–6.

[132] M. Di R. et al. "Smart Radio Environments Empowered by AI Reconfigurable Meta-Surfaces: An Idea Whose Time Has Come". In: (2019).

[133] C. Huang et al. "Reconfigurable Intelligent Surfaces for Energy Efficiency in Wireless Communication". In: *IEEE Wireless Commun.* 18.8 (2019), pp. 4157–4170.

[134] Z. Ding et al. "A Survey on Non-Orthogonal Multiple Access for 5G Networks: Research Challenges and Future Trends". In: *IEEE J. Select. Areas Commun.* 35.10 (2017), pp. 2181–2195.

[135] Z. Ding et al. "A State-of-the-Art Survey on Reconfigurable Intelligent Surface-Assisted Non-Orthogonal Multiple Access Networks". In: *Proc. IEEE* (2022), pp. 1–22.

[136] B. Zheng, Q. Wu, and R. Zhang. "Intelligent Reflecting Surface-Assisted Multiple Access With User Pairing: NOMA or OMA?" In: *IEEE Commun. Lett.* 24.4 (2020), pp. 753–757.

[137] F. E. Bouanani et al. "Performance Analysis of Intelligent Reflecting Surface Aided Wireless Networks With Wireless Power Transfer". In: *IEEE Commun. Lett.* 25.3 (2021), pp. 793–797.

[138] Z. Ding, R. Schober, and H. V. Poor. "On the Impact of Phase Shifting Designs on IRS-NOMA". In: *IEEE Commun. Lett.* 9.10 (2020), pp. 1596–1600.

[139] T. Hou et al. "Reconfigurable Intelligent Surface Aided NOMA Networks". In: *IEEE J. Select. Areas Commun.* 38.11 (2020), pp. 2575–2588.

[140] J. Zhu et al. "Power Efficient IRS-Assisted NOMA". In: *IEEE Trans. Commun.* 69.2 (2021), pp. 900–913.

[141] F. Fang et al. "Energy-Efficient Design of IRS-NOMA Networks". In: *IEEE Trans. Veh. Technol.* 69.11 (2020), pp. 14088–14092.

[142] B. M. ElHalawany et al. "Performance Analysis of Downlink NOMA Systems Over κ-μ Shadowed Fading Channels". In: *IEEE Trans. Veh. Technol.* 69.1 (2020), pp. 1046–1050.

[143] H. Shao et al. "QoE-Aware Downlink User-Cell Association in Small Cell Networks: A Transfer-matching Game Theoretic Solution With Peer Effects". In: *IEEE Access* 4 (2016), pp. 10029–10041.

[144] Y. Sun et al. "QoE-Oriented Resource Allocation for Downlink Non-Orthogonal Multiple Access". In: *IEEE Commun. Lett.* 25.7 (2021), pp. 2362–2365.

[145] J. Cui et al. "QoE-Based Resource Allocation for Multi-Cell NOMA Networks". In: *IEEE Wireless Commun.* 17.9 (2018), pp. 6160–6176.

[146] A. A. Kilbas and M. Saigo. "On the H-function". In: *J. Appl. Math. Stoch. Anal.* 12.2 (1999), pp. 191–204.

[147] K. Peppas et al. "Simple, accurate formula for the average bit error probability of multiple-input multiple-output free-space optical links over negative exponential turbulence channels". In: *Opt. Lett.* 37 (Aug. 2012), pp. 3243–3245.

[148] M. Rugelj et al. "Novel Cross-Layer QoE-Aware Radio Resource Allocation Algorithms in Multiuser OFDMA Systems". In: *IEEE Trans. Commun.* 62.9 (2014), pp. 3196–3208.

[149] P. Ameigeiras et al. "QoE oriented cross-layer design of a resource allocation algorithm in beyond 3G systems". In: *Comp. Commun.* 33.5 (2010), pp. 571–582.